Universiteit Utrecht

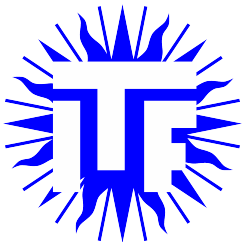

Master thesis

Anomalous Magnetic Effects in Three-Dimensional Weyl Semimetals

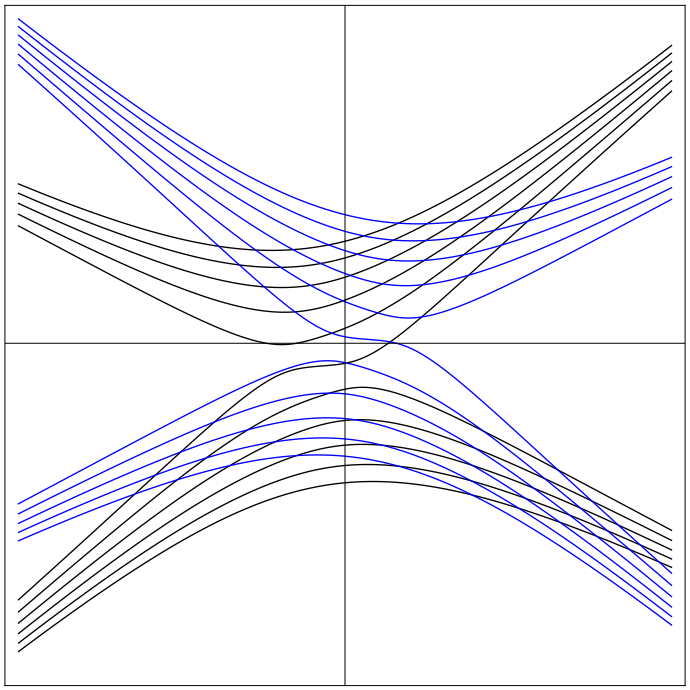

Author:

Thijs van Gogh, BSc.
Institute for Theoretical Physics
Utrecht University

Supervisors:

Prof. dr. ir. Henk Stoof
Institute for Theoretical Physics
Utrecht University

Erik van der Wurff, MSc.
Institute for Theoretical Physics
Utrecht University

June 2017

Abstract

We calculate the energy spectrum of a Weyl semimetal near the band touching points in the presence of a magnetic field. In this calculation we include the effect of the anomalous magnetic moment, coming from a vertex correction to the action. We show that this effect breaks the spin degeneracy, which is present in all states except the chiral ground state. Additionally, we calculate the effect of introducing a time reversal symmetry breaking vector, which separates the two Weyl nodes in momentum space. We find that having the vector along the direction of the magnetic field yields analytically computable states. In contrast, having the vector perpendicular to the direction of the magnetic field requires numerical computation of the energy levels and leads to a non-linear dispersion relation for the ground state. This conclusion is supported by perturbation theory.

Furthermore, we consider the influence of magnetic fields on bound surface states. We show that within a WKB approximation, a magnetic field parallel to the boundary does not affect the surface state dispersion relation. However, the anomalous magnetic moment terms do alter the dispersion relation, as well as the region in reciprocal space in which the dispersion relation is a solution.

Contents

Chapter 1

Introduction

Condensed matter physics is one of the largest and most active fields of research in physics. It encompasses a vast amount of different topics, from liquid crystals to Bose-Einstein condenstates. Both experimentally and theoretically it is a quickly advancing field and many Nobel prizes have been awarded for significant advancements. For instance, in 2016 the Nobel prize was awarded to Thouless, Haldane and Kosterlitz for the theoretical discovery of topological phase transitions and topological phases of matter [1]. In this thesis we consider one such topological phase of matter, a Weyl semimetal, classified through its conductive properties. We start off by sketching the theoretical background. The aim of this thesis is to further our understanding of the energy states of the semimetal under the influence of magnetic fields, more specifically when considering interaction effects such as the anomalous magnetic moment from quantum electrodynamics (QED).

1.1 Solid-state physics

In order to understand the general concepts used and calculations done in this thesis, a short introduction to solid-state physics and semimetals is in order.

The current paradigmatic model that is used in solid-state physics is that of electronic band structures. These bands dictate which energy states the system is allowed to take and are found using quantum mechanical calculations of the wave function of the electrons in the material. The allowed energies are the bands, while the energies that are forbidden are called the band gaps. The electrons will try to minimize the energy of the system, so they will try to occupy a lower energy band before a higher one. However, since they are fermions, they are subject to the Pauli exclusion principle. This forbids them to occupy the same quantum state. Thus, when one state is filled, remaining electrons will have to occupy higher energetic states. The level to which these bands are generaly occupied is called the Fermi level. When the Fermi level lies inside of a band gap, we call the closest band below the gap the valence band, while we call the band above the gap the conduction band. The size of the band gap is denoted by the parameter Δ, which is the difference between the lowest energy of the conduction band and the highest energy of the valence band.

To classify materials according to their conductivity, we will need to define what conductivity is. Conductivity is related to the ability for electrons to move between energetic states, from occupied states to vacant states. Since states below the Fermi level will be occupied, while those above it will be empty, it is natural to see that the position of the Fermi level with regard to the energy bands is important. If the Fermi level lies inside a band, having $\Delta = 0$, the energy difference between occupied states and unoccupied ones will be very small, so it is easy to move between states, yielding high conductivity. This situation is the case for metals. On the other hand, if the Fermi level lies in between

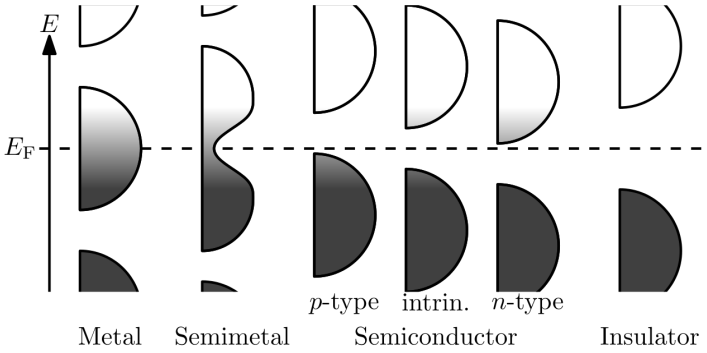

Figure 1.1 – Classification of the materials by their conductance. Black indicates completely filled states, while white indicates completely empty ones. Image taken from Wikipedia.

bands, having $\Delta > 0$, then the energy difference between the highest occupied state and lowest empty state will be very large and movement will be very difficult, yielding very low conductivity. Materials with this property are called insulators.

Furthermore, we have the classes of semimetals and semiconductors. For semiconductors, the Fermi level lies inside of a band gap, but the gap is not as big as in the case of an insulator. So $\Delta_{sc} < \Delta_i$. It is difficult to move to a higher energetic state, but not nearly as hard as for an insulator. Semiconductors can be doped, in which case the Fermi level is shifted closer to the valence band (p-type), or to the conduction band (n-type). In the semimetal case, the Fermi level lies inside a band, so Δ_{sm}=0, but the density of states around the Fermi level is not as high as for a metal. In the case of the classes of semimetals that we consider in this thesis, the valence and conduction band precisely touch at a singular point. In this case the density of states is exactly zero at that point. This band touching point will be considered to be at the Fermi level, or very close to it. For a schematic view of the different classes, see Fig. 1.1.

1.2 Weyl semimetals

We will proceed by describing the different classes of topological materials and how they relate to each other. We start with topological insulators, before moving on to Dirac and Weyl semimetals and their properties. Furthermore, we show that the Weyl semimetal is topologically non-trivial.

1.2.1 Topological insulators

Up until recently, the above classification of solids was thought to contain the full range of possible materials. However, in 2005, a new class of materials was discovered by Mele and Kane, namely the topological insulator (TI) [2]. Topological insulators are a class of materials that behave like an insulator in bulk, having the Fermi level lie inside a band gap, but support conducting surface states. So no current will flow in its interior, but it can flow along its surface. However, conducting surface states are also allowed in trivial insulators, so this property alone is not enough to make it a topological insulator. The property that does make it a topological material is that its surface states are topologically protected through symmetries [3]. This means that these surface states cannot simply be destroyed through very small perturbations, given that those perturbations do not break the protecting symmetries. A schematic overview of a typical band structure for these TI's is shown in Fig. 1.2.

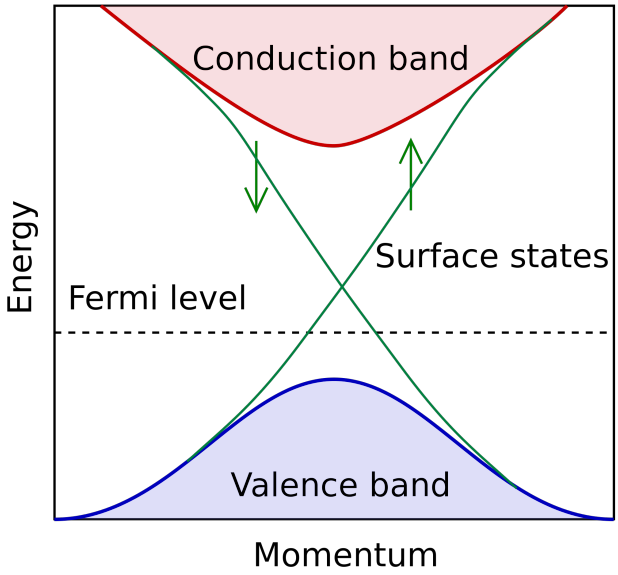

Figure 1.2 – Typical band structure for a topological insulator. The Fermi level lies inside the gap, which can only be crossed by surface states. Image taken from Wikipedia.

1.2.2 Dirac and Weyl semimetals

One of the defining features of the semimetals that we consider in this thesis is that they have a linear dispersion around their band touching point. The most general Hamiltonian that we can write down for a two-band model, linearized around the band touching point, is given by

$$H(\mathbf{k}) = \epsilon \hbar v_F \boldsymbol{\sigma} \cdot \mathbf{k}, \tag{1.2.1}$$

where $\boldsymbol{\sigma}$ is the vector of Pauli matrices, $\mathbf{k}$ is the crystal wavevector in the first Brillouin zone and $\epsilon = \pm 1$, which is called the chirality. Three dimensional condensed matter systems with a band touching point that can be described by this Hamiltonian are called Weyl semimetals (WSM). The eigenvalues associated with this Hamiltonian are given by

$$E(\mathbf{k}) = \pm \hbar v_F \sqrt{k_x^2 + k_y^2 + k_z^2}. \tag{1.2.2}$$

This result is independent of the chirality.

We see that we have a band touching point at exactly $\mathbf{k} = 0$, which is doubly degenerate. This is what we call a Weyl node. Now we can look at what happens when we add a small perturbation to the Hamiltonian. Since the Pauli matrices and the unit matrix together form a basis for all 2×2 matrices, any perturbation can be expressed as a linear combination of these matrices. Any perturbation proportional to one of the Pauli matrices will simply shift the corresponding momentum. Any perturbation proportional to the unit matrix will only shift the energy by a constant. From this we can then conclude that any small pertubation added to the Hamiltonian can only move the Weyl node around in energy-momentum space, but cannot actually destroy it and gap out the system. As will be shown shortly, this is due to the topological nature of the Weyl node. This stability of the node is a consequence of the von Neumann-Wigner theorem [4], which states that we require three changeable parameters in order to be able to have a band touching point. In the Weyl semimetal, we have all three momenta as parameters. This also the reason why a Weyl semimetal cannot exist for lower dimensions.

We have yet to motivate the names that we have given so far, especially the Weyl part. Looking back at the Hamiltonian for this band touching, we see that it has exactly the form of the Weyl Hamiltonian, which is known from particle physics [5]. The only difference here is that we have changed c, the speed of light, to v_F, which is the Fermi

velocity. The Fermi velocity is the characteristic speed in condensed matter systems and is typically 300 times smaller than the speed of light. The quasi-particle excitations of this Hamiltonian are then massless Weyl fermions. Since they have no mass, we know that they have a definite chirality. This also justifies why we call ϵ the chirality. Depending on the sign of the Hamiltonian, the Weyl fermions that arise as excitations will be either right-handed (RH), corresponding to $\epsilon = 1$, or left-handed (LH), corresponding to $\epsilon = -1$.

However, simply having a linear band touching described by the above Hamiltonian is not sufficient for a Weyl node to exist. The other condition that needs to be satisfied is that either time-reversal (TR) symmetry, or inversion (I) symmetry, or both need to be broken. Under time-reversal, we find that $\mathbf{k} \to -\mathbf{k}$ and $\boldsymbol{\sigma} \to -\boldsymbol{\sigma}$, hence we require $E_\sigma(\mathbf{k}) = E_{-\sigma}(-\mathbf{k})$. Under inversion we have $\mathbf{k} \to -\mathbf{k}$, thus we require $E_\sigma(\mathbf{k}) = E_\sigma(-\mathbf{k})$. So if now both TR and I symmetries are present in the system, we require that $E_\sigma(\mathbf{k}) = E_{-\sigma}(\mathbf{k})$. Switching the sign on $\boldsymbol{\sigma}$ in the Hamiltonian is equivalent to switching the sign of the chirality. So we can conclude from this that in order to have both symmetries present in the system, we must have two Weyl nodes of opposite chirality at the same point in momentum space. This is what we call a Dirac point. From Kramer's degeneracy theorem [6], we find that all energies must be doubly degenerate everywhere. The only exception being at the Dirac point, where it is four-fold degenerate. The low-energy Hamiltonian that is associated with this is then given as

$$H(\mathbf{k}) = \hbar v_F \begin{pmatrix} -\boldsymbol{\sigma}\cdot\mathbf{k} & 0 \\ 0 & \boldsymbol{\sigma}\cdot\mathbf{k} \end{pmatrix}, \tag{1.2.3}$$

where its quasi-particle excitation are then massless Dirac fermions. For this reason, a condensed matter system that is described through this Hamiltonian is called a Dirac semimetal. Here we can also see why we will require our Weyl nodes to be separated in order for a stable semimetal to exist. Looking at just the Weyl Hamiltonian, we see that we cannot add anything that will open up a gap. However, looking at the Hamiltonian above, we see that we can add terms to the off-diagonal part, which then can actually gap out the system.

Dirac semimetals can exist in either $(2+1)$-dimensions or $(3+1)$-dimensions, as opposed to Weyl semimetals, which can only exist in $(3+1)$ dimensions. Perhaps the most famous example of a $(2+1)$-dimensional Dirac semimetal is graphene. When Weyl semimetals are discussed, it is often described as a three dimensional analogue to graphene. Graphene was first discovered in 2004 [7], for which the Nobel prize was awarded in 2010 [8]. However, this parallel is somewhat deceptive, as we will show shortly. In $(2+1)$-dimensions, the Hamiltonian is then given as

$$H = \pm\hbar v_F \left(k_x\sigma^x + k_y\sigma^y\right).$$

Since there is no term proportional to σ^z, we can add a small perturbation proportional to that to the Hamiltonian, which will then gap out the system and destroy the Dirac point. So in order for a Dirac semimetal to be stable, we cannot allow perturbations of this form. This can be achieved through protecting symmetries. In the case of graphene, we have TR symmetry which protects this Dirac point [9].

From the above discussion, we see that in $(3+1)$-dimensions we have a Dirac semimetal when both TR and I symmetries are present, and a Weyl semimetal when at least one of these symmetries is broken. So one can view the Dirac semimetal as a special case of the Weyl semimetal, or vice versa. Both of these states of matter have been experimentally observed recently. The three dimensional Dirac semimetal in 2014 [10], and finally the Weyl semimetal in 2015 [11].

1.2.3 Topological nature of Weyl semimetals

One of the many interesting properties of a Weyl semimetal is its topological nature, which we hinted at earlier. Here we show that the Weyl nodes are topological objects,

acting as either a source or a sink of so-called Berry flux. Whether they are a sink or source depends on the chirality of the node. This implies, since the total Berry flux of a semimetal has to vanish, that the Weyl nodes can only appear in pairs, with opposite chirality.

Assume we have a system that is described by a Hamiltonian $H(\mathbf{R}(t))$, where $\mathbf{R}(t)$ is a time-dependent vector parameter. When $\mathbf{R}(t)$ undergoes a cyclic, adiabatic evolution, such that $\mathbf{R}(0) = \mathbf{R}(T)$, the corresponding eigenstate may not return to its original value, but rather pick up a geometrical phase factor. This factor, denoted by γ_n, is called the Berry phase, and this result was shown by Berry in 1984 [12]. Writing $|n(\mathbf{R})\rangle$ as the eigenstates of the Hamiltonian corresponding to the n-th eigenvalue $E_n(\mathbf{R})$, the Berry phase can be computed as

$$\gamma_n = \imath \oint_{\mathcal{C}} d\mathbf{R} \langle n(\mathbf{R}) | \nabla_{\mathbf{R}} | n(\mathbf{R}) \rangle = \oint_{\mathcal{C}} d\mathbf{R} \cdot \mathcal{A}_n(\mathbf{R}), \tag{1.2.4}$$

where we define the Berry connection $\mathcal{A}_n(\mathbf{R}) = \imath \langle n(\mathbf{R}) | \nabla_{\mathbf{R}} | n(\mathbf{R}) \rangle$. The $\mathcal{C}$ denotes a loop integral over a closed curve.

From here, we can obtain the Berry curvature $\mathbf{\Omega}_n(\mathbf{R})$, by taking the rotation with respect to the parameter space:

$$\mathbf{\Omega}_n(\mathbf{R}) = \nabla_{\mathbf{R}} \times \mathcal{A}_n(\mathbf{R}). \tag{1.2.5}$$

Recalling Stokes' theorem, we can rewrite the formula for the Berry phase from a contour integral over the Berry connection to a surface integral over the Berry curvature:

$$\gamma_n = \int_{\mathcal{S}} d\mathbf{S} \cdot \mathbf{\Omega}_n(\mathbf{R}). \tag{1.2.6}$$

If we now let this integral be over a closed manifold, then the Chern theorem tells us that this integral will be quantized in units of 2π [13]. The number that comes out of the integral is called the Chern number and is a measure for the amount of sources and sinks of Berry flux within that manifold.

So far this discussion has been general and abstract, so how do we apply this to semimetals? The above statements hold systems dependent on an arbitrary parameter $\mathbf{R}$. The Hamiltonian for semimetals depends on $\mathbf{k}$, so we take $\mathbf{R}$ to be our momentum wavevector $\mathbf{k}$. Thus we can write the Berry curvature in the semimetal system as

$$\mathbf{B}_n(\mathbf{k}) = \nabla_{\mathbf{k}} \times \mathcal{A}_n(\mathbf{k}). \tag{1.2.7}$$

Here we suggestively denoted the Berry curvature with a $\mathbf{B}$. Now the analogue to the magnetic field becomes obvious, but then in reciprocal space instead of real space. The Berry connection here plays the role of the electromagnetic vector potential, while the Berry curvature plays the role of the magnetic field.

Now that we have this expression in reciprocal space, it is a very natural next step to calculate the Berry phase over a closed surface in that space. Since it is known that the topology of this space is indeed a manifold, this Berry phase will then give us a Chern number. It can be easily shown that calculating the Berry phase over a positive chiral node gives a Chern number of +1, while that of a negative node gives −1. So this then characterizes the topological nature of the Weyl nodes. They are analogous to magnetic monopoles in reciprocal space, one node is the source, while the opposite note is the sink for the Berry flux. Just like magnetic poles, they never appear alone, and one can never destroy just one node. They are created in pairs, and get annihilated in pairs, since the total Chern number of the reciprocal space has to remain constant, namely zero.

At this point does the analogy between graphene and Weyl semimetals breaks down. Having a Dirac point, as opposed to two Weyl nodes, does not give any Chern number, as the source and sink of the Berry flux are the same point. So while Weyl semimetals are topological materials, Dirac semimetals are not.

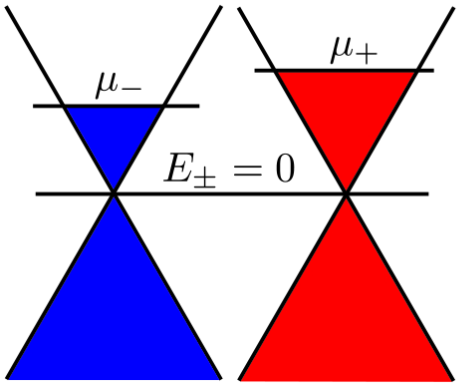

Figure 1.3 – Chiral imbalance due to chiral potential for undoped Weyl nodes.

1.3 Topological electromagnetic properties

Owing to its topological nature, the Weyl semimetal has quite a few interesting properties. Here two of those properties will be explained, being the chiral magnetic effect (CME) and the anomalous Hall effect (AHE), which arise by applying an external electromagnetic field.

1.3.1 Chiral magnetic effect

The CME is one of the novel effects that can be measured in Weyl semimetals and is related to the chiral anomaly found in quantum field theory. It has been predicted for these systems in 1983 [14]. It only arises in chiral systems where a chiral charge imbalance can occur, such as in Dirac and Weyl semimetals or a quark-gluon plasma. The effect is the generation of an electric current along the direction of the applied external magnetic field. If this chiral imbalance is present, the current associated with this effects is found to be

$$\mathbf{j} = \frac{e^2 \mu_5}{2\pi^2} \mathbf{B}, \tag{1.3.1}$$

where the constant of proportionality to the magnetic field is called the CME conductivity [15]. $\mu_5 = \mu_+ - \mu_-$ denotes the chiral chemical potential. This effect is illustrated in Fig. 1.3. The CME has recently been observed in the Dirac semimetal $ZrTe_5$ [16].

1.3.2 Anomalous Hall effect

When an external magnetic field is applied to a conductor, a voltage difference is produced transverse to the direction of the electric current and perpendicular to the magnetic field. This is called the Hall effect, and was discovered by Edwin Hall in 1879 [17]. Shortly thereafter, it was found to be much stronger in magnetic conductors than in non-magnetic conductors [18]. This stronger version of the Hall effect was then dubbed the anomalous Hall effect. It took well over a century before this effect was well understood. This because it relies on concepts such as the Berry phase, which was not discovered until 1984.

The AHE has its origins in two different terms [19]. The first is due to intrinsic properties of the material, which can be related to the Berry phase effect in momentum space, and for this reason is called the intrinsic AHE. The second is due to disorder and impurity scattering, and is called the extrinsic AHE. In the WSM case, it has been shown that only the intrinsic part of the AHE contributes [20]. The current that is then produced

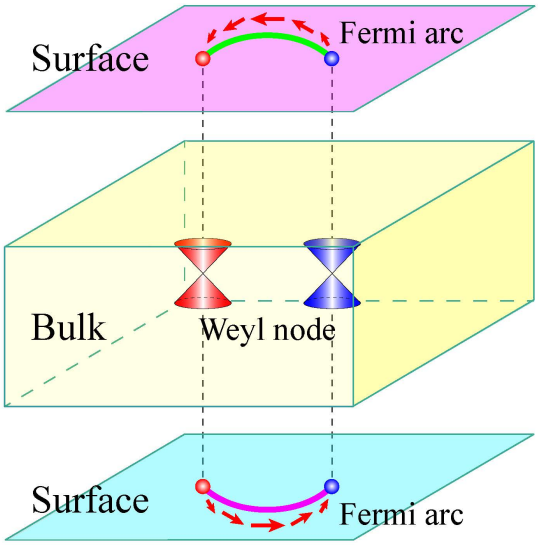

Figure 1.4 – Schematic of a Weyl semimetal with its conducting surface Fermi arcs. Image taken from Ref. [22].

by the intrisic AHE is found to be

$$j^{\mu} = \frac{e^2}{2\pi^2}\epsilon^{\mu\nu\rho\sigma} b_{\nu}\partial_{\rho}A_{\sigma}, \tag{1.3.2}$$

where b_{μ} is the vector that separates the two Weyl nodes in energy-momentum space, $\epsilon^{\mu\nu\rho\sigma}$ is the totally anti-symmetric Levi-Civita tensor and A_{σ} is the four-potential of the external electromagnetic field. Interesting to note here is that the strength of the induced current is proportional to the separation of the Weyl nodes. Moreover, we see that this effect occurs even in the absence of a magnetic field. Indeed, having just an external electric field is enough to give rise to this effect.

1.4 Topological surface states

Another fascinating property, which we expand upon in detail in this thesis, is the appearence of topological surface states. This is a property of topological states of matter, and they also appear on the surface of topological insulators. However, the Weyl semimetal surface states are very different from those of a TI. Whereas usually we find a Fermi surface, which is a topologically closed object, in Weyl semimetals we find topologically open Fermi arcs [21]. These arcs connect the projections of the Weyl nodes on the surface of the Brillouin zone through conducting states. In order for these projections to not be at the same point on the surface, it is insufficient to have a Weyl semimetal with just a broken I symmetry. So for these surface states to exist, we require that we have a WSM with broken TR symmetry. A schematic view is given in Fig. 1.4. The region in which the Fermi arc and surface states exist are exactly the regions in the Weyl semimetal where the Chern number is not equal to zero. However, as we will find later, this is only true in the absence of interaction. Introducing interactions will change the region in which the surface states exist, but will not affect the Chern number. We will compute these surface states in chapter 4.

These Fermi arcs are a hallmark for experimentally observing Weyl semimetal states. Using angle-resolved photoemission spectroscopy (ARPES), information can be gained on both the energy and momenta of electrons at a surface. Using this technique, the Fermi arc and surface states can be experimentally shown [23].

1.5 This thesis

After this introduction to the world of semimetal physics, we will now go into detail on some of its properties. While there are many interesting effects that can occur in this system, we will focus on gaining a deeper understanding of the effects of magnetic fields. Specifically, we will focus on the influence of the anomalous magnetic moment on the energy states, both in bulk and at the surface. The anomalous magnetic moment arises from performing a vertex correction to the action, and will turn out to have interesting consequences.

This thesis is structured in the following way: In chapter 2 we will explicitly perform the quantization of the Weyl Hamiltonian and its energy levels under influence of magnetic fields. This forms the basis for the chapters thereafter. After solving the non-interacting case, we investigate the effect of the anomalous magnetic moment on the energy levels in bulk in chapter 3. From that we find that it breaks the spin degeneracy present in the Landau levels. Next we introduce a term that separates the Weyl points of the two chiralities in energy- momentum space, breaking I and/or TR symmetry. The effect of this is studied using both analytical and numerical tools. Introducing this term will then also break the spin degeneracies. Having thoroughly investigated the effects on bulk states, we move the focus from bulk states to surface states in chapter 4. Here we demand solutions in bulk have to be matched with those in a Dirac vacuum on the interface between them, giving us states localized to the surface. These states are a consequence of the topological nature of the Weyl semimetal. However, finding solutions under the effect of magnetic fields turns out to be non-trivial, so appendix A is devoted to setting up the mathematical framework for these computations, employing a first order WKB approximation. After having obtained the results in both the bulk and at the surface of the Weyl semimetal, chapter 5 will summarize the results obtained in this thesis and looks ahead at the questions that remain open and could be interesting to answer in future work.

1.5.1 A note on notation

To avoid confusion, we specify our choice of notations and definitions here. First and foremost, as with any work that employs field-theoretical computations, Einstein notation will be used. Any repeated indices will be implicitly summed over, unless otherwise specified, such as when summing over a range excluding some values.

When dealing with tensors and vectors, Greek letters will indicate spacetime indices, while roman letters will denote spatial indices.

When considering units, in general SI units will be used, unless otherwise specified. However, dimensionless equations will be useful at some point, especially when considering numerics. When this happens, dimensionless variables will be indicated with a bar, and it will be stated how they are made dimensionless.

We work in flat Minkowski space, where we choose our sign convention for the metric to be $(+,-,-,-)$.

Since we will often be working with the Dirac equation and variations thereof, we will make extensive use of the Dirac gamma matrices γ^μ. The matrices obey the Clifford algebra, which is defined by the anti-commutation relations $\{\gamma^\mu,\gamma^\nu\} = 2\eta^{\mu\nu}$, with $\eta^{\mu\nu}$ the Minkowski metric. There are a couple different choices of basis that we can use. Because chirality will be very important in this work, we shall use the chiral basis for our Dirac matrices. Along with our choice for the metric signature, we find them to be

$$\gamma^0 = \begin{pmatrix} 0 & \mathbb{I}_2 \\ \mathbb{I}_2 & 0 \end{pmatrix}, \qquad \gamma^i = \begin{pmatrix} 0 & \sigma^i \\ -\sigma^i & 0 \end{pmatrix}, \qquad \gamma^5 = \imath\gamma^0\gamma^1\gamma^2\gamma^3 = \begin{pmatrix} -\mathbb{I}_2 & 0 \\ 0 & \mathbb{I}_2 \end{pmatrix}.$$

Chapter 2

Landau Levels

The basis for calculating the effects of a magnetic field on free, charged particles lies in the so-called Landau quantization: the quantization of the radius of their cyclotron orbits in a perpendicular magnetic field. This also forms the basis for much of the work that is done later in this thesis.

In this chapter we will explicitly perform this quantization on both the non-relativistic (Section 2.2) and relativistic (Section 2.3) Hamiltonians of the semimetal around the Weyl points. Furthermore we calculate the so-called Landau levels, the quantized energy levels, that result from this.

2.1 Introduction

When a uniform magnetic field is applied in a certain direction, charged particles will move in closed orbits around the axis of the magnetic field due to the (magnetic) Lorentz force, given by $\mathbf{F}_{\text{mag}} = q\mathbf{v} \times \mathbf{B}$. These closed orbits are called cyclotron orbits.

When considering these orbits quantum mechanically, one finds that the radius of these orbits actually becomes quantized. However, this quantization of the energy levels is only observed when the mean thermal energy of the particles is much lower than the separation between the energy levels. This means that $k_B T \ll \hbar\omega_c$, where ω_c is the cyclotron frequency, classically defined as $\omega_c = qB/m$ for a particle with mass m and charge q in a magnetic field with strength B. Otherwise the thermal spread will obscure the difference between the energy levels. This boils down to having very low temperatures, and very strong magnetic fields. In general we will consider $T = 0$ in this thesis.

In this part the energy levels in the bulk of a Weyl semimetal with an applied magnetic field are investigated. The charged particles that are considered here are massless, spin-1/2 Weyl fermions, which obey the Weyl equation. The Weyl equation is derived from the Dirac equation, which describes relativistic, massive spin-1/2 particles, and was formulated by Paul Dirac in 1928 [24]. The Dirac equation is given by

$$(\imath\hbar\partial\!\!\!/ - mc)\psi = 0, \tag{2.1.1}$$

where $\partial\!\!\!/ = \partial_\mu \gamma^\mu$, with γ^μ the Dirac matrices, which obey the Clifford algebra defined by $\{\gamma^\mu, \gamma^\nu\} = 2\eta^{\mu\nu}$. From this equation the eigenstates and energies can be determined. If we couple this equation with a magnetic field, then we find quantized energy levels. These quantized energy levels are called the Landau levels (LL), named after the Soviet physicist Lev Landau.

In order to arrive at the Hamiltonians that we will work with, we need to keep in mind that we are dealing with solids, so the system will be electrons on a 3D lattice, consisting of 2 inequivalent sublattices. The Hamiltonian will be that of of a discrete lattice, with hopping between sites on the lattice. The Hamiltonian can be rewritten as a function of

momenta instead, as long as we keep in mind that we use the momenta corresponding to the crystal momenta in the first Brillouin zone. To obtain the Hamiltonians below, we make a low energy expansion around the band touching points. For a derivation in two spatial dimensions, see section 2.1.2 in Ref. [25]. The derivation in three spatial dimensions is analogous to this derivation.

2.2 Non-relativistic case

The calculations in this section will be along the lines of those done in Ref. [25]. In the non-relativistic case, the Hamiltonian in absence of magnetic fields simply reads

$$H = \frac{\mathbf{p}^2}{2m_B}, \tag{2.2.1}$$

where m_B is not the free electron mass, but rather the band mass, also often called the effective mass.

If we now add a magnetic field, we can make use of the principle of minimal coupling, which is given by

$$\mathbf{p} \to \mathbf{\Pi} = \mathbf{p} - q\mathbf{A}, \tag{2.2.2}$$

with q the charge of the particle and $\mathbf{A}$ the magnetic vector potential. Note that neither $\mathbf{p}$ nor $\mathbf{A}$ are gauge invariant quantities, but $\mathbf{\Pi}$ is. This substitution takes into account the effects of charge distributions, but neglects higher order multipole effects. Up to monopole order this expression is exact. Since we consider single electrons, which we take to be monopole charges, we can consider this expression to be exact.

Since we consider electrons, which have a charge of $q = -e$, the Hamiltonian reads

$$H = \frac{(\mathbf{p} + e\mathbf{A})^2}{2m_B} \equiv \frac{\mathbf{\Pi}^2}{2m_B}. \tag{2.2.3}$$

If we now take the magnetic field to be uniform and in the positive z-direction, since the magnetic field is given by $\mathbf{B} = \nabla \times \mathbf{A}$, we find that $\mathbf{A} = B(-y, 0, 0)$ is a valid choice of gauge.

Note that this is only one of the possible choices for $\mathbf{A}$ and is known as the Landau gauge. Another possibility is taking $\mathbf{A} = B(0, x, 0)$, which is also called the Landau gauge. We can also take $\mathbf{A} = B(-y, x, 0)/2$, which is known as the symmetric or radial gauge. In fact, there are infinitely many choices here: $\mathbf{A} = B(-ay, bx, 0)$, with $a + b = 1$ will all give the correct result for the magnetic field. Of course, all gauges will yield the same physical result, but not all gauges will be easy to work with, hence only two of the infinite amount of choices have names and are generally used. Which of those is used is generally dependent on the geometry of the system. If it is useful to retain a translational invariance, then the Landau gauge is more suitable. If rotational invariance is present, then the radial gauge may be a better choice.

Using the Landau gauge, we find

$$\Pi_x = p_x - eBy, \quad \Pi_y = p_y, \quad \Pi_z = p_z.$$

Note that the Hamiltonian now explicitly depends on y, so it is no longer translationally invariant along that direction. This then implies that its associate momentum p_y is no longer a good quantum number. Since the system remains invariant in the other two directions, their associated momenta will still be good quantum numbers. From the canonical commutation relations, we know that all momentum operators commute with each other, but do not commute with the position operators in the same direction of the momentum. So the only non-zero commutation relations are given by:

$$[x, p_x] = [y, p_y] = [z, p_z] = \imath\hbar.$$

From this, we see that the operators Π_i also commute, with the exception of Π_x and Π_y. Their commutation relation reads

$$\begin{aligned}[\Pi_x, \Pi_y] &= [p_x - eBy, p_y] \\ &= \underbrace{[p_x, p_y]}_{=0} - eB[y, p_y] \\ &= -\imath\hbar eB.\end{aligned}$$

Since their commutator is non-zero, we conclude that these are conjugate variables. Using this commutator, we can rewrite the Hamiltonian in Eq. 2.2.3. We note that

$$\begin{aligned}(\Pi_x + \imath\Pi_y)(\Pi_x - \imath\Pi_y) &= \Pi_x^2 + \Pi_y^2 + \imath\Pi_y\Pi_x - \imath\Pi_x\Pi_y \\ &= \Pi_x^2 + \Pi_y^2 + \imath[\Pi_y, \Pi_x] \\ &= \Pi_x^2 + \Pi_y^2 - \hbar eB,\end{aligned}$$

yielding the Hamiltonian

$$H = \frac{1}{2m_B}\left[(\Pi_x + \imath\Pi_y)(\Pi_x - \imath\Pi_y) + \hbar eB + \Pi_z^2\right]. \tag{2.2.4}$$

Next we want to write this in terms of creation and annihilation operators. We define $\tilde{a}^\dagger = \Pi_x + \imath\Pi_y$ and $\tilde{a} = \Pi_x - \imath\Pi_y$. In order for them to be proper ladder operators, we require that the commutator $[a, a^\dagger] = 1$, so we need to normalize them first. After normalization, the creation and annihilation operators are defined as

$$a^\dagger = \frac{1}{\sqrt{2\hbar eB}}(\Pi_x + \imath\Pi_y), \quad a = \frac{1}{\sqrt{2\hbar eB}}(\Pi_x - \imath\Pi_y). \tag{2.2.5}$$

We can now introduce the magnetic length, which is a measure for the smallest radius of the cyclotron orbit that is allowed by the uncertainty principle. It is defined as

$$l_B = \sqrt{\frac{\hbar}{eB}},$$

such that our ladder operators then read

$$a^\dagger = \frac{l_B}{\sqrt{2}\hbar}(\Pi_x + \imath\Pi_y), \quad a = \frac{l_B}{\sqrt{2}\hbar}(\Pi_x - \imath\Pi_y). \tag{2.2.6}$$

In terms of the original momenta, we can write these operators as

$$a^\dagger = \frac{l_B}{\sqrt{2}\hbar}[(p_x - eBy) + \imath p_y], \quad a = \frac{l_B}{\sqrt{2}\hbar}[(p_x - eBy) - \imath p_y], \tag{2.2.7}$$

where we see that these are simply the ladder operators for a harmonic oscillator, with a shifted coordinate. Finally, we arrive at the following expression for the Hamiltonian:

$$H = \frac{1}{2m_B}\left(\frac{2\hbar^2}{l_B^2}a^\dagger a + \frac{\hbar^2}{l_B^2} + p_z^2\right) = \frac{\hbar^2}{l_B^2 m_B}\left(a^\dagger a + \frac{1}{2}\right) + \frac{p_z^2}{2m_B}. \tag{2.2.8}$$

Since the Hamiltonian is now in the form of a harmonic oscillator, we know that the eigenstates are given by $|n, p_x, p_z\rangle \equiv |n\rangle \otimes |p_x\rangle \otimes |p_z\rangle$. Here $|n\rangle$ are the harmonic oscillator

states, which are eigenstates of the number operator $a^\dagger a$, such that $a^\dagger a|n\rangle = n|n\rangle$ and $n \in \mathbb{N}$. The energies, which are the eigenvalues corresponding to the eigenstates, are then given by

$$\begin{aligned} H|n, p_x, p_z\rangle &= \left(\frac{\hbar^2}{l_B^2 m_B}\left(a^\dagger a + \frac{1}{2}\right) + \frac{\Pi_z^2}{2m_B}\right)|n, p_x, p_z\rangle \\ &= \left(\frac{\hbar^2}{l_B^2 m_B}\left(n + \frac{1}{2}\right) + \frac{\Pi_z^2}{2m_B}\right)|n, p_x, p_z\rangle \\ &= E_{n,p_z}|n, p_x, p_z\rangle. \end{aligned}$$

In order to be able to consider effects of spin, we need to introduce a spin-structure to the Hamiltonian. This is done for spin-1/2 particles by having the Hamiltonian be a 2×2 matrix, with its corresponding eigenvalues being two component spinors. The Hamiltonian under consideration does not have any spin effects incorporated, and will simply be proportional to $\mathbb{I}_2$. We can now add a spin-field interaction term, given by $-\boldsymbol{\mu} \cdot \mathbf{B}$, where $\boldsymbol{\mu} = g\mu_B \boldsymbol{\sigma}/2$, with g the Lande g factor, μ_B the Bohr magneton and $\boldsymbol{\sigma}$ the vector of spin-1/2 Pauli matrices. This term gives the tendency for the spins to align with the magnetic field. If the spins are (anti-)aligned with the field, then the term as a whole gives a negative (positive) contribution to the energy. So it is energetically favourable for the spins to align with the magnetic field.

Since we consider a magnetic field along the z-direction, the term that gets added to the Hamiltonian is given by $-g\mu_B\sigma_z/2$. Since this term is diagonal and does not act on the eigenstates, we simply find that this contributes to the energy levels as $-g\mu_b\sigma/2$, where $\sigma = \pm 1$. From this, we find that the full energy levels are given by

$$E_{n,p_z,\sigma} = \frac{p_z^2}{2m_B} + \frac{\hbar^2}{l_B^2 m_B}\left(n + \frac{1}{2}\right) - \frac{g}{2}\mu_B B\sigma = \frac{p_z^2}{2m_B} + 2\mu_B\left(n + \frac{1}{2} - \frac{\sigma}{2}\right)B \equiv \frac{p_z^2}{2m_B} + 2\mu_B l B. \tag{2.2.9}$$

Here we have used that $\mu_B = e\hbar/2m_B = \hbar^2/l_B^2 m_B B$, and that $g = 2$ for electrons, which is true in the absence of interactions, which will be accounted for in the next chapter. We have also defined the Landau level $l \equiv n + (1-\sigma)/2$, which is a non-negative integer. Note that, besides $l = 0$ which can only be constructed using the values $n = 0$ and $\sigma = +1$, there are always two configurations that lead to the same value for l. This leads us to conclude that the ground state is non-degenerate, while all other levels are doubly degenerate in spin. There is a second degeneracy in p_x, which is actually an infinite degeneracy and is present in all levels, including the lowest level. A plot of the non-relativistic energy levels is given in Fig. 2.1.

Care needs to be taken here when taking the limit $B \to 0$. The reason for this is that the magnetic field quantizes the directions transverse to its direction, which allowed us to introduce the ladder operators that we then used to compute the energy spectrum. This quantization breaks down in the zero magnetic field limit. Instead, if we consider $B = 0$, then all three components of $\mathbf{p}$ are good quantum numbers and the energy spectrum will simply be given by $E = (p_x^2 + p_y^2 + p_z^2)/2m_B$.

2.3 Relativistic case

We can do the same calculation for relativistic electrons. The Hamiltonian for the relativistic case can be derived from the Dirac equation, given by

$$(\Pi_\mu \gamma^\mu - m v_F)\psi = 0, \tag{2.3.1}$$

where $\Pi_\mu = \imath\hbar\partial_\mu - eA_\mu$ and $A_\mu = (\phi, \mathbf{A})$ the four-potential. In the four-potential, ϕ is the scalar potential from which the electric field can be derived, and $\mathbf{A}$ is again the magnetic

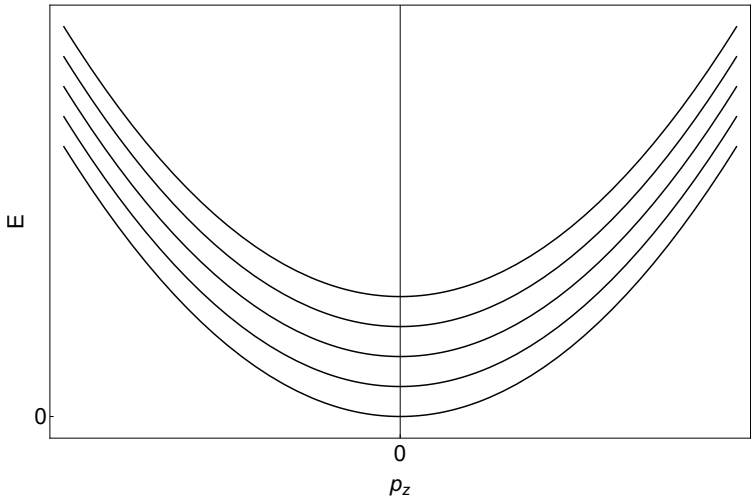

Figure 2.1 – Non-relativistic energy levels as a function of momentum along the magnetic field. The values $m_B = \mu_B = B = 1$ were used.

vector potential. Taking $m = 0$ and noticing that the momentum operators are given by $p_i = -\imath\hbar\partial_i$, we find two Schrödinger equations, given by

$$\imath\hbar\partial_t \begin{pmatrix}\psi_1\\ \psi_2\end{pmatrix} = \begin{pmatrix}-\mathbf{\Pi}\cdot\boldsymbol{\sigma}\psi_1\\ \mathbf{\Pi}\cdot\boldsymbol{\sigma}\psi_2\end{pmatrix} = H\begin{pmatrix}\psi_1\\ \psi_2\end{pmatrix},$$

where both ψ_1 and ψ_2 are 2 component spinors. We see that the two equations for ψ_1 and ψ_2 are identical, except for a minus sign. This difference in minus sign turns out to be exactly the difference in chirality between the two different Weyl cones. Using the parameter $\epsilon = \pm 1$ for the chirality, we can conveniently write our full 4×4 Hamiltonian as a 2×2 Hamiltonian with a factor of ϵ to take the sign difference into account. In this case our Hamiltonian reads

$$H = -\epsilon v_F \mathbf{\Pi}\cdot\boldsymbol{\sigma} = -\epsilon v_F \begin{pmatrix}\Pi_z & \Pi_x - \imath\Pi_y\\ \Pi_x + \imath\Pi_y & -\Pi_z\end{pmatrix}. \tag{2.3.2}$$

Note that the Hamiltonian only explicitly depends on y, so p_x and p_z are good quantum numbers here, and the wave function will depend on those. Another thing to note is that the relativistic Hamiltonian automatically incorporates the effects of spin, so the magnetic moment does not need to be added here, it is already included in the Dirac equation through the gamma matrices. The creation and annihilation operators that we derived in the previous section still hold here, so we can immediately rewrite this Hamiltonian as

$$H = -\epsilon\frac{\sqrt{2}\hbar v_F}{l_B}\begin{pmatrix}0 & a\\ a^\dagger & 0\end{pmatrix} - \epsilon v_F p_z \sigma_z. \tag{2.3.3}$$

Again the eigenstates are two component spinors, given by $|\psi\rangle = \begin{pmatrix}\psi^+\\ \psi^-\end{pmatrix}$. We now want to solve the eigenvalue equation

$$H\begin{pmatrix}\psi^+\\ \psi^-\end{pmatrix} = \left[-\epsilon\frac{\sqrt{2}\hbar v_F}{l_B}\begin{pmatrix}0 & a\\ a^\dagger & 0\end{pmatrix} - \epsilon v_F p_z\sigma_z\right]\begin{pmatrix}\psi^+\\ \psi^-\end{pmatrix} = E\begin{pmatrix}\psi^+\\ \psi^-\end{pmatrix}.$$

This then gives us a set of two equations:

$$-\epsilon\frac{\sqrt{2}\hbar v_F}{l_B}a\psi^- = (E + \epsilon v_F p_z)\psi^+, \quad -\epsilon\frac{\sqrt{2}\hbar v_F}{l_B}a^\dagger\psi^+ = (E - \epsilon v_F p_z)\psi^-. \tag{2.3.4}$$

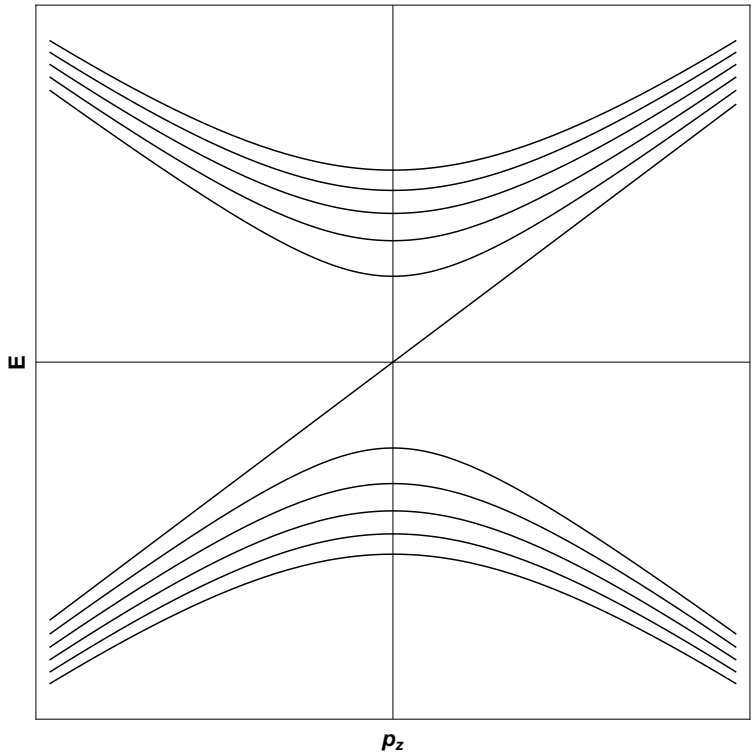

Figure 2.2 – Relativistic energy levels as a function of momentum along the magnetic field for right handed fermions. The values $v_F = \hbar = l_B = 1$ were used here.

Solving the first one for ψ^+ yields

$$\psi^+ = -\frac{\epsilon\sqrt{2}\hbar v_F}{l_B(E + \epsilon v_F p_z)} a\psi^-.$$

Substituting that into the other equation gives us

$$\frac{2\hbar^2 v_F^2}{l_B^2(E + \epsilon v_F p_z)} a^\dagger a\psi^- = (E - \epsilon v_F p_z)\psi^-.$$

From this we then find that

$$a^\dagger a\psi^- = \frac{l_B^2(E^2 - v_F^2 p_z^2)}{2\hbar^2 v_F^2}\psi^-, \quad \text{or} \quad (\frac{2\hbar^2 v_F^2}{l_B^2} a^\dagger a + v_F^2 p_z^2)\psi^- = E^2\psi^-.$$

From this form of the equation we see that the eigenstates are again harmonic oscillator states, since the only operator acting on the eigenstates is a number operator.

So we find that the state ψ^- is proportional to the harmonic oscillator states, so we can write $\psi^- = c|n, p_x, p_z\rangle$, where c is a constant that we can determine later through normalization.

Using this, we find that the energy levels are given by:

$$E_{n,p_z} = \pm v_F\sqrt{p_z^2 + \frac{2\hbar^2}{l_B^2}n}. \tag{2.3.5}$$

We plot these energy levels in Fig. 2.2.

Since we now know ψ^- and E, we can use it to find ψ^+. For the sake of brevity, we define $\alpha \equiv \sqrt{2}\hbar v_F/l_B$. From Eq. 2.3.4, we know that

$$\psi^+ = -\frac{\alpha}{E + \epsilon v_F p_z} a\psi^-.$$

Inserting the found expression for ψ^-, we find:

$$\begin{aligned}
\psi^+ &= \frac{-\epsilon\alpha}{E_{n,p_z} + \epsilon v_F p_z} a\psi^- \\
&= \frac{-\epsilon\alpha}{E_{n,p_z} + \epsilon v_F p_z} ac|n, p_x, p_z\rangle \\
&= \frac{-\epsilon\alpha(E_{n,p_z} - \epsilon v_F p_z)}{E_n^2 - v_F^2 p_z^2} ac|n, p_x, p_z\rangle \\
&= \frac{-\epsilon E_{n,p_z} + v_F p_z}{\alpha n} ac|n, p_x, p_z\rangle \\
&= c\frac{-\epsilon E_{n,p_z} + v_F p_z}{\alpha\sqrt{n}}|n-1, p_x, p_z\rangle.
\end{aligned}$$

From this we find that the eigenstates are given by

$$|\psi_{n\neq 0,p_x,p_z}\rangle = c\begin{pmatrix} \frac{-\epsilon E_{n,p_z} + v_F p_z}{\alpha\sqrt{n}}|n-1, p_x, p_z\rangle \\ |n, p_x, p_z\rangle \end{pmatrix}, \tag{2.3.6}$$

for $n > 0$, and for $n = 0$

$$|\psi_{n=0,p_x,p_z}\rangle = c\begin{pmatrix} 0 \\ |n=0, p_x, p_z\rangle \end{pmatrix}. \tag{2.3.7}$$

We see that if we simply insert $n = 0$ into our equation for the energy, we find that it is given by $E_{n=0,p_z} = \pm v_F p_z$. However, explicitly calculating the ground state energy using the lowest level eigenstate shows that

$$\begin{aligned}
H|\psi_{n=0,p_x,p_z}\rangle &= -\epsilon\alpha\begin{pmatrix} 0 & a \\ a^\dagger & 0 \end{pmatrix}\begin{pmatrix} 0 \\ |n=0, p_x, p_z\rangle \end{pmatrix} - \epsilon v_F p_z \sigma_z \begin{pmatrix} 0 \\ |n=0, p_x, p_z\rangle \end{pmatrix} \\
&= -\epsilon v_F p_z \begin{pmatrix} 1 & 0 \\ 0 & -1 \end{pmatrix}\begin{pmatrix} 0 \\ |n=0, p_x, p_z\rangle \end{pmatrix} \\
&= \epsilon v_F p_z \begin{pmatrix} 0 \\ |n=0, p_x, p_z\rangle \end{pmatrix} \\
&= \epsilon v_F p_z |\psi_{n=0,p_x,p_z}\rangle.
\end{aligned}$$

So there is in fact no ambiguity in the sign of the ground state energy. Since the sign of the ground state energy depends on the chirality ϵ, we call this state chiral or spin-polarized. We shall call the $\epsilon = 1$ states right-handed (RH) and the $\epsilon = -1$ states left-handed (LH). The higher states currently do not depend on the chirality. Later we shall see that they do also depend on the chirality through effects that will be introduced in the next chapter.

For the non-zero values of n, we know that the harmonic oscillator states form an orthonormal basis, so we can use that to determine the normalization constant c.

We require that $\langle\psi_{n,p_x,p_z}|\psi_{n,p_x,p_z}\rangle = c^2\left(1 + \frac{(-\epsilon E_{n,p_z} + v_F p_z)^2}{\alpha^2 n}\right) = 1$.

Defining the function

$$f(n, p_z) \equiv \frac{v_F^2 p_z^2 + \epsilon v_F p_z\sqrt{\alpha^2 n + v_F^2 p_z^2}}{\alpha^2 n},$$

where we demand that $n > 0$, the normalization constant is found to be equal to

$$c_{n,p_z} = \pm\frac{1}{\sqrt{2}}\left[1 + f(n, \lambda p_z)\right], \tag{2.3.8}$$

where $\lambda = \pm 1$, depending on whether we consider the postive or negative energy solutions, so $\lambda = \mathrm{Sgn}(E_n)$. Another way to describe this is to say that $\lambda = +1$ describes the particle states, while $\lambda = -1$ describes the hole states.

Furthermore, looking at the limit of $p_z \to \pm\infty$, we see that the levels decouple again.

Writing the eigenstates as

$$|\psi_n\rangle = \begin{pmatrix} a_{n,p_z}|n-1,p_x,p_z\rangle \\ b_{n,p_z}|n,p_x,p_z\rangle \end{pmatrix},$$

with the normalization constants a_n and b_n given by

$$a_{n,p_z} = c_{n,p_z}, \qquad b_{n,p_z} = c_{n,p_z}\frac{-\epsilon E_{n,p_z} + v_F p_z}{\alpha\sqrt{n}},$$

we find that if we take $\lambda = 1$, $p_z \to \infty$ gives $a_n = 1$ and $b_n = 0$, while for $p_z \to -\infty$ gives $a_n = 0$ and $b_n = 1$. Changing the sign of λ then also reverses the outcome of the limits. Taking the limit of $p_z \to 0$, we find that $a_n = b_n = \pm 1/\sqrt{2}$.

Note that the Zeeman effect is already accounted for in this calculation, as it is included in the Dirac equation from which the used Hamiltonian is derived. This also means that the the energy spectrum is again doubly degenerate in spin. To explicitly show this level degeneracy, instead of considering just the Hamiltonian, we can consider the square of the Hamiltonian, which has the eigenvalues E^2. Using the commutation relation between Π_x and Π_y, we can write this operator as

$$H^2 = \begin{pmatrix} \mathbf{\Pi}^2 - e\hbar B & 0 \\ 0 & \mathbf{\Pi}^2 + e\hbar B \end{pmatrix} = \mathbf{\Pi}^2\mathbb{I}_2 - e\hbar B\sigma_z.$$

This gives us the eigenvalues

$$E^2 = p_z^2 + 2e\hbar B\left(n + \frac{1}{2}\right) - \sigma e\hbar B = p_z^2 + 2e\hbar B l.$$

We now explicitly see again that the ground state is non-degenerate, while all other levels are doubly degenerate.

However, we must note that the square of the Hamiltonian is equal for both the RH and LH cases, since they only differ a minus sign in their original Hamiltonian. Also, we expect two values of E for each cone, while we now find two values for E^2. This yields four values after taking the square root, which gives us the particle and hole states for both chiralities. The chiral lowest Landau levels are an exception to this argument of course.

So we conclude that taking the square of the Hamiltonian gives us the eigenvalues for both the RH and LH system, and that the degeneracy stems from the combination of both Weyl cones, rather than a single cone. This is because the two Weyl cones are implicitly assumed to be located at the same position in momentum space. In the next chapter we shall see that the degeneracy is broken when we include the effects of the anomalous magnetic moment, since it couples to the two chiralities in a different way.

We also want to note the symmetries currently present in the system. We have two cones, one for each chirality. We have absorbed a term that provides separation in reciprocal space into the momentum terms, meaning that the two Weyl points are still located at the same point in reciprocal space. This then implies that both inversion (I) and time reversal (TR) symmetries are intact. In order to have a stable Weyl semimetal, we need to break either of those two symmetries, which will be done in the next chapter. There is also a third symmetry in play here: particle-hole symmetry. This symmetry gives us a relation between the two cones of opposite chirality and is given by $E_n(k_z, \epsilon = 1) = E_n(-k_z, \epsilon = -1)$. This symmetry will be unaffected by either the anomalous magnetic moment or breaking TR symmetry by moving the Weyl nodes apart in reciprocal space. Breaking I symmetry by moving the nodes in energy space will turn out to break particle-hole symmetry in this form.

2.4 Conclusion

In this chapter we have shown the effect of the magnetic field on the energy levels of a Weyl semimetal. The energy levels for both a non-relativistic and relativistic system have been computed and the Landau levels have been explicitly constructed through Landau quantization. We have also shown that this leads to chiral ground states, in which the sign of the (linear) dispersion relation of the lowest Landau level is dependent on the chirality of the cone. Finally we have shown that all states, except for the chiral ground states, are doubly degenerate.

With this relatively simple case thoroughly analyzed, we have now built the foundation upon which the rest of the work will continue to build in the chapters to come. In the next chapter we will consider the effect of a vertex correction to the action on the Landau levels. Furthermore, we explicitly break the symmetries currently present in the system by shifting the cones in energy-momentum space.

Chapter 3

Anomalous Effects

In this chapter we will look at the effect of the anomalous magnetic moment, which stems from quantum electrodynamics (QED), on the energy levels in bulk. In section 3.1 we calculate this effect for both the relativistic and non-relativistic case, and we look for the tensorial structure of this correction term.

Up until now, we also tacitly assumed that the two Weyl nodes of the cones are at the same point in momentum space. This, however, is not true in physical situation. Having the two nodes at the same position can lead to the annihilation of the two Weyl nodes, thereby gapping out the system. In section 3.2 we investigate the effect of this separation in momentum space on the energy levels, which turns out to be non-trivial, giving rise to some interesting effects, such as a non-linear ground state dispersion.

3.1 Anomalous magnetic moment

In the previous calculations we assumed that the g factor for electrons, which shows up as a multiplicative factor in the magnetic moment, is exactly equal to 2. However, this is the case only in the absence of interactions. So to account for interactions, we want to allow the factor to have values different from its non-interacting value. To account for that, we shall denote the factor as $g = 2 + g'$, where g' is the difference from 2 and is called the anomalous magnetic moment.

A quick note on units in this chapter to avoid confusion: k_i will denote wavenumbers, while p_i will label momenta, with their relation being $p_i = \hbar k_i$.

3.1.1 Non-Relativistic case

We start by adding the anomalous magnetic moment to the non-relativistic energies. Putting back the general factor g into Eq. 2.2.9, we see that the energies are given by

$$E_{n,p_z,\sigma} = \frac{p_z^2}{2m_B} + 2\mu_B\left(n + \frac{1}{2}\right)B - \frac{g}{2}\mu_B B\sigma. \tag{3.1.1}$$

Using that $g = 2 + g'$, we write this as

$$E_{n,p_z,\sigma} = \frac{p_z^2}{2m_B} + 2\mu_B\left[n + \frac{1}{2} - \frac{\sigma}{2}\left(1 + \frac{g'}{2}\right)\right]B \equiv \frac{p_z^2}{2m_B} + 2\mu_B l' B. \tag{3.1.2}$$

Now the values that l' can take are no longer integers. If we look at the lowest Landau level, given by $n = 0$, $\sigma = 1$, we see that $l' = -g'/4$. For all the other values, we find that $l' = k \pm g'/4$, where k is an integer. With this anomalous magnetic moment, the spin degeneracy that is present in all excited states has is lifted. All values for n and σ

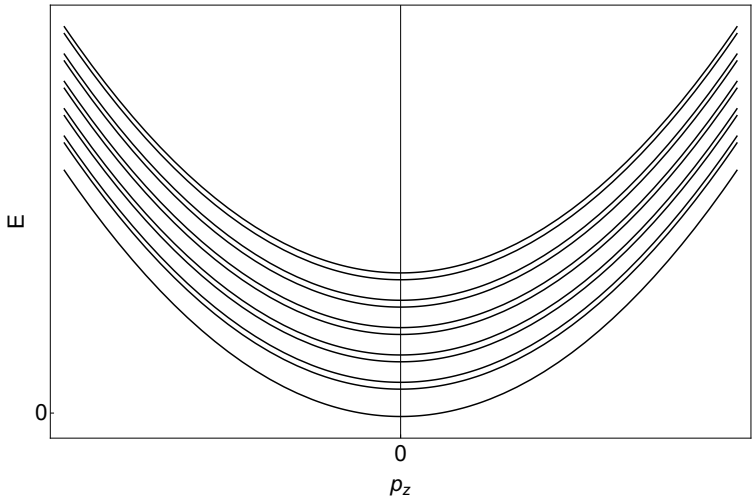

Figure 3.1 – Non-relativistic energy levels as a function of the momentum along the direction of the magnetic field with an anomalous magnetic moment term. The values $m_B = \mu_B = B = 1$ and $g' = 1/2$ were used here.

now give unique values for l'. The energy levels when also accounting for the anomalous magnetic moment are given in Fig. 3.1. Clearly, all previously degenerate levels have now split up.

3.1.2 Relativistic case

In the Hamiltonian for the relativistic case, given in Eq. 2.3.2, the non-anomalous Zeeman effect has already been accounted for. At this point it becomes imperative to differentiate between the massive and massless case. We work with Weyl fermions, but to illustrate the subtle differences that arise when treating massive fermions instead of massless ones, the massive case will be shown as well.

Massive particles

To start with the massive case, it can be found, through calculating the vertex correction, that we have the term $g'\mu_B\sigma_{\mu\nu}F^{\mu\nu}$ to the Dirac equation, where $F^{\mu\nu}$ is the electromagnetic field tensor given by $F^{\mu\nu} = \partial^\mu A^\nu - \partial^\nu A^\mu$, and $\sigma_{\mu\nu} = \frac{\imath}{2}[\gamma_\mu, \gamma_\nu]$ [26]. Calculating this contraction, using that only the components $F^{21} = -B = -F^{12}$ are non-zero in the field tensor due to only considering a magnetic field in the z-direction, we find that the equations of motion are given by

$$(\gamma^\mu\partial_\mu - m + g'\mu_B B\Sigma_3)\psi = 0,$$

where $\Sigma_3 = \imath\gamma^1\gamma^2 = \sigma_z \otimes \mathbb{I}_2$.

Transforming the gradient back to momentum space, we find that we can write this equation in its matrix form, which is given by

$$\begin{pmatrix} g'\mu_B B\sigma_3 - m\mathbb{I}_2 & \imath\hbar\partial_t - \boldsymbol{\sigma}\cdot\mathbf{p} \\ \imath\hbar\partial_t + \boldsymbol{\sigma}\cdot\mathbf{p} & g'\mu_B B\sigma_3 - m\mathbb{I}_2 \end{pmatrix}\psi = 0.$$

So in the massive case, we see that the term that is added through the vertex correction couples like a mass term, which then will couple the right and left chiral states.

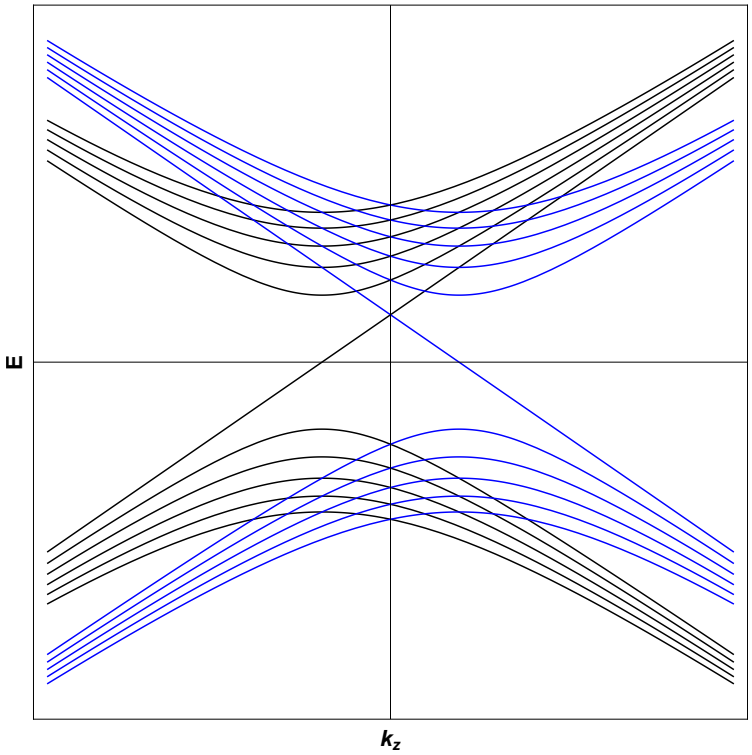

Figure 3.2 – Relativistic energy levels as a function of the momentum along the direction of the magnetic field with an anomalous Zeeman term. Black: RH fermions. Blue: LH fermions. The values $v_F = l_B = B = \mu_B = g' = 1$ were used here.

Massless particles

Since we work in the massless case, we expect that the right-handed (RH) and left-handed (LH) states remain uncoupled and that the anomalous magnetic moment will couple like a Zeeman term instead of a mass-like term. So instead of a term proportional to $\sigma_{\mu\nu}F^{\mu\nu}$, we need to consider a term proportional to $\sigma^\mu p^\nu \left(F_{\mu\nu} - *F_{\mu\nu}\right)$, where $*F_{\mu\nu}$ is the Hodge dual of the EM tensor, defined as $*F^{\mu\nu} = \epsilon^{\mu\nu\rho\lambda}F_{\rho\lambda}/2$, where $\epsilon^{\mu\nu\rho\lambda}$ is the totally anti-symmetric Levi-Civita tensor [27]. The convention for the Levi-Civita tensor used here is $\epsilon^{0123} = 1$. Assuming absence of electric fields, this leads to both a Zeeman like term, proportional to $\mathbf{B}\cdot\boldsymbol{\sigma}$ and a Rashba spin-orbit like term, proportional to $\mathbf{B}\cdot(\boldsymbol{\sigma}\times\mathbf{p})$.

Adding the Zeeman like term to the Hamiltonian, we find that the Hamiltonian for the right chiral Weyl cone is given by

$$H = -\frac{\sqrt{2}\hbar v_F}{l_B}\begin{pmatrix} 0 & a \\ a^\dagger & 0 \end{pmatrix} - (v_F p_z + g'\mu_B B)\sigma_z. \tag{3.1.3}$$

From this it is clear how to incorporate this into to the already calculated energies $E(n, p_z)$: it is simply a shift of the vertical momentum $p_z \to p_z' = p_z + g'\mu_B B/v_F$.

Next we note that this shift is for a RH fermion. If we consider a LH fermion, going through the calculations will reveal that the shift is instead given by $p_z \to p_z' = p_z - g'\mu_B B/v_F$. This change of sign is then also what breaks the degeneracy at the relativistic level: instead of both RH and LH giving the same value for the energies, with exception of the lowest Landau level, the excited state energies are now shifted in momentum space. The form of these shifted energies are plotted in Fig. 3.2.

The above can be made more precise. For this, the form of the vertex correction has already been calculated, so we want to check that it is consistent with the statements made above. Specifically, we consider the transverse part of the vertex correction for

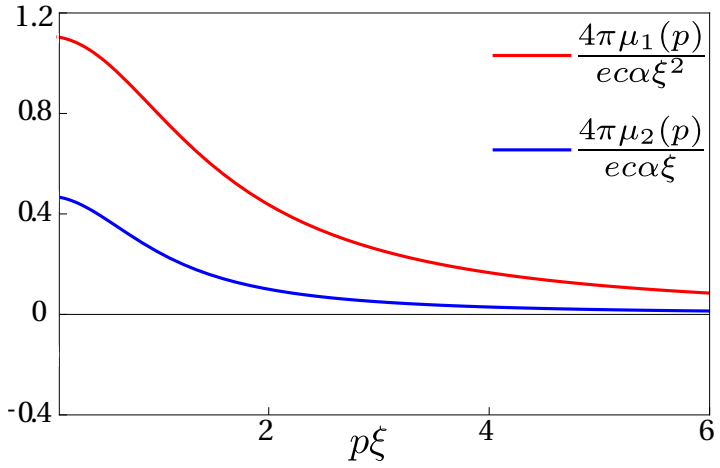

Figure 3.3 – Dimensionless magnetic moments as a function of momentum. Values for $k_F\xi = 1/4$. Figure adapted from Ref. [28].

massless fermions. The correction to the action, which has been calculated in Ref. [28], is given by

$$-ev_F A_\mu \Gamma^\mu_{\text{transv.}}(\mathbf{k}) = -[\boldsymbol{\mu}_1(\mathbf{k}) \times \boldsymbol{\sigma}] \cdot \frac{\mathbf{E}}{v_F} - [\boldsymbol{\mu}_2(k) - \epsilon\boldsymbol{\mu}_1(\mathbf{k})] \cdot \mathbf{B}, \tag{3.1.4}$$

where $\boldsymbol{\mu}_1(\mathbf{k}) \equiv \mu_1(k)\mathbf{k}$, $\boldsymbol{\mu}_2(k) \equiv \mu_2(k)\boldsymbol{\sigma}$ and $\epsilon = \pm 1$ the chirality. Looking at Fig. 3.3, we see that the μ_i depend on the momenta, but are finite in the long wavelength limit. Since we work in the low-energy limit in this thesis, we will consider them to be constants, which we take to be the long wavelength limits. So we define $\mu_i \equiv \mu_i(0)$.

The first term on the right-hand side of the equation gives a Rashba-like spin-orbit coupling term. Looking at the other two terms, we see a term proportional to $\boldsymbol{\sigma} \cdot \mathbf{B}$, which has the form of a Zeeman shift, and a term proportial to $\mathbf{k} \cdot \mathbf{B}$, which will turn out to be a tilt term. If we consider the absence of electric fields, we can discard the Rashba term. We want to investigate the tensorial structure of the first order correction term given by $(\mu_2\boldsymbol{\sigma} - \mu_1\mathbf{k}) \cdot \mathbf{B}$. To write this in its tensorial form, we shall consider the Hodge dual of the EM tensor. In the absence of electric fields, it is given by

$$*F_{\mu\nu} = \frac{1}{2}\epsilon_{\mu\nu\rho\lambda}F^{\rho\lambda} = \begin{pmatrix} 0 & B_x & B_y & B_z \\ -B_x & 0 & 0 & 0 \\ -B_y & 0 & 0 & 0 \\ -B_z & 0 & 0 & 0 \end{pmatrix}.$$

So we see that $B_i = *F_{0i}$. This means that we can write $\boldsymbol{\sigma} \cdot \mathbf{B} = \sigma^i * F_{0i}$. Since $*F_{00} = 0$, we can easily extend it to read $\boldsymbol{\sigma} \cdot \mathbf{B} = \sigma^\nu * F_{0\nu}$, where $\sigma^0 = \mathbb{I}_2$. Similarly, we can write the $-\mathbf{k} \cdot \mathbf{B}$ term as $k^\mu * F_{\mu 0}$. Now we see that since $*F_{ij} = 0$, that with a proper choice of σ^0 and k^0 we can write the required term as $k^\mu\sigma^\nu * F_{\mu\nu}$. In order to not need a redefintion of the Pauli matrices, we shall take the μ_1 outside of the brackets. If we then define $k^0 = \mu_2/\mu_1$, we see that we can then write this as

$$\mu_1 \left(\frac{\mu_2}{\mu_1}\boldsymbol{\sigma} - \mathbf{k}\right) \cdot \mathbf{B} = \mu_1 k^\mu \sigma^\nu * F_{\mu\nu}. \tag{3.1.5}$$

However, the above equation is valid for a single Weyl cone only, since we considered only one of the two possible chiralities of the fermions. So we want to generalize it to include both the cones. The other possible term is given by $(\mu_2\boldsymbol{\sigma} + \mu_1\mathbf{k}) \cdot \mathbf{B}$. Since we do not want to break the chiral symmetry, the full tensor form should give us a block diagonal matrix, which can be written as

$$M = \begin{pmatrix} (\mu_2\boldsymbol{\sigma} - \mu_1\mathbf{k})\cdot\mathbf{B} & 0 \\ 0 & (\mu_2\boldsymbol{\sigma} + \mu_1\mathbf{k})\cdot\mathbf{B} \end{pmatrix}.$$

Thus we see that the $\boldsymbol{\sigma}\cdot\mathbf{B}$ term keeps the same sign, while the $\mathbf{k}\cdot\mathbf{B}$ term changes its sign. This 4×4 matrix can be constructed by using the Dirac gamma matrices instead of just the Pauli matrices. In our basis we have

$$\gamma^5\gamma^0\gamma^0 = \gamma^5 = \begin{pmatrix} -\mathbb{I}_2 & 0 \\ 0 & \mathbb{I}_2 \end{pmatrix}, \qquad \gamma^5\gamma^0\gamma^i = \begin{pmatrix} \sigma_i & 0 \\ 0 & \sigma_i \end{pmatrix}.$$

From this we see that if we substitute $\sigma^\mu \to \gamma^5\gamma^0\gamma^\mu$, that we get the desired result. However, if we use the same convention for k^0, we see that we end up with the chiralities reversed. To counter this, we reverse the sign of k^0. This then gives us the correct order of chiralities, but also an overall minus sign, which is easily dealt with, for instance by swapping the indices of the dual EM tensor, since it is anti-symmetric. Finally we can write the transversal part of the vertex correction as

$$(\mu_2\boldsymbol{\sigma} - \epsilon\mu_1\mathbf{k})\cdot\mathbf{B} \to \mu_1\gamma^0\gamma^5 k^\mu\gamma^\nu * F_{\nu\mu}, \tag{3.1.6}$$

where $k^\mu = \left(-\frac{\mu_2}{\mu_1}, \mathbf{k}\right)$.

The left-hand side of this equation is clearly time-reversal invariant, since under time-reversal we find that $\mathbf{B} \to -\mathbf{B}$, $\mathbf{k} \to -\mathbf{k}$ and $\boldsymbol{\sigma} \to -\boldsymbol{\sigma}$. Of course the right-hand side is then also invariant, but we want to make this explicit by looking at how the terms transform. Since the components of $*F_{\mu\nu}$ are the components of the magnetic field, we see that $*F_{\mu\nu} \to -*F_{\mu\nu}$. Because under time-reversal $\sigma^i \to -\sigma^i$, we also see that $\gamma^i \to -\gamma^i$. We also already found that $k^i \to -k^i$. However, time-reversal transforms $k^0 \to k^0$ and $\gamma^0 \to \gamma^0$. Because either we have a term $k^i\gamma^0$ or $k^0\gamma^i$, we see that the combination $k^\mu\gamma^\nu * F_{\nu\mu}$ is invariant under this transformation.

Finally we need to check that $\gamma^0\gamma^5$ is invariant. We see that we can write this as $\imath\gamma^1\gamma^2\gamma^3$. All three gamma matrices get a minus sign, but because we also need to consider the conjugation, we find that the imaginary unit also gets a minus sign, which then leaves the whole operator invariant, so $\gamma^0\gamma^5 \to \gamma^0\gamma^5$. From this we conclude that $\gamma^0\gamma^5 k^\mu\gamma^\nu * F_{\nu\mu} \to \gamma^0\gamma^5 k^\mu\gamma^\nu * F_{\nu\mu}$, meaning that the right-hand side of the equation indeed is invariant under time-reversal, as it of course should be.

3.1.3 Effect on energy levels

Again taking $\mathbf{E} = 0$ and $\mathbf{B} = B\hat{z}$, we can now determine what the effect of the anomalous magnetic moment is on the energy spectrum that we have calculated before. The Hamiltonian is given by the sum of the non-interacting Hamiltonian H_0 and the Hamiltonian corresponding to the correction H_1. Taking into account both Weyl cones, we can write it as

$$H = H_0 + H_1 = \epsilon\left[-\frac{\sqrt{2}\hbar v_F}{l_B}\begin{pmatrix} 0 & a \\ a^\dagger & 0 \end{pmatrix} - (v_F\hbar k_z + \epsilon\mu_2 B)\sigma_z + \mu_1 B k_z \mathbb{I}_2\right]. \tag{3.1.7}$$

By using what we already know of the eigenstates of H_0, we see that the μ_2 term simply gives a shift in the vertical momentum in the energy that we have already calculated, while the μ_1 term simply adds a term linear in p_z to the energy. Taking into account the effect of the ϵ, we find that the energy levels in this case are given by

$$E_{n,p_z,\epsilon} = \pm v_F\sqrt{\left(\hbar k_z + \epsilon\frac{\mu_2}{v_F}B\right)^2 + \frac{2\hbar^2}{l_B^2}n} + \epsilon\mu_1 B k_z. \tag{3.1.8}$$

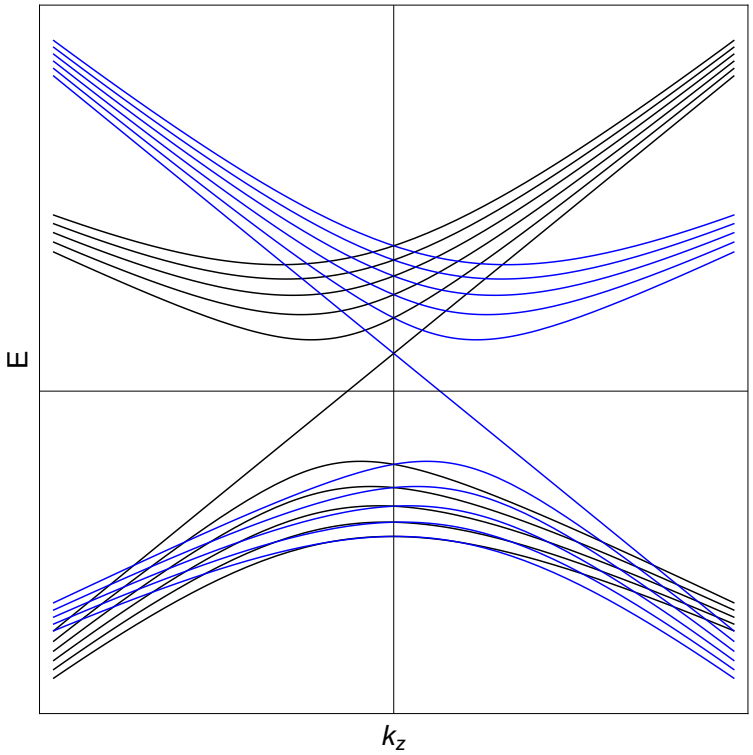

Figure 3.4 – Relativistic energy levels as a function of the momentum along the direction of the magnetic field with the anomalous magnetic moment terms. Black: RH fermions. Blue: LH fermions. The values $\hbar = v_F = B = 1$, $\mu_1 = 0.25$ and $\mu_2 = 0.85$ were used.

Doing the calculation explicitly, in a similar fashion as was done earlier in this chapter,we find the exact same result. The energy levels as function of k_z and μ_1 are plotted in Fig. 3.4. From the image one can see that not only does this separate the two Weyl cones in momentum space, but it also tilts them, justifying our name for the $\mathbf{k} \cdot \mathbf{B}$ term.

Finally we could consider the electric field. The reason that we have not included it in our calculation of the energy levels is that there are no stable states. When considering a magnetic field, the cyclotron orbits form the eigenstates. However, an electric field does not induce similar orbits. Instead, we effectively have a linear potential that will simply accelerate the electrons in a linear fashion. This would then induce a current, but not stable states of single electrons. While currents and conductivity are certainly interesting in these materials, we will not consider them in this thesis.

3.2 Separation of the Weyl nodes

In the previous calculations, we have assumed that there was no separation between the two Weyl nodes. However, the nodes could very well be separated both in energy and momentum. In fact, they should be separated in at least one of the two to ensure that the Weyl points do not annihilate each other. This separation is denoted by the four-vector b^μ, where the temporal component is the separation in energy space, while the spatial components give the separation in the momenta. A non-zero b_0 breaks inversion symmetry, while a non-zero b_i breaks time-reversal symmetry. For this reason we call this the symmetry breaking vector.

In the calculations above, we have simply absorbed the separation in the momentum term, by defining $\mathbf{p} \equiv \hbar(\mathbf{k} - \epsilon\mathbf{b})$. We can now also do the calculations by re-inserting the explicit dependence on initial separation. For the most part this is an easy task, since the p_0 and p_z appear explicitly in the calculations. Thus they are easily shifted,

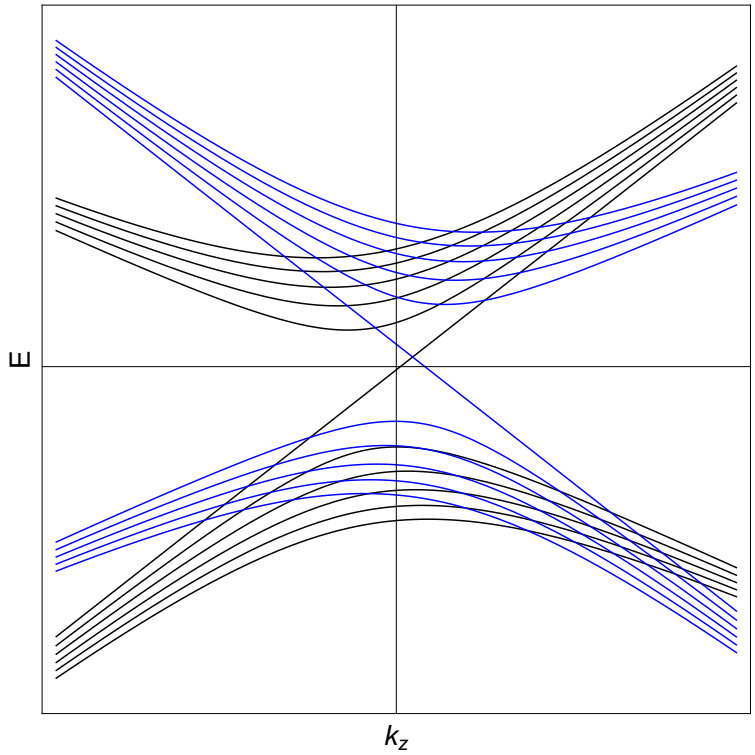

Figure 3.5 – Relativistic energy levels as a function of the momentum along the direction of the magnetic field with the anomalous magnetic moment terms and non-zero values for b_0 and b_z. Black: RH fermions. Blue: LH fermions. The values $\hbar = v_F = B = 1$, $\mu_1 = 0.25$, $\mu_2 = 0.85$, $b_0 = 0.3$ and $b_z = 0.5$ were used.

obtaining the desired result. However, since we have used the p_x and p_y terms to form the ladder operators, we need to take a closer look at how the b_x and b_y terms affect these operators. Reinserting this shift into Eq. 2.3.2, we find

$$H = -\epsilon v_F \left(\mathbf{\Pi} - \epsilon\hbar\mathbf{b}\right)\cdot\boldsymbol{\sigma} = -\epsilon v_F \mathbf{\Pi}\cdot\boldsymbol{\sigma} + \hbar v_F \mathbf{b}\cdot\boldsymbol{\sigma}. \tag{3.2.1}$$

So we find the original Hamiltonian, which we have studied already, plus the effect of the symmetry breaking vector, which has a form reminiscent of a Zeeman effect. It is good to note that this vector is not an operator, but simply a vector containing real numbers.

For the b_0 and b_z terms, we see that they shift the origin of the energy and vertical momentum in a chirality dependent way. So from this, we expect that in the energy versus vertical momentum plots b_0 will shift the energy levels up or down, while the b_z term will shift them to the right or left. Note that b_0 will make an energy difference between the two Weyl points. This, however, is not the same as introducing an axial chemical potential, which would effectively shift the Fermi level up or down for the two cones, while potentially leaving the Weyl points at the same level in energy space.

Using this, we find that the energy levels are given by

$$E_{n,k_z,\epsilon} = \pm\hbar v_F \sqrt{\left(k_z - \epsilon b_z + \epsilon\frac{\mu_2}{\hbar v_F}B\right)^2 + \frac{2}{l_B^2}n} + \epsilon\mu_1 B(k_z - \epsilon b_z) - \epsilon b_0. \tag{3.2.2}$$

Using this expression, we plot the energy levels as a function of p_z in Fig. 3.5.

Next we explore the effects of having a time-reversal symmetry breaking vector with components perpendicular to the magnetic field. It is fairly easy to see that, since the b^μ commute with both position and momentum operators, there is no change in the commutator $[\Pi_x, \Pi_y]$. This then means that we can define the same ladder operators,

but with k_i instead of p_i. The z part of this vector, as argued above, can very easily be incorporated in the energy levels of the system. So the part that is truly new here and needs to be investigated is

$$H_1 = \hbar v_f \mathbf{b}\cdot\boldsymbol{\sigma} = \hbar v_F \begin{pmatrix} 0 & b_x - \imath b_y \\ b_x + \imath b_y & 0 \end{pmatrix}.$$

To do this, we look at the Hamiltonian in the basis of the eigenvectors we found earlier, given by

$$|\psi_i\rangle = \begin{pmatrix} c_{i,1}|i-1, p_x, p_z\rangle \\ c_{i,2}|i, p_x, p_z\rangle \end{pmatrix}, \tag{3.2.3}$$

where $|i\rangle$ are again the harmonic oscillator states. Note that the normalization constants, previously called a_n and b_n, are not the same as computed earlier, due to having introduced more terms to the Hamiltonian. The precise normalization will be determined later, but this form will suffice to illustrate the effect.

Assume for the moment that $i > 0$. We already know that this basis diagonalizes the part of the Hamiltonian excluding H_1, with known eigenvalues. We can now check whether this also is the case for H_1:

$$\begin{aligned}
M_{ij} &= \langle i|H_1|j\rangle \\
&= \hbar v_F \begin{pmatrix} c_{i,1}\langle i-1|, & c_{i,2}\langle i|\end{pmatrix} \begin{pmatrix} 0 & b_x - \imath b_y \\ b_x + \imath b_y & 0 \end{pmatrix} \begin{pmatrix} c_{j,1}|j-1\rangle \\ c_{j,2}|j\rangle \end{pmatrix} \\
&= \hbar v_f \begin{pmatrix} c_{i,2}(b_x + \imath b_y)\langle i|, & c_{i,1}(b_x - \imath b_y)\langle i-1|\end{pmatrix} \begin{pmatrix} |j-1\rangle \\ |j\rangle \end{pmatrix} \\
&= c_{j,1}c_{i,2}\hbar v_f(b_x + \imath b_y)\langle i|j-1\rangle + c_{i,1}c_{j,2}\hbar v_F(b_x - \imath b_y)\langle i-1|j\rangle \\
&= c_{j,1}c_{i,2}\hbar v_f(b_x + \imath b_y)\delta_{i,j-1} + c_{i,1}c_{j,2}\hbar v_F(b_x - \imath b_y)\delta_{i-1,j} \\
&= c_{j,1}c_{i,2}\hbar v_f(b_x + \imath b_y)\delta_{i,j-1} + c_{i,1}c_{j,2}\hbar v_F(b_x - \imath b_y)\delta_{i,j+1}.
\end{aligned}$$

From this we find that the matrix elements in this basis are given by

$$M_{ij} = \begin{cases} c_{i,1}c_{j,2}\hbar v_F(b_x - \imath b_y) & i = j-1 \\ c_{i,2}c_{j,1}\hbar v_F(b_x + \imath b_y) & i = j+1 \\ 0 & \text{otherwise} \end{cases} \tag{3.2.4}$$

From this we immediately see that this part of the Hamiltonian is not diagonal in this basis, but actually provides off-diagonal terms. Hence in this basis the full Hamiltonian is no longer diagonal, but rather tri-diagonal.

In order to now find the energy levels with this effect incorporated, we want to diagonalize this infinite dimensional tri-diagonal matrix. To calculate this, the normalization factors of the eigenstates come into play. On the diagonals, the normalization factors don't matter:

$$\langle\psi_i|H|\psi_i\rangle = E_i\langle\psi_i|\psi_i\rangle = E_i.$$

On the off-diagonal elements though, the factors do play a role, so we need to know their exact form before we can perform any meaningful calculation. For this we have to revisit the calculation of the eigenstates that we did before. However, we cannot simply use the already found result due to the addition of terms, changing our eigenstates. So a recalculation is in order, but the same steps of calculation can still be used.

We know that the basis of harmonic oscillator states that were found diagonalizes a part of the Hamiltonian, wich we shall call H_0, with eigenvalues given by Eq. 3.2.2:

$$\epsilon\begin{pmatrix} -\hbar v_F k_z - \epsilon\mu_2 B + \mu_1 k_z B - b_0 & -\alpha a \\ -\alpha a^\dagger & \hbar v_F k_z + \epsilon\mu_2 B + \mu_1 k_z B - b_0 \end{pmatrix}\begin{pmatrix}\psi^+\\ \psi^-\end{pmatrix} = E\begin{pmatrix}\psi^+\\ \psi^-\end{pmatrix}. \quad (3.2.5)$$

Note that the substitution $k_z \to k_z - \epsilon b_z$ will be made later for convenience of notation. Rewriting this, we find

$$\psi^+ = -\frac{\alpha a}{\epsilon E + b_0 + (\hbar v_f k_z + \epsilon\mu_2 B - \mu_1 k_z B)}\psi^-.$$

This can then be used to explicitly find the energy levels that were found through reasoning above. However, that will not add anything of value to this section, so instead we shall use this result to find the normalization factor of the eigenstates.

We know that $\psi^- = c|n\rangle$, with c the constant of proportionality that we want to determine. So from this we then immediately see that

$$\psi^+ = -\frac{\alpha c\sqrt{n}}{\epsilon E + b_0 + (\hbar v_f k_z + \epsilon\mu_2 B - \mu_1 k_z B)}|n-1\rangle.$$

Normalization then demands that

$$c^2\left(1 + \frac{\alpha^2 n}{[\epsilon E + b_0 + (\hbar v_f k_z + \epsilon\mu_2 B - \mu_1 k_z B)]^2}\right) = 1.$$

We now also see that the b_0 term here cancels the term in the expression for the energy, since $\epsilon E + b_0 = \epsilon(E + \epsilon b_0)$, and there is a term $-\epsilon b_0$ in the energy. So we can get rid of the b_0 term in this calculation, and keep in mind that we then use a modified energy, which we shall denote by E'. The solution to this, though fairly complicated in structure, is easily found through elementary algebra:

$$c = \pm\frac{|(\mu_1 B - \hbar v_F)k_z - \epsilon(\mu_2 B + E')|}{\sqrt{\left[(\mu_1 B - \hbar v_F)k_z - \epsilon(\mu_2 B + E')\right]^2 + \alpha^2 n}}. \quad (3.2.6)$$

In order to compactly write the resulting eigenstates, especially after substituting $k_z \to k_z - \epsilon b_z$, we introduce some definitions:

$$\delta_n \equiv (\mu_1 B - \hbar v_F)(k_z - \epsilon b_z) - \epsilon(\mu_2 B + E'_n),$$
$$\gamma_n \equiv \sqrt{\delta_n^2 + \alpha^2 n}.$$

Note that the delta still depends on the level through the energy, where we have now explicitly denoted its level dependence with n. This allows us to write the normalization as $c_n = \pm|\delta_n|/\gamma_n$. Since $|\delta_n|/\delta_n = \mathrm{Sgn}(\delta_n) = \pm 1$, the eigenstates can be written as

$$|\psi_n\rangle = \pm\frac{1}{\gamma_n}\begin{pmatrix}\mathrm{Sgn}(\delta_n)\alpha\sqrt{n}|n-1\rangle \\ |\delta_n||n\rangle\end{pmatrix}, \quad (3.2.7)$$

where we need to keep in mind that α depends on B. Using these normalization factors, it is also immediately obvious that for $n = 0$ we have the ground state $|\psi_0\rangle = (0, \pm|0\rangle)^T$, since $|\delta_0|/\gamma_0 = 1$. Using the results found in Eq. 3.2.4, we can now write down the Hamiltonian in this basis:

$$H_{ij} = \frac{\alpha\sqrt{j}\,\mathrm{Sgn}(\delta_j)|\delta_i|}{\gamma_i\gamma_j}\hbar v_F(b_x + \imath b_y)\delta_{i,j-1} + E_i\delta_{i,j} + \frac{\alpha\sqrt{i}\,\mathrm{Sgn}(\delta_i)|\delta_j|}{\gamma_i\gamma_j}\hbar v_F(b_x - \imath b_y)\delta_{i,j+1}. \quad (3.2.8)$$

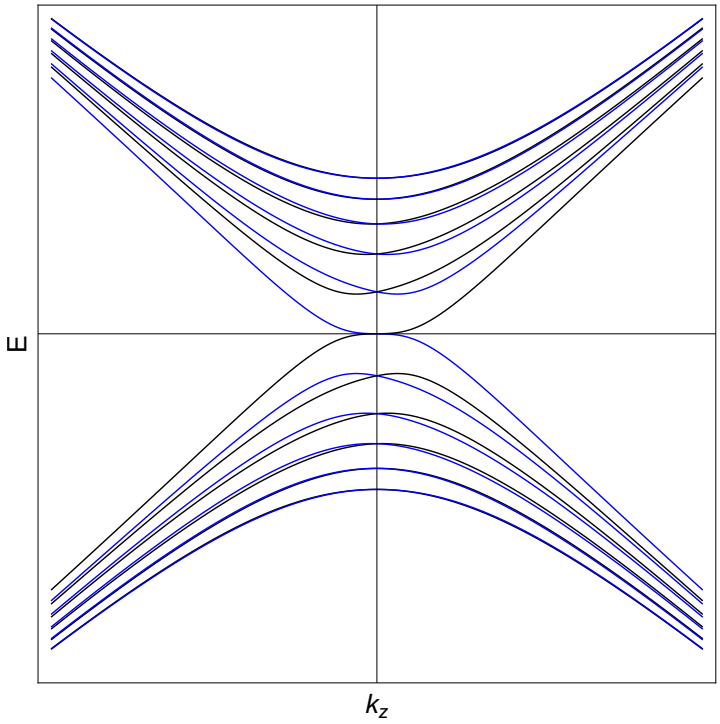

Figure 3.6 – Numerically computed energy levels of the Hamiltonian from Eq. 3.2.10 as a function of the momentum along the direction of the magnetic field with $\bar{b}_x = 2.3$, without anomalous magnetic moment. Black: right chiral states. Blue: left chiral states.

Although it is not diagonal, it is easy to check that this matrix is still Hermitian, as is expected of a Hamiltonian. This also ensures that our eigenvalues are real valued.

With the exact form of the Hamiltonian known, we can now attempt to diagonalize it by finding its eigenvalues. However, this procedure will be a numerical one, and since the matrix is in principle infinite dimension, we will need to introduce a cut-off in the amount of terms that we consider. Later on some analytical results are derived using perturbation theory, but those results are only valid in a regime where the $b_{x,y}$ are fairly small. So numerical results are necessary in order to compute the energy spectrum for higher values of those components. Since the energy levels do not explicitly depend on either k_x or k_y, we expect that the seperations in either of these directions are equivalent, and that only the absolute separation in this plane is what affects the energies.

3.2.1 Numerical procedure & results

For the diagonalization procedure, we do not want to construct two different matrices, depending on whether we consider positive or negative states, but rather a single matrix. Doing the former would lead to shifting the ground state in two different ways, effectively splitting it up, which is incorrect. Instead we construct a matrix of the form

$$H_{ij} = \begin{pmatrix} \ddots & \vdots & \vdots & \vdots & \iddots \\ \cdots & E_1 & b & 0 & \cdots \\ \cdots & b^* & E_0 & a & \cdots \\ \cdots & 0 & a^* & E_{-1} & \cdots \\ \iddots & \vdots & \vdots & \vdots & \ddots \end{pmatrix},$$

where the E_{-i} represent the negative energy states. The stars on the off-diagonal entries denote complex conjugation, as we consider a Hermitian matrix. In order to be able to perform numerical computation, the relevant variables are scaled dimensionless. Di-

mensionless variables will be denoted with with a bar. The parameters are scaled in the following way: k_z and b_z are scaled with $1/l_B^1$, μ_1 is scaled with $ev_F l_B^2$, μ_2 is scaled with $ev_F l_B$ and finally E and b_0 are scaled with $\hbar v_F/l_B$. With this scaling, the energy levels are given by

$$\bar{E}_n = \pm\sqrt{(\bar{k}_z - \epsilon\bar{b}_z + \epsilon\bar{\mu}_2)^2 + 2n} + \epsilon\bar{\mu}_1(\bar{k}_z - \epsilon\bar{b}_z) - \epsilon\bar{b}_0. \tag{3.2.9}$$

However, we must also then rescale the other entries of the matrix. This is done by introducing the same scaled variables as before. The normalization factor, in its scaled version, is now given by

$$c_n = \pm\frac{|\bar{\delta}_n|}{\bar{\gamma}_n},$$

where now

$$\begin{aligned}\bar{\delta}_n &= (\bar{\mu}_1 - 1)(\bar{k}_z - \epsilon\bar{b}_z) - \epsilon(\bar{\mu}_2 + \bar{E}'_n)\\ \bar{\gamma}_n &= \sqrt{\bar{\delta}_n^2 + 2n}.\end{aligned}$$

The scaled matrix that we use for numerical computations is then given by

$$\bar{H}_{ij} = \frac{\sqrt{2j}\mathrm{Sgn}(\bar{\delta}_j)|\bar{\delta}_i|}{\bar{\gamma}_i\bar{\gamma}_j}(\bar{b}_x + \imath\bar{b}_y)\delta_{i,j-1} + \bar{E}_i\delta_{i,j} + \frac{\sqrt{2i}\mathrm{Sgn}(\bar{\delta}_i)|\bar{\delta}_j|}{\bar{\gamma}_i\bar{\gamma}_j}(\bar{b}_x - \imath\bar{b}_y)\delta_{i,j+1}. \tag{3.2.10}$$

An interesting footnote to this scaling is that the only dependence on the magnetic field now resides in the anomalous magnetic moment terms. Additionally, note that the magnetic length scales with $B^{-1/2}$, so it diverges for $B \to 0$. This then implies that the scaling term will also diverge in this limit. However, since we are only interested in the situation where there is a non-zero magnetic field, and the behaviour without a magnetic field is known, we simply accept that this is the case. If we wanted to take the zero field limit, we would have to carefully look at how all the different terms scale. Of course it is still possible, because the physical system has not changed, but one has to be a little more careful.

We perform this numerical diagonalization on the above matrix, with a cut-off in the dimension of the matrix. Additionally, we set all other terms to zero, so we do not consider the anomalous magnetic moment terms or separation in any other direction here. The energy levels under influence of a non-zero $\bar{b}_x$ is plotted in Fig. 3.6. From this figure it is clear that a non-zero $\bar{b}_x$ affects the lower energetic states more strongly, with the most obvious diference being the curvature of the lowest Landau level, which was not present before. This behaviour is interesting, because the lowest level normally has a linear dispersion, while now it seems to become non-linear instead. The difference between the two chiralities is also stronger in the lower states than in the higher ones.

To see what the effect is of this b_x, we can also compare it with the energy levels when considering b_x, but with all other parameters kept the same. A comparison of $b_x \neq 0$ and $b_x = 0$ is plotted in Fig. 3.7. It is interesting to note that this separation in momentum space appears to make the band gaps smaller, as the energy levels are shifted closer to each other.

Finally, we can include all the effects that we have calculated up until now. The result of this is plotted in Fig. 3.8. In this figure we see all the effects we discussed up until now combined. The levels are both shifted and tilted through the parallel component of the TR breaking vector and anomalous magnetic moment terms, and are distorted by the perpendicular components of the TR breaking vector.

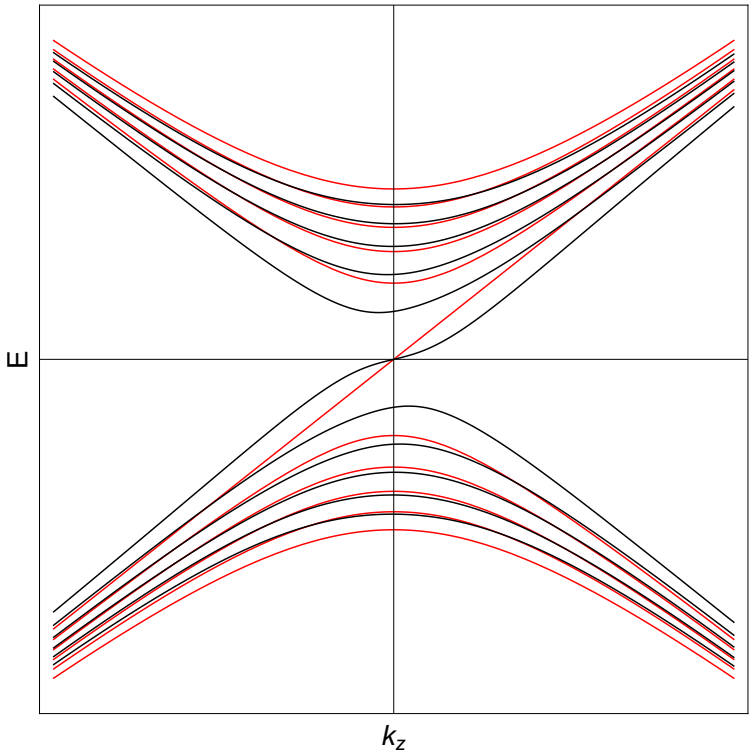

Figure 3.7 – Comparison of the energy levels as a function of the momentum along the direction of the magnetic field with both a zero and a non-zero b_x term, without anomalous magnetic moment. The black curves denote the numerically computed states for $\bar{b}_x = 2$. The red curves denote the analytical solutions for $\bar{b}_x = 0$. Both are the solutions for right chiral fermions.

Since we, consider an infinite dimensional system, but for obvious reasons cannot do that numerically, we need to investigate the effects of this dimensional cut-off. In Fig. 3.9 the first five excited states are shown, which have been computed using two different cut-offs. For the black curves, we have placed the cut-off at ten levels, while for the red curves the cut-off is placed at five levels. The ground state and the first excited state are barely affected by the cut-off, but the discrepancy becomes very clear for the higher levels. So it is clear that care needs to be taken in placing the cut-off.

Taking a higher amount of computed states can reduce this numerical error to a minimum. In Fig. 3.10 we compare the first five levels again, but now with respectively 10 and 20 computed levels before the cut-off. One can clearly see that now the first three excited states match very well, while the error in the highest two levels are visible, but noticably reduced in comparison with the previous example. Taking 15 and 20 levels shows that the discrepancy is no longer visible when looking at the first five excited states. From this we can conclude that the numerical errors introduced by a cut-off in the computed amount of terms is very much relevant, but that it can be effectively compensated by computing many more terms than one is interested in, since the error is mainly in the higher terms.

Another curious thing to take a look at is the behaviour of the chiral ground state near zero, where it curves a bit. One can wonder how this energy scales with momentum, and whether it is still linear around this point, as it was in the case without the symmetry breaking vector having components perpendicular to the magnetic field. Unfortunately, we cannot do this analytically, since this curvature seems to stem from the higher order terms: simply calculating the ground state using just the first excited states, a first order correction if you will, does not yield the form we see when using higher order corrections. Trying to analytically calculate it using a 11 by 11 matrix is simply too much work, especially given the complicated form of its entries, so numerics will have to suffice here.

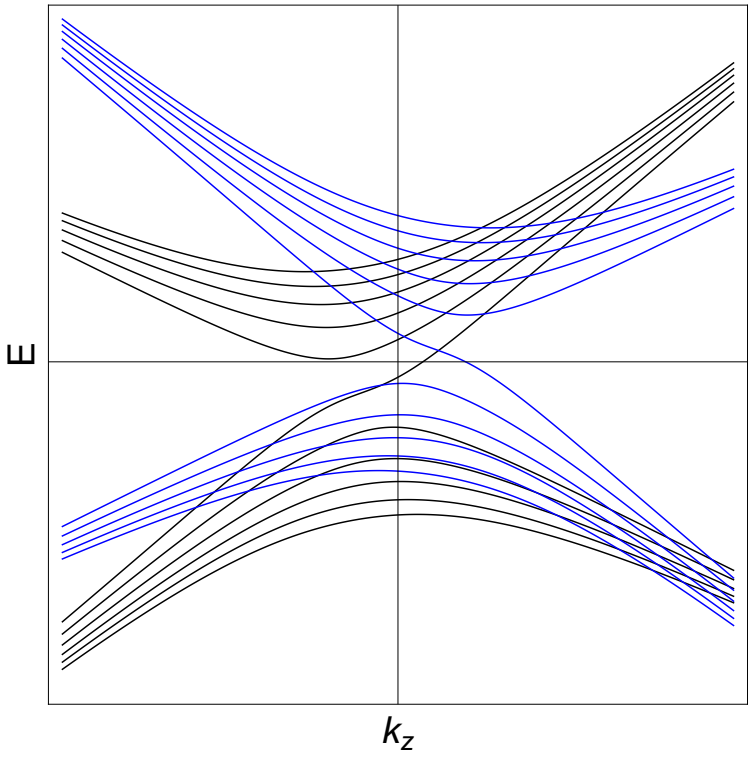

Figure 3.8 – Energy levels as a function of the momentum along the direction of the magnetic field with $\bar{b}_x = 2$, $\bar{b}_0 = 0.5$, $\bar{b}_z = 0.3$, $\bar{\mu}_1 = 0.25$ and $\bar{\mu}_2 = 0.85$. Black: right chiral states. Blue: left chiral states.

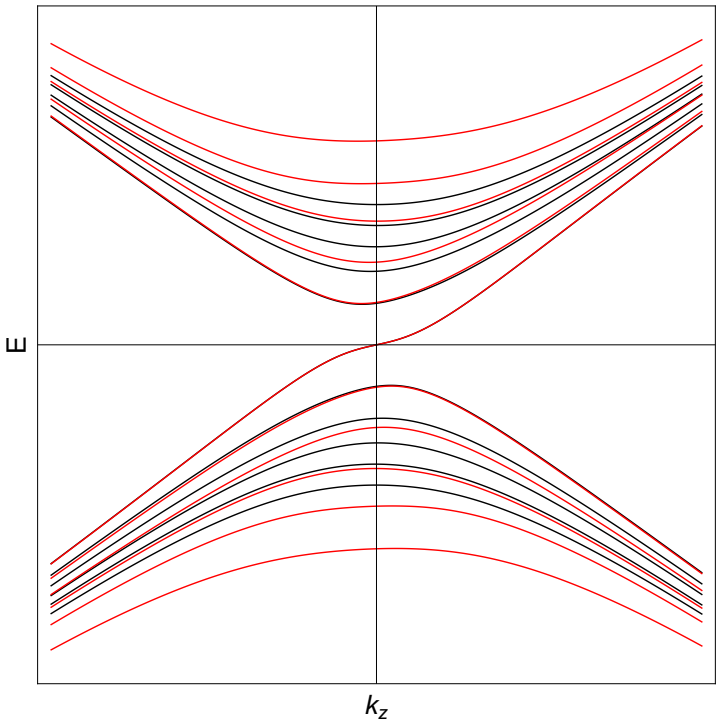

Figure 3.9 – Numerically computed energy levels of the Hamiltonian Eq. 3.2.10 as a function of the momentum along the direction of the magnetic field with $\bar{b}_x = 2$. Different cut-offs in the dimensions are used here. For the black curves we used 10 excited states. For the red curves we used 5 excited states.

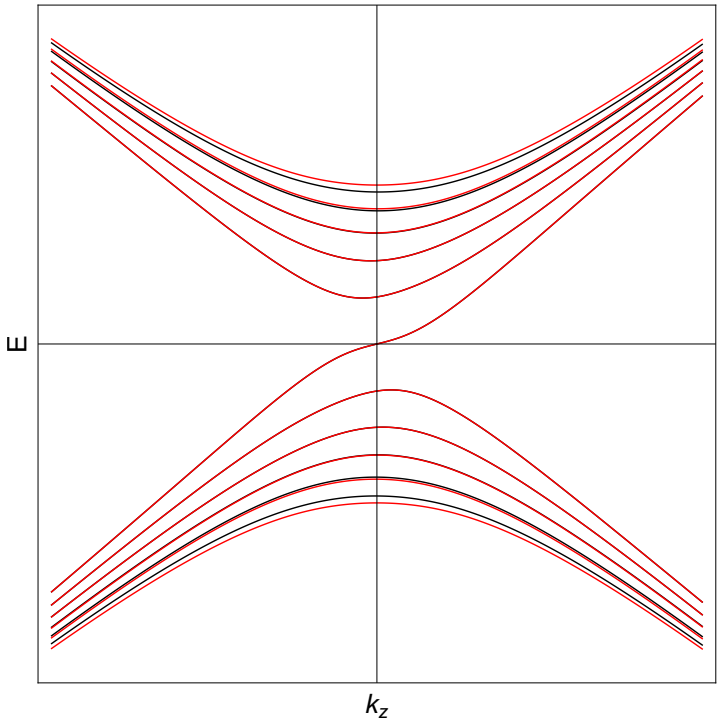

Figure 3.10 – Numerically computed energy levels of the Hamiltonian Eq. 3.2.10 as a function of the momentum along the direction of the magnetic field with $\bar{b}_x = 2$. Different cut-offs in the dimensions are used here. For the black curves we used 20 excited states. For the red curves we used 10 excited states.

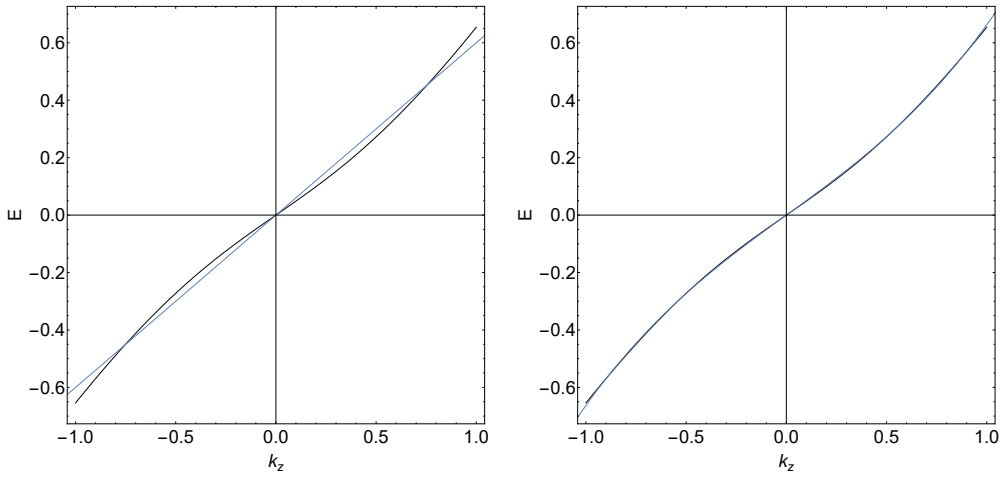

Figure 3.11 – Two different fits for the behaviour of the lowest Landau level with $\bar{b}_x = 1.8$ near $\bar{k}_z = 0$. a shows a fit of the form $a\bar{k}_z$ and b shows a fit of the form $a\bar{k}_z + b\bar{k}_z^3$, where a and b are constants.

In Fig. 3.11 we compare two fitted curves to the points, one with a purely linear fit of the form ax, which is shown in subfig. 3.11a, and one with an added third order term of the form $ax + bx^3$, which is shown in subfig. 3.11b. It is clear that the added third order term makes for a much better fit, so we can conclude from this that the behaviour around zero is no longer linear, but also has a cubic term for this value of $\bar{b}_x$.

For higher values of $\bar{b}_x$ we find that the non-linear effect becomes more pronounced. One of the consequences of this is that above a certain value, the level actually can rise above the Fermi level before crossing the origin and then dip below the Fermi level again briefly.

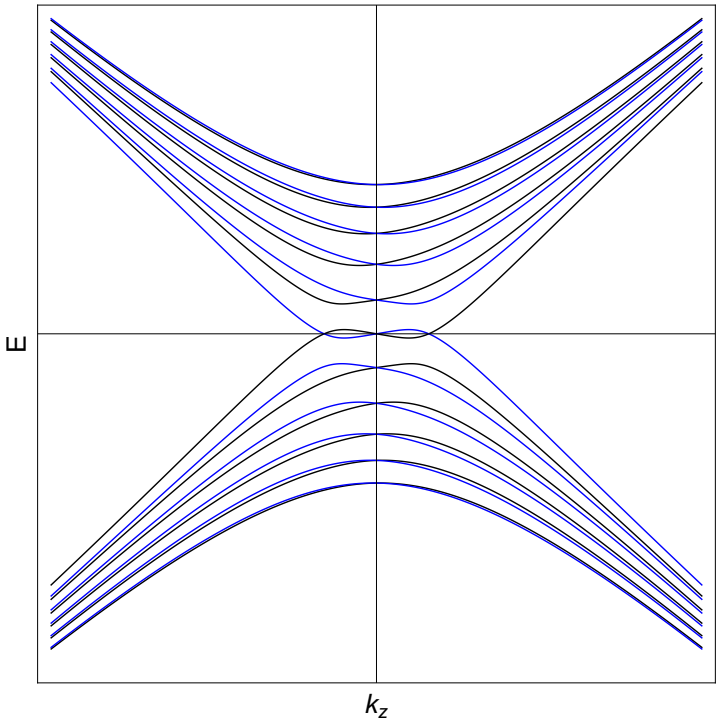

Figure 3.12 – Energy states as a function of the momentum along the direction of the magnetic field for $\bar{b}_x = 2.7$, calculated using 50 excited states. The black and blue curves are respectively the right and left chiralities. Both ground state curves cross the Fermi level three times.

This effect can be clearly seen in Fig. 3.12. The higher the $\bar{b}_x$ is, the more erratic the curve becomes. In the absence of anomalous magnetic moment contributions, the curve will remain anti-symmetric around the origin, thus we can attempt to decribe it using a power series of odd powers of $\bar{k}_z$, where the coefficients themself can depend on the parameter $\bar{b}_x$

$$E(\bar{k}_z) = \sum_{l=1,3,\ldots}^{\infty} a_l(\bar{b}_x)\bar{k}_z^l \tag{3.2.11}$$

From this it is clear that larger $\bar{b}_x$ will then require increasingly more terms in order to describe the behaviour accurately. The values for the coefficient of the first 4 terms are given in Fig. 3.13. From here we can also determine at which point we get the phase transition, as this will occur when the linear coefficient changes sign. This has been numerically determined to happen around $\bar{b}_x \approx 2.318$.

As can be seen from this figure, the higher the value of $\bar{b}_x$, the less linear the system behaves. Up until around $\bar{b}_x = 1.5$ the system can be described approximately linearly, because we consider $|\bar{k}_z| < 1$, so the higher order terms contribute less if their coefficient is not large enough. Above that, the contributions from higher order terms can no longer be ignored. Above $\bar{b}_x = 2.6$ even an approximation up to $\bar{k}_z^5$ becomes insufficient. Taking this to the extremes, at $\bar{b}_x = 4$ even an approximation with terms up to $\bar{k}_z^{21}$ is not enough. So it is clear that this system can become complicated very quickly.

In light of the phase transition that was found for the ground state, thinking about the effect of b_0, one can see that a similar effect may occur. If we make b_0 large enough, we can shift the first Landau level to actually have its minimum below the Fermi level, creating an additional hole pocket, giving us another way to make a phase transition occur in this system. However, we need to be careful in using b_0 in the system if we want to retain our semimetallic behaviour. Shifting the Weyl point away from the Fermi level means that we actually have the Fermi level inside the conduction band, which simply gives us metallic behaviour.

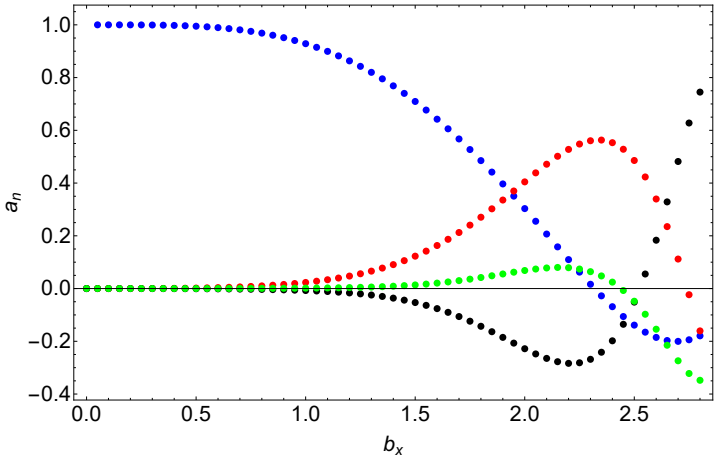

Figure 3.13 – Values for the first four coefficients a_l of the power series given in Eq. 3.2.11 as function of $\bar{b}_x$. Blue: $l = 1$. Red: $l = 3$. Black: $l = 5$. Green: $l = 7$.

3.2.2 Perturbative results

We can also attempt to compute the ground state using perturbation theory. This allows us to write the energy as

$$E_0(\lambda) = \sum_{m=0}^{\infty} \lambda^m E_0^{(m)}, \tag{3.2.12}$$

where λ is our perturbation parameter, which we take to be b_x for this system. The power in brackets is the order of perturbation. Since we know that the perturbative part of the Hamiltonian is side-diagonal, we can immediately discard a first order perturbation, since those are given by the diagonal part of the perturbative Hamiltonian. So we will look at a second order correction for the ground state, which is given by

$$E_0^{(2)} = \sum_{k\neq 0} \frac{|\langle 0|V|k\rangle|^2}{E_0^{(0)} - E_k^{(0)}} \equiv \sum_{k\neq 0} \frac{|V_{0,k}|^2}{E_{0,k}}, \tag{3.2.13}$$

where V is the perturbative part of the Hamiltonian, and we define $V_{i,j} \equiv \langle i|V|j\rangle$ and $E_{i,j} \equiv E_i^{(0)} - E_j^{(0)}$.

For simplicity's sake, we shall not include any anomalous effects in this calculation. We also take $b_y = 0$. Using this, we can write our perturbative part of the Hamiltonian, leaving out the b_x, since it is our perturbation parameter λ, as

$$V_{i,j} = \frac{\sqrt{2j}\mathrm{Sgn}(\bar{\delta}_j)|\bar{\delta}_i|}{\bar{\gamma}_i\bar{\gamma}_j}\delta_{i,j-1} + \frac{\sqrt{2i}\mathrm{Sgn}(\bar{\delta}_i)|\bar{\delta}_j|}{\bar{\gamma}_i\bar{\gamma}_j}\delta_{i,j+1}. \tag{3.2.14}$$

Since $V_{0,j}$ only couples to neighbouring states, we see that we can only have $V_{0,1}$ and $V_{0,-1}$. So the perturbation is given by

$$E_0^{(2)} = \frac{|V_{0,1}|^2}{E_{0,1}} + \frac{|V_{0,-1}|^2}{E_{0,-1}}.$$

Since we defined that $\delta_0/\gamma_0 = 1$, we find that we can write

$$|V_{0,\pm 1}|^2 = \frac{2\delta_0^2}{\gamma_0^2\gamma_{\pm 1}^2} = \frac{2}{\delta_{\pm 1}^2 + 2}.$$

Next we note that $E_0^{(0)} = \epsilon k_z$ and $E_{\pm n}^{(0)} = \pm\sqrt{k_z^2 + 2n}$, and we note that

$$E_{0,1}E_{0,-1} = (\epsilon k_z - \sqrt{k_z^2+2})(\epsilon k_z + \sqrt{k_z^2+2}) = -2,$$

which then allows us to write

$$E_0^{(2)} = \frac{E_{-1,0}}{\delta_1^2+2} + \frac{E_{1,0}}{\delta_{-1}^2+2}.$$

We have $\delta_{\pm 1} = -(k_z + \epsilon E_{\pm 1}) = -(k_z \pm \epsilon\sqrt{k_z^2+2})$. Calculating the delta terms explicitly, we find that $\delta_{\pm 1}^2 + 2 = 2(k_z^2 \pm \epsilon k_z\sqrt{k_z^2+2}+2)$. This allows us to write

$$\begin{aligned}\frac{1}{\delta_{\pm 1}^2+2} &= \frac{1}{2}\frac{1}{k_z^2+2\pm\epsilon k_z\sqrt{k_z^2+2}} \\ &= \frac{1}{4}\left(1 \mp \frac{\epsilon k_z}{\sqrt{k_z^2+2}}\right) \\ &= \frac{1}{4E_1}\left(E_1 \mp E_0\right).\end{aligned}$$

Making use of the symmetry $E_{\pm 1} = \pm E_1$, we can now write

$$\begin{aligned}\frac{E_{\mp 1}-E_0}{\delta_{\pm 1}^2+2} &= \frac{\mp E_1 - E_0}{\delta_{\pm 1}^2+2} \\ &= -\frac{1}{4E_1}(E_0 \pm E_1)(E_1 \mp E_0) \\ &= \mp\frac{1}{2E_1}.\end{aligned}$$

Finally we find the perturbation to be given by

$$E_0^{(2)} = \frac{E_{-1,0}}{\delta_1^2+2} + \frac{E_{1,0}}{\delta_{-1}^2+2} = -\frac{1}{2E_1} + \frac{1}{2E_1} = 0. \tag{3.2.15}$$

So we conclude that the second order perturbation is also zero in the case of no anomalous effects. We expect that this is not the case when considering anomalous effects, since the symmetry $E_{\pm n} = \pm E_n$ will no longer hold in that case.

The next step is to then look at the third order perturbation. This is given by

$$E_0^{(3)} = \sum_{k\neq 0, l\neq 0}\frac{V_{0,l}V_{l,k}V_{k,0}}{E_{k,0}E_{l,0}} - V_{0,0}\sum_{k\neq 0}\frac{|V_{0,k}|^2}{E_{k,0}^2}. \tag{3.2.16}$$

Since $V_{0,0} = 0$, we can discard the second term immediately, so we are left to look at

$$E_0^{(3)} = \sum_{k\neq 0, l\neq 0}\frac{V_{0,l}V_{l,k}V_{k,0}}{E_{k,0}E_{l,0}}. \tag{3.2.17}$$

We know that $V_{0,l}$ is non-zero only if $l = \pm 1$, and the same for $V_{k,0}$. However, since $V_{\pm 1,\pm 1} = 0$, we can immediately deduce that the third order perturbation is also zero. In fact, due to our form of the perturbative Hamiltonian, we see that all odd orders of perturbations vanish, since an odd combination of V_{ij} cannot create combinations such that it is of the form $V_{0,k_1}\cdots V_{k_i,k_{i+1}}\cdots V_{k_n,0}$, since we require $|k_i - k_{i+1}| = 1$. The first term that turns out to be non-zero is the fourth order correction, which is given by

$$E_0^{(4)} = \sum_{k\neq 0, l\neq 0, m\neq 0}\frac{V_{0k}V_{kl}V_{lm}V_{m0}}{E_{0k}E_{0l}E_{0m}} - E_0^{(2)}\frac{|V_{0k}|^2}{E_{0k}^2} - 2V_{00}\frac{V_{0k}V_{kl}V_{l0}}{E_{0l}^2E_{0k}} + V_{00}^2\frac{|V_{0k}|^2}{E_{0k}^3}. \tag{3.2.18}$$

Now fortunately we know that $E_0^{(2)} = 0$ and $V_{0,0} = 0$, so we can discard all terms except the first. Next we go over the possible combination for $V_{0k}V_{kl}V_{lm}V_{m0}$, such that none of the four terms is zero, and such that neither k, l or m are zero. This leaves us with only two possiblities: $V_{0,1}V_{1,2}V_{2,1}V_{1,0} = |V_{0,1}|^2|V_{1,2}|^2$ and $V_{0,-1}V_{-1,-2}V_{-2,-1}V_{-1,0} = |V_{0,-1}|^2|V_{-1,-2}|^2$. So we find that the fourth order correction is given by

$$E_0^{(4)} = \frac{|V_{0,1}|^2|V_{1,2}|^2}{E_{0,1}^2 E_{0,2}} + \frac{|V_{0,-1}|^2|V_{-1,-2}|^2}{E_{0,-1}^2 E_{0,-2}}, \tag{3.2.19}$$

and is determined by the nearest two levels. So here we also see that all even orders of perturbation will consist of terms with products $|V_{i,i\pm1}|^2 \propto (b_x^2 + b_y^2)$. This justifies our reasoning for ignoring b_y in these computations, since we only concern ourselves with the length of the vector (b_x, b_y) instead of its direction. So anything we calculate here simply using b_x will also be valid for b_y. For the following computation we will assume, to avoid getting lost in all indices and powers, that if no order of perturbation is mentioned the unperturbed state is meant. So $E_i \equiv E_i^{(0)}$. At the end it will be denoted properly again. Writing out the expressions for the matrix elements, we get

$$E_0^{(4)} = \frac{8\delta_1^2}{(\delta_1^2+2)^2(\delta_2^2+4)}\frac{1}{(E_0-E_1)^2(E_0-E_2)} + \frac{8\delta_{-1}^2}{(\delta_{-1}^2+2)^2(\delta_{-2}^2+4)}\frac{1}{(E_0-E_{-1})^2(E_0-E_{-2})}.$$

Using the symmetry $E_{-n} = -E_n$, for $n > 0$, we can rewrite this. If we also see that $\delta_{\pm n} = -\epsilon(E_0 + E_{\pm n}) = -\epsilon(E_0 \pm E_n)$, then we can write $\delta_{\pm n}^2 = (E_0 \pm E_n)^2$. This allows us to write

$$\begin{aligned} E_0^{(4)} =& \frac{8(E_0+E_1)^2}{[(E_0+E_1)^2+2]^2[(E_0+E_2)^2+4]}\frac{1}{(E_0-E_1)^2(E_0-E_2)} \\ &+ \frac{8(E_0-E_1)^2}{[(E_0-E_1)^2+2]^2[(E_0-E_2)^2+4]}\frac{1}{(E_0+E_1)^2(E_0+E_2)}. \end{aligned}$$

Using $(E_0+E_n)(E_0-E_n) = E_0^2 - E_n^2 = -2n$. We can finally cast the fourth order correction to the ground state energy into a somewhat compact form:

$$E_0^{(4)} = -\frac{1}{2}\left[\frac{(E_0+E_1)^4(E_0+E_2)}{[(E_0+E_2)^2+2][(E_0+E_2)^2+4]} + \frac{(E_0-E_1)^4(E_0-E_2)}{[(E_0-E_2)^2+2][(E_0-E_2)^2+4]}\right].$$

As much as it may not look like it, this is expression can be very much simplified. This will be shown, but not in full detail. Instead we show some intermediate results. We first equalize the denominator. To do this we use the following results:

$$\begin{aligned} [(E_0+E_1)^2+2]^2[(E_0-E_1)^2+2]^2 &= 64E_1^4, \\ [(E_0+E_2)^2+4][(E_0-E_2)^2+4] &= 16E_2^2. \end{aligned}$$

So the denominator becomes $1024E_1^4E_2^2$. Now we calculate the products in the enumerator:

$$\begin{aligned} [E_0 \pm E_1]^4[(E_0 \mp E_1)^2+2]^2 &= 32E_1^2(1 + E_0^2 \pm E_0E_1) \\ [E_0 \pm E_2][(E_0 \mp E_2)^2+4] &= \pm 8E_2. \end{aligned}$$

Using these results, we conclude that

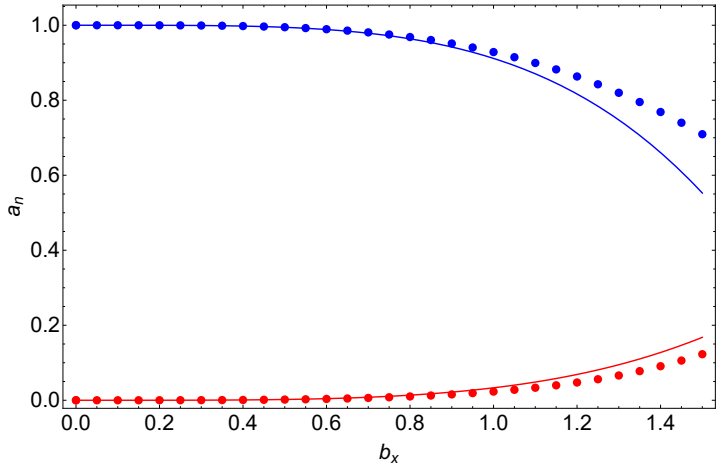

Figure 3.14 – Values for the first two coefficients a_n of the power series given in Eq. 3.2.11 as function of $\bar{b}_x$. Blue: $n = 1$. Red: $n = 3$. Dots are numerical data points, while the solid curves denote the perturbative results.

$$E_0^{(4)} = -\frac{1}{4}\frac{E_0}{E_1 E_2}.$$

So after some extensive algebra, we find that this is actually a fairly simple correction:

$$E_0^{(4)} = -\frac{1}{4}\frac{E_0^{(0)}}{E_1^{(0)} E_2^{(0)}} = -\frac{1}{4}\frac{\epsilon k_z}{\sqrt{k_z^2+2}\sqrt{k_z^2+4}}, \tag{3.2.20}$$

where we have now reinserted the perturbative orders again. Thus, up to fourth order in perturbation, the ground state energy is given by

$$E_0(b_x) = E^{(0)} + b_x^4 E_0^{(4)} = E_0^{(0)}\left(1 - \frac{b_x^4}{4E_1^{(0)}E_2^{(0)}}\right), \tag{3.2.21}$$

which we expect to hold for small b_x. If we now take a Taylor expansion of the fourth order correction around $p_z = 0$, we obtain

$$E_0^{(4)} = -\frac{\epsilon k_z}{8\sqrt{2}} + \frac{3\epsilon k_z^3}{64\sqrt{2}} + \mathcal{O}(k_z^5). \tag{3.2.22}$$

This is then also a good indication that we were justified in ignoring any even order of k_z in our numerical analysis, since all even powers are zero in this expansion. We can also compare these coefficients to Fig 3.13, where we computed these coefficients as a function of b_x numerically for $\epsilon = 1$. We would then expect that the linear and cubic coefficients will be given, for small b_x , by

$$a_1 = 1 - \frac{b_x^4}{8\sqrt{2}}, \qquad a_3 = \frac{3b_x^4}{64\sqrt{2}}$$

The result of the perturbation theory for the linear and cubic coefficients is plotted in Fig. 3.14. From the figure it is clear that the perturbatively computed coefficients indeed match the numerically calculated values for small b_x. So the pertubative approach works well for smaller b_x, while it starts to deviate more and more for higher values, which is as expected. While it is obvious that a perturbative approach is not valid for higher values of b_x, it is still a good check on the numerical calculation, giving confidence in the obtained results, since it matches the analytical calculation in the perturbative regime quite well.

3.3 Conclusion

In this chapter we have computed the effects of the anomalous magnetic moment terms and the separation of the Weyl cones in energy-momentum space on the Landau levels. From the vertex correction, two anomalous magnetic moment terms were derived. The first is an anomalous Zeeman shift, which simply shifted the two Weyl cones with respect to each other. The second term had the effect of tilting the Weyl cones. The effect of both these terms on the energy levels have been analytically computed. Both effects also broke the level degeneracy that was present at tree level.

The second major part of this chapter has been calculating the effect of explicitly shifting the Weyl cones in energy-momentum space in a chiral dependent way. From this, we concluded that the effect on the energy levels is easily computed when the shift is in the energy direction or in the direction along the magnetic field and does exactly what you would expect: the states are unaltered, but the entire cone is simply shifted. However, shifts in the direction perpendicular to the direction of the magnetic field give highly non-trivial results. First of all, the harmonic oscillator basis, which is used to find the Landau levels, is no longer diagonalizes Hamiltonian. Instead, the Hamiltonian has to be diagonalized numerically and the energy states are then somewhat distorted and the lowest level then gives a non-linear dispersion. This result has been verified through perturbation theory for low values of this shift parameter.

With these results, we now have a framework to compute the energy spectrum in the presence of a magnetic field, incorporating the anomalous magnetic moment terms, and with a symmetry breaking vector in an arbitrary direction with respect to the orientation of the magnetic field. In the next chapter we move away from the bulk problem and attempt to find the energetic states at the interface between the Weyl semimetal and a massive Dirac vacuum.

Chapter 4

Surface States

As mentioned in the introduction, one of the interesting properties of Weyl semimetallic materials, just like in topological insulators, is the existence of conducting surface states. These states are generally topologically protected by symmetries and are localized at the surface, with a wave function rapidly decaying away from the surface.

The aim of this chapter is to build a framework for computing these surface states and their dispersion relation. We will start by computing the surface states in the absence of any gauge fields in section 4.1. Next we show the effects of an electric field and the influence of the Rashba-like term in section 4.2. After that we will compute them in the presence of a uniform magnetic field. To finish, we compute the effects of the anomalous magnetic moment on the surface state dispersion in section 4.3.

In this chapter we will work with $\hbar = c = v_F = 1$ for most of the part, and switching to dimensionless variables when concerning things that have to be computed numerically. This choice was made for the reason that it makes it clear exactly what the structure of the Hamiltonians is and where the dependences on different parameters come into play. For the dimensionless variables we use the same scaling factors as before.

4.1 Zero electromagnetic field

In order to simulate the edge of a Weyl semimetal, we consider a Weyl semimetal bordering a Dirac vacuum at $x = 0$. We solve the Dirac equation in both the Dirac vacuum of mass m and in the massless Weyl semimetal with a TR symmetry breaking vector $\mathbf{b} = b\hat{z}$, $b > 0$. We take a large mass for the Dirac part, which acts as a work function, preventing the particles from leaving the semimetal freely. This model is similar to the one used in Ref. [29]. A schematic illustration of this model is given in Fig. 4.1.

The Hamiltonian of the system then reads

$$H = \gamma^0 \left[\boldsymbol{\gamma} \cdot (-\imath\nabla + \theta(x)\gamma^5 \mathbf{b}) + \theta(-x)m \right], \tag{4.1.1}$$

where $\theta(x)$ is the Heaviside step function, equaling one if the argument is positive and zero otherwise. Since we have translational invariance in the $\hat{y}$ and $\hat{z}$ direction, we can insert a plane-wave ansatz for the wave functions in those directions, giving

$$\Psi(\mathbf{x}) = e^{\imath(k_y y + k_z z)}\psi(x), \tag{4.1.2}$$

leaving us with a one-dimensional problem for $\psi(x)$.

The Hamiltonian described above is explicitly dependent on the coordinate x now. Since it is different in the both halves of the space, we cannot simply solve the system in one go. Instead, we shall solve the equation in both halves of our space separately, and then

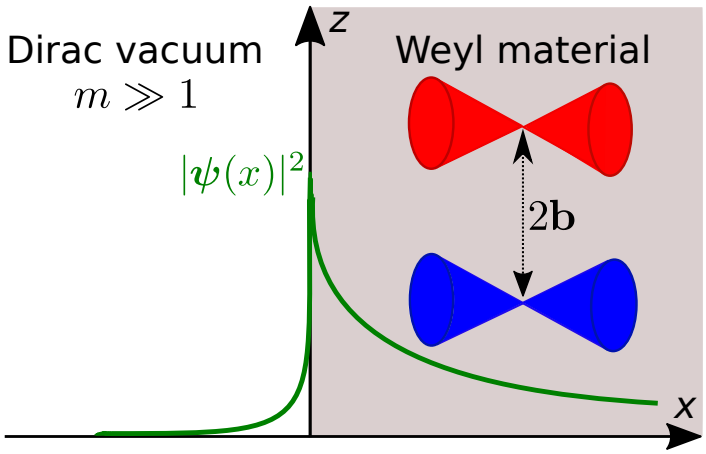

Figure 4.1 – Model for the construction of surface states. For $x < 0$ we have a Dirac vacuum with a large mass, acting as a work function. For $x > 0$ we have a Weyl semimetal with a broken TR symmetry. The green curves denote the amplitude of the wave function, which is localized at the surface.

demand the solutions to match at their boundary. Using our ansatz, we find that the Hamiltonian can be further rewritten as

$$H = \gamma^0 \left[-\imath\gamma^1 \partial_x + \gamma^2 k_y + \gamma^3 (k_z + \theta(x)\gamma^5 b) + \theta(-x)m \right], \tag{4.1.3}$$

We will now solve these equations separately for the two regions in space before matching them up and computing the allowed states.

4.1.1 Semimetal regime

In the semimetallic part of the space, our Hamiltonian reads

$$H = \gamma^0 \left[-\imath\gamma^1 \partial_x + \gamma^2 k_y + \gamma^3 (k_z + \gamma^5 b) \right]. \tag{4.1.4}$$

To make this into a solvable system, we will use an exponential ansatz for $\psi(x)$:

$$\psi(x) = e^{\lambda_i x} \mathbf{u}_i, \tag{4.1.5}$$

where $\mathbf{u}_i$ is a constant, four-component vector. Using this ansatz, we see that $\partial_x \psi(x) = \lambda_i \psi(x)$. Now our problem is reduced to a one-dimensional problem, which is solving the differential equation

$$\partial_x \psi(x) = Q\psi(x) = \lambda_i \psi(x), \tag{4.1.6}$$

where

$$Q = -\imath\gamma^1 \left[\gamma^0 E - \gamma^2 k_y - \gamma^3 (k_z + \gamma^5 b) \right], \tag{4.1.7}$$

which we shall call the effective matrix. With the ansatz we make, this is simply an eigenvalue equation given by $Q\mathbf{u}_i = \lambda_i \mathbf{u}_i$. Finding the eigenvalues of the above effective matrix is straightforward and yields

$$\pm\lambda_>^{\pm} \equiv \sqrt{-E^2 + k_y^2 + (k_z \pm b)^2}. \tag{4.1.8}$$

Since we are interested in those solutions that do not blow up in the bulk for $x \to \infty$, we discard the positive values, leaving us with $-\lambda^{\pm}$. Hence, the solution for $\psi(x)$ in this regime is given by

$$\psi_{>}(x) = A_1 e^{-\lambda^{-}x}\mathbf{u}_{>,1} + A_3 e^{-\lambda^{+}x}\mathbf{u}_{>,3}, \tag{4.1.9}$$

with the two vectors given by

$$\mathbf{u}_{>,1} = \begin{pmatrix} 0 \\ 0 \\ \frac{\imath(-k_y+\sqrt{k_y^2+(k_z-b)^2-E^2})}{E-k_z+b} \\ 1 \end{pmatrix}, \qquad \mathbf{u}_{>,3} = \begin{pmatrix} \frac{\imath(k_y-\sqrt{k_y^2+(k_z+1)^2-E^2})}{E+k_z+b} \\ 1 \\ 0 \\ 0 \end{pmatrix}.$$

4.1.2 Dirac vacuum

In the vacuum part, the Hamiltonian is given by

$$H = \gamma^0\left(-\imath\gamma^1\partial_x + \gamma^2 k_y + \gamma^3 k_z + m\right). \tag{4.1.10}$$

Solving this will proceed in a similar fashion to the semimetallic part. Setting $H\psi(x) = E\psi(x)$, we can again rewrite this into $\partial_x\psi(x) = Q\psi(x)$, where we have

$$Q = -\imath\gamma^1\left(\gamma^0 E - \gamma^2 k_y - \gamma^3 k_z - m\right). \tag{4.1.11}$$

Again, if we now make the ansatz $\psi(x) = e^{\lambda_i x}\mathbf{u}_i$, we are reduced to the eigenvalue equation $Q\mathbf{u}_i = \lambda_i\mathbf{u}_i$. So we again want to find the eigenvalues and eigenvectors of Q. This time, there are only two unique eigenvalues:

$$\pm\lambda_{<} \equiv \pm\sqrt{-E^2 + k_y^2 + k_z^2 + m^2}. \tag{4.1.12}$$

We now require this solution to not blow up for $x \to -\infty$, so we discard the negative solutions here, leaving just $+\lambda_{<}$. The solution for $\psi(x)$ in this part is then given by

$$,\psi_{<}(x) = e^{\lambda_{<}x}\left(B_3\mathbf{u}_{<,3} + B_4\mathbf{u}_{<,4}\right), \tag{4.1.13}$$

with the two vectors given by

$$\mathbf{u}_{<,3} = \frac{1}{m}\begin{pmatrix} \imath\left(k_y + \sqrt{-E^2+m^2+k_y^2+k_z^2}\right) \\ E + k_z \\ 0 \\ m \end{pmatrix}, \qquad \mathbf{u}_{<,4} = \frac{1}{m}\begin{pmatrix} E - k_z \\ \imath\left(-k_y + \sqrt{-E^2+m^2+k_y^2+k_z^2}\right) \\ m \\ 0 \end{pmatrix}.$$

4.1.3 Matching at the boundary

Now that we found the solutions for both regimes, we demand the full solution to be continuous at the boundary $x = 0$, so $\psi_{<}(0) = \psi_{>}(0)$. Since our wave function has four components, this gives us four matching equations and hence allows us to find values for four unknowns. However, we have a fifth unknown, namely the energy. So we need a fifth equation to solve the system, which is provided by the normalization of the wave function:

$$\int_{-\infty}^{\infty} dx\psi^{\dagger}(x)\psi(x) = 1. \tag{4.1.14}$$

We can succinctly write the four matching equations in matrix form:

$$M \cdot (A_1, A_3, B_3, B_4)^T = 0. \tag{4.1.15}$$

As usual, this only has non-trivial solutions when $\mathrm{Det}(M) = 0$. This is what will tell us the allowed values for the energy, namely exactly those values that allow the determinant of the matchings matrix to vanish. From the matching equations, we see that the matrix we need to consider is given by

$$M = (\mathbf{u}_{<,1}, \mathbf{u}_{<,3}, -\mathbf{u}_{>,3}, -\mathbf{u}_{>,4}), \tag{4.1.16}$$

So its columns consist of the normalized eigenvectors, with either a plus or minus sign.

Setting the determinant to zero and then solving for E is generally not doable by hand, since it will contain both roots and higher powers in the energy. In general, its solutions need to be determined numerically. However, analyical solutions can be found. One such solution is $E = -k_y$, existing for $|k_z| < b$. This shows us that a gapless, chiral surface state exists, since $E = +k_y$ is not a solution. There is a way to have $E = +k_y$ be a solution, which is done by switching the chiralities of the Weyl nodes. Doing so will reverse the current. This effect can also be achieved by switching the WSM and Dirac vacuum.

With this dispersion relation and taking the limit $m \to \infty$, the matching matrix is given by

$$M = \begin{pmatrix} 0 & -\imath & -\imath & 0 \\ 0 & 1 & 0 & -\imath \\ \imath & 0 & 0 & -1 \\ 1 & 0 & -1 & 0 \end{pmatrix}. \tag{4.1.17}$$

Hence we find that $A_3 = -B_3$, $A_1 = A_3$ and $B_4 = \imath A_3$. Defining $A_3 \equiv c$, the normalization constant, we then find the wave function to be

$$\psi_>(x) = ce^{-(b+k_z)x} \begin{pmatrix} \imath \\ -1 \\ 0 \\ 0 \end{pmatrix} + ce^{-(b-k_z)x} \begin{pmatrix} 0 \\ 0 \\ \imath \\ 1 \end{pmatrix} \quad \text{and} \quad \psi_<(x) = ce^{\sqrt{k_z^2+m^2}x} \begin{pmatrix} \imath \\ -1 \\ \imath \\ 1 \end{pmatrix}. \tag{4.1.18}$$

Thus, we find that the components of the wave function indeed decay exponentially on both sides of the boundary. This means that the state is localized at the surface, which we shall call a surface state. We plot the form of the wave function Eq. 4.1.18 in Fig. 4.2. Due to the degeneracy of the eigenvalues, there are only two different decay rates for the solution in the bulk, while there is only one for the vacuum.

A last remark on the above calculation is that care needs to be taken when taken the limit $m \to \infty$. Looking at the wave function that we obtained for the vacuum part, we see that an infinite mass would lead to simply a zero wave function. For this reason you should not take this limit until after the surface state is constructed, otherwise matching will become impossible. In this case the mass is left in the wave function in order to illustrate the decay into the vacuum, without having it be a step function.

4.2 With electric field

Now that the solution in absence of electromagnetic fields is known, we can start to consider the influence of electromagnetic fields. The results of this section are derived in Ref. [28], and are simply stated here to provide a comparison with its magnetic counterpart in the next section. Note for this section that we have denoted the energy as ω instead of E, to avoid confusion with the electric field, which is called E here.

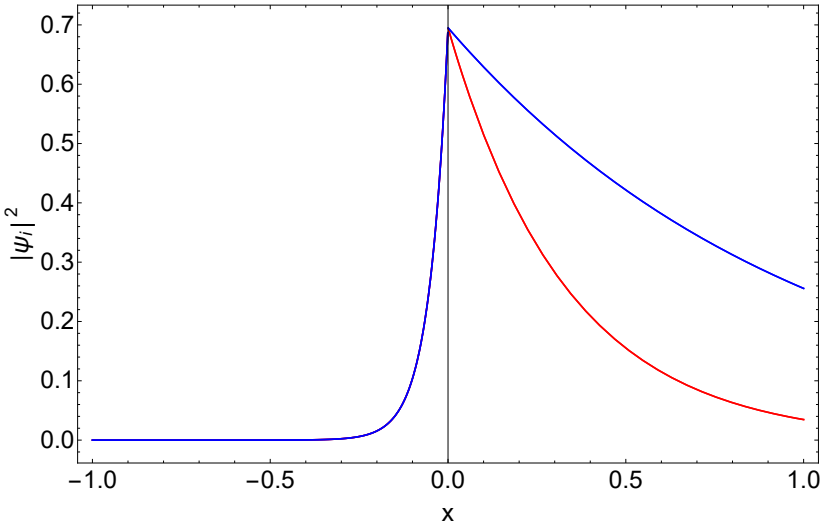

Figure 4.2 – Components of the wave function given in Eq. 4.1.18 as a function of position x. Image for the values $b = 2$, $k_z = 1$ and $m = 19$.

The electric field influences the bound states through the anomalous Rashba spin-orbit coupling. This adds a term $[\bar{\mathbf{E}}\times(\mathbf{k}-\epsilon\mathbf{b})]\cdot\boldsymbol{\sigma}$ to the Hamiltonian, where we define $\bar{\mathbf{E}} = \mu_1\mathbf{E}$. In terms of Dirac matrices, the Hamiltonian in real space reads

$$H = \gamma^0\boldsymbol{\gamma}\cdot\left[-\imath\nabla - \gamma^5\mathbf{b} + (\bar{\mathbf{E}}\times\mathbf{b}) - \imath\gamma^5(\bar{\mathbf{E}}\times\nabla)\right]. \tag{4.2.1}$$

Using the same ansatz as before, in which the y and z directions are assumed to be plane-waves, and introducing the notation $\mathbf{k}_\perp = (0, k_y, k_z)$, we can rewrite the above Hamiltonian to read

$$H = -\imath\gamma^0(\gamma^1 + \gamma^2\gamma^5\bar{E}_z - \gamma^3\gamma^5\bar{E}_y)\partial_x + \gamma^0\boldsymbol{\gamma}\cdot\left[\mathbf{k}_\perp - \gamma^5\mathbf{b} + (\bar{\mathbf{E}}\times\mathbf{b}) + \gamma^5(\bar{\mathbf{E}}\times\mathbf{k}_\perp)\right]. \tag{4.2.2}$$

Now define the matrix in front of the partial derivative as M_x and call the eigenstates of the Hamiltonian ω to avoid confusion with the electric field components. Then the effective matrix in this case is given by

$$\tilde{H} = M_x^{-1}\left\{\omega - \gamma^0\boldsymbol{\gamma}\cdot\left[\mathbf{k}_\perp - \gamma^5\mathbf{b} + (\bar{\mathbf{E}}\times\mathbf{b}) + \gamma^5(\bar{\mathbf{E}}\times\mathbf{k}_\perp)\right]\right\}, \tag{4.2.3}$$

where the inverse of M_x is given by

$$M_x^{-1} = \frac{\imath}{1+\bar{E}_y^2+\bar{E}_z^2}\gamma^0(\gamma^1 + \bar{E}_z\gamma^2\gamma^5 + \bar{E}_y\gamma^3\gamma^5). \tag{4.2.4}$$

The above equations are true for electric fields and TR breaking vectors in arbitrary (spatial) directions. In order to not over-complicate the problem, we shall consider only one direction for the electric field at a time, and assume that $\mathbf{b} = b\hat{z}$ in all three cases. When coupling the electric field to the Weyl semimetal, no explicit dependence on position is introduced, so we can still make use of the exponential ansatz from the previous section. So here the name of the game is again to find eigenvalues and eigenvectors of the effective matrix. In the case of $\bar{\mathbf{E}} = \bar{E}\hat{z}$, we find that the effective matrix is given by

$$Q = \frac{1}{1+\bar{E}^2}\begin{pmatrix}\boldsymbol{\sigma}\cdot\mathbf{v}_+^z & 0\\ 0 & \boldsymbol{\sigma}\cdot\mathbf{v}_-^z\end{pmatrix},$$

where $\mathbf{v}_\pm^z = (\mp\imath\omega \mp \bar{E}(k_z \pm b), \imath\bar{E}\omega - (k_z \pm b), k_y(1+\bar{E}^2))$.

This matrix has the eigenvalues

$$\pm\lambda_{\pm}^{z} = \pm\sqrt{\frac{(k_z \pm b)^2 + k_y^2(1+\bar{E}^2) - \omega^2}{1+\bar{E}^2}}. \tag{4.2.5}$$

Using this to find the matching matrix and compute for which dispersion relation a vanishing determinant is supported, we find $\omega = -k_y\sqrt{1+\bar{E}^2}$, existing when $|k_z| < b$. While the dispersion relation is altered from the zero field case, we do not find a qualitative difference. The dispersion relation is still linear in k_y and in the same direction as before, so it has only been multiplied with a constant. This only implies that the surface electrons have a higher velocity, but nothing else.

In the case of $\bar{\mathbf{E}} = \bar{E}\hat{y}$, we find that the effective matrix is given by

$$Q = \frac{1}{1+\bar{E}^2}\begin{pmatrix} \boldsymbol{\sigma}\cdot\mathbf{v}_{+}^{y} & 0 \\ 0 & \boldsymbol{\sigma}\cdot\mathbf{v}_{-}^{y} \end{pmatrix},$$

with $\mathbf{v}_{+}^{y} = (\mp\bar{E}k_y \mp \imath\omega, -(1+\bar{E}^2)(k_z \pm b), k_y - \imath\bar{E}\omega)$. This matrix has the eigenvalues

$$\pm\lambda_{\pm}^{y} = \pm\sqrt{\frac{(k_z \pm b)^2(1+\bar{E}^2) + k_y^2 - \omega^2}{1+\bar{E}^2}}. \tag{4.2.6}$$

This then yields the same dispersion relation as in the case of no electric field: $\omega = -k_y$ when $|k_z| < b$. So this yields no difference with the zero field case at all.

Finally we can consider the case where $\bar{\mathbf{E}} = \bar{E}\hat{x}$, which is perpendicular to the surface. In this case we find that the effective matrix is given by

$$Q = \begin{pmatrix} \boldsymbol{\sigma}\cdot\mathbf{v}_{+}^{x} & 0 \\ 0 & \boldsymbol{\sigma}\cdot\mathbf{v}_{-}^{x} \end{pmatrix},$$

with $\mathbf{v}_{+}^{x} = (\mp\imath\omega, \bar{E}k_y \mp (k_z \pm b), k_y \pm \bar{E}(k_z \pm b))$. It has the eigenvalues

$$\pm\lambda_{\pm}^{x} = \pm\sqrt{(k_z \pm b)^2(1+\bar{E}^2) + k_y^2(1+\bar{E}^2) - \omega^2}. \tag{4.2.7}$$

Computing from this the surface state dispersion, we find a result very different from the other two cases. We find the relation

$$\omega = -\frac{(1-\bar{E}^2)bk_y + \bar{E}(k_y^2 + k_z^2 - b^2)}{\sqrt{(b+\bar{E}k_y)^2 + \bar{E}^2k_z^2}},$$

which is valid only in the exterior of the two circles that are defined by

$$\left[k_y - \frac{b}{\bar{E}}\right]^2 + \left[k_z \pm \frac{b}{2}\left(1 + \frac{1}{\bar{E}^2}\right)\right]^2 = \frac{b^2}{4}\left[1 + \frac{1}{\bar{E}^2}\right]^2.$$

Now this result is very different from the previously considered cases. We see that the dispersion relation now also depends on k_z, and is no longer linear in nature. We conclude that an electric field perpendicular to the interface does yield very different behaviour from the zero field case.

With these results, the effect of the electric field on the surface states including a vertex correction have been computed. These results show us that surface states remain under influence of electric fields. Moreover, we see that the Rashba term of the anomalous magnetic moment can influence the dispersion relation and the region in which the surface states exist. For this reason, we are interested to see if the other two terms of the anomalous magnetic moment, the Zeeman and tilt terms, can also influence this dispersion relation. To investigate this, we first need to compute the surface states in the presence of magnetic fields in absence of interactions.

4.3 With magnetic field

In the presence of a magnetic field, we have to again use minimal substitution in the form $-\imath\nabla \to -\imath\nabla + e\mathbf{A}$. We will consider a magnetic field in the $\hat{z}$ direction, as before. Because we now have a boundary at $x = 0$, we slightly change our gauge as used before from $\mathbf{A} = B(-y, 0, 0)$ to $\mathbf{A} = B(0, x, 0)$ in order to preserve translational invariance along the $\hat{y}$ direction, ensuring that k_y remains a good quantum number.

Before we do any calculations, we can argue what the effects on the surface states are. Specifically in this gauge, we see that it adds a term proportional to eBx to the Hamiltonian. At the boundary, which is $x = 0$, we note that this does not give any contribution. Therefore, when confined to the interface, there is no change in the Hamiltonian. Hence we expect that in the absence of interaction effects, a magnetic field parallel to the boundary will have no effect. However, keeping in mind that we also will compute the anomalous magnetic moment, it is still very much possible that these correction terms will in fact alter these states.

Another way to argue that this magnetic field should not change the dispersion is to consider how magnetic fields act on charged particles. As we know, they will tend to form closed orbits, the cyclotron orbits. Near the surface, the particles will not be able to make full orbits due to the surface obstructing their path, forcing them along the boundary. This is also known as skipping orbits or extended states. The direction they are forced in is exactly already the direction of the dispersion relation in the zero field case. So based on this physical argument we again expect to see no change in the dispersion due to this field.

Due to the Hamiltonian now explicitly depending on position, the exponential ansatz that we used previously to find surface states is no longer useful. So we need to look for a new method to solve this problem. The full solution to the Dirac equation with a magnetic field is provided in Appendix A. As can be read there, the analytical solution only provides us with the classically allowed harmonic oscillator states. In order to find the exponentially decaying states, we need to look at the classically forbidden regime. This is found making use of a WKB approximation, which constitutes a power series expansion in gradients. We terminate this power series after first order. The full derivation and computation of these WKB states can be found in Appendix A.2. Its results will simply be used here.

Looking at the found results, we see that at $x = 0$, the computed wave functions are actually exactly the same as in the case without magnetic fields. This automatically means that we obtain the same matchings matrix as before and hence the same surface state dispersion relation. This is what we already argued above. So we find a chiral, gapless surface mode, given by $E = -k_y$. So no change in the dispersion is found for a magnetic field parallel to the boundary, a conclusion that is also supported in Ref. [30].

We can construct the wave function for these bound states. Because the matching matrix and dispersions are the same as in the case without a field, we find that the matching matrix with the disperion relation inserted is the same as in Eq. 4.1.17, and hence the same relations hold.

So we find the wave function in both halves of the plane to be

$$\begin{aligned}\psi_>(x) =& c\sqrt{\frac{\lambda^>_{-,0}}{\lambda^>_-(x)}}\sqrt{\frac{\alpha(x)+\lambda^>_-(x)}{k_y+\lambda^>_{-,0}}}\begin{pmatrix}0\\0\\-\imath\frac{\alpha(x)-\lambda^>_-(x)}{E-k_z+b}\\1\end{pmatrix}e^{\int_0^x dy\lambda^>_-(y)}\\ &+c\sqrt{\frac{\lambda^>_{+,0}}{\lambda^>_+(x)}}\sqrt{\frac{\alpha(x)+\lambda^>_+(x)}{k_y+\lambda^>_{+,0}}}\begin{pmatrix}\imath\frac{\alpha(x)-\lambda^>_+(x)}{E+k_z+b}\\1\\0\\0\end{pmatrix}e^{\int_0^x dy\lambda^>_+(y)},\end{aligned}$$

and

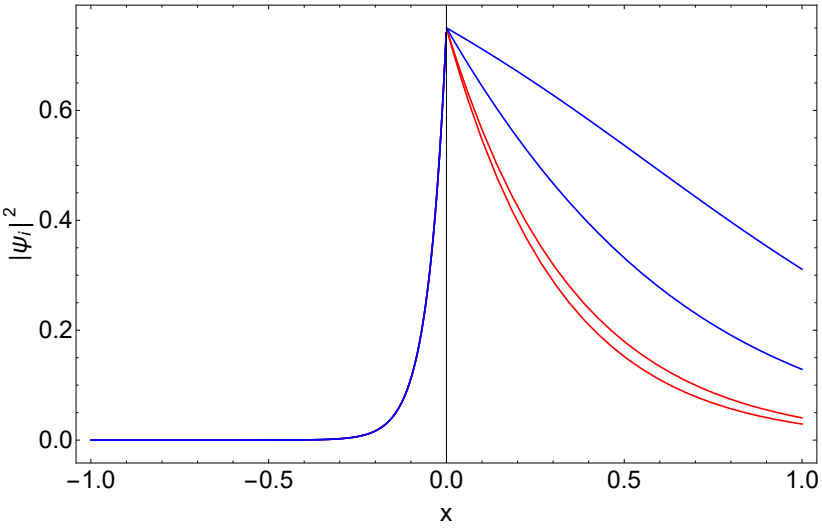

Figure 4.3 – Components of the wave function as a function of position. Image for the values $b = 2$, $k_z = 1$, $B = 1$ and $m = 19$.

$$\psi_<(x) = c \begin{pmatrix} \imath \\ \imath \\ 1 \\ 1 \end{pmatrix} e^{-\int_0^x dy \lambda^<(y)},$$

where we defined $\alpha(x) \equiv k_y + eBx$, $\lambda_\pm^>(x) = \sqrt{-k_y^2 + \alpha(x)^2 + (k_z \pm b)^2}$, $\lambda^<(x) = \sqrt{-k_y^2 + k_z^2 + \alpha(x)^2 + m^2}$, $\lambda_{\pm,0}^> \equiv \lim_{B\to 0} \lambda_\pm^>$ and c is just an overall constant of normalization.

We see that even though the surface state dispersion relation is the same as we found without magnetic fields, the found states are not exactly the same. Beside the exponent, the vectors themself now also depend on position. The exponents with which the modes decay is different and dependent on the magnetic field, so the same goes for the overall normalization. In particular, we find for the WSM part that all four components of the wave function decay differently, as opposed to having two pairs with the same decay as in the previous case. This is plotted in Fig. 4.3.

4.3.1 Interaction effects

In the part above we have concluded that a magnetic field parallel to the boundary does not influence the surface state at the tree level, which is given by the Hamiltonian

$$H_0 = \gamma^0 \left[-\imath\gamma^1 \partial_x + \gamma^2 (k_y + eBx) + \gamma^3 (k_z - \gamma^5 b) \right] \tag{4.3.1}$$

in the Weyl semimetal. Now we once again turn to a correction, which is given by the anomalous magnetic moment. To take into account this effect, we add the following term to the Hamiltonian:

$$H_1 = -\gamma^5 \left[\gamma^0 \gamma^3 \mu_2 + \mu_1 (k_z + \gamma^5 b) \right] B, \tag{4.3.2}$$

which takes into account both the separation of the Weyl nodes in momentum space and the interaction terms with the magnetic field. We assume here that both the magnetic field and the separation of the nodes is in the z-direction. In matrix form, this interaction

Hamiltonian is given by

$$H_1 = \begin{pmatrix} (\mu_2\sigma_z - \mu_1 k_z)B & 0 \\ 0 & (\mu_2\sigma_z + \mu_1 k_z)B \end{pmatrix}. \tag{4.3.3}$$

Zeeman term

The easier of the two terms to compute is the μ_2 term, which is the Zeeman term. To incorporate this effect, we add the term

$$H_1 = -\gamma^5\gamma^0\gamma^3\mu_2 B \tag{4.3.4}$$

to the Hamiltonian.

Inserting this term, we find that the new effective matrix $Q(x)$ is given by

$$Q(x) = -\imath\gamma^1\left\{\gamma^0 E - \gamma^2[k_y + eBx] - \gamma^3[k_z - \gamma^5(b + \mu_2 B)]\right\} \tag{4.3.5}$$

So this term simply shifts our separation of the Weyl nodes by $b \to b + \mu_2 B$. Note that this is of course due to our choice of the separation vector, which is in the same direction of the magnetic field. If the two were not parallel, the effect would be very different. Now this is a very simple substitution to make into the previous results for the surface states. Going through the computations again we quickly find that the surface state dispersion is still given by $E = -k_y$, but now with a Fermi arc modified by the magnetic field as $|k_z| < b + \mu_2 B$, as was to be expected.

Tilt term

The μ_1 term, which we showed to be a tilt term in Fig. 3.4, is a lot less trivial to compute. In this case the term

$$H_1 = -\gamma^5\mu_1(k_z - \gamma^5 b)B \tag{4.3.6}$$

has to be added to the Hamiltonian. Computing from this the effective matrix, we find that it reads

$$Q(x) = -\imath\gamma^1\left\{\gamma^0\left[E + \gamma^5\mu_1(k_z - \gamma^5 b)B\right] - \gamma^2[k_y + eBx] - \gamma^3[k_z - \gamma^5 b]\right\}. \tag{4.3.7}$$

It is clear from this equation that the tilt term does not provide a simple shift in one of the variables. This is mainly due to its chiral nature, since it affects the two Weyl cones differently, as opposed to the Zeeman term, which affects them equally. Going through the same calculations as before, we find in this case a novel dispersion relation, which is given by

$$E = \mu_1 B b\left[1 - \left(\frac{k_z}{b}\right)^2\right] - k_y\sqrt{1 - (\mu_1 B)^2\left(\frac{k_z}{b}\right)^2}. \tag{4.3.8}$$

In the case where we set $\mu_1 = 0$, or equivalently, set $B = 0$, the regular $E = -k_y$ dispersion relation is again recovered. In dimensionless units, the dispersion relation reads

$$\bar{E} = \bar{B}(1 - \bar{k}_z^2) - \bar{k}_y\sqrt{1 - \bar{B}^2\bar{k}_z^2}, \tag{4.3.9}$$

where we have defined the dimensionless variables to be

$$\bar{E} \equiv \frac{E}{\hbar v_F b}, \quad \bar{B} \equiv \frac{\mu_1 B}{\hbar v_F} \text{ and } \bar{k}_{y,z} \equiv \frac{k_{y,z}}{b}.$$

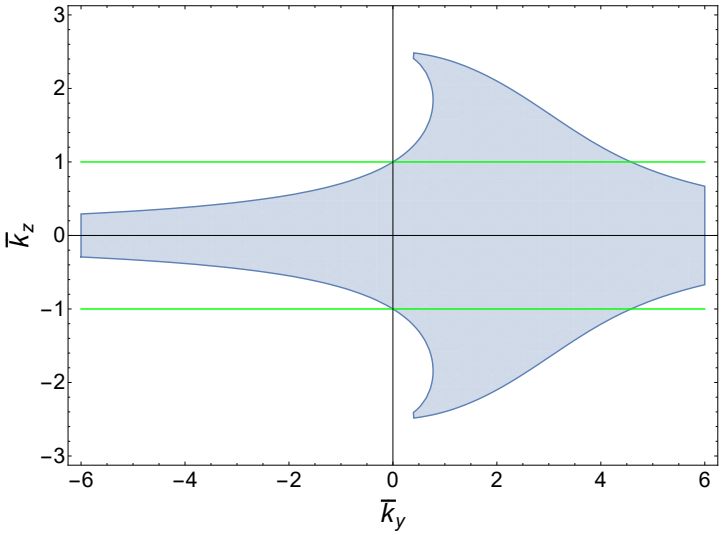

Figure 4.4 – Shaded in blue is the region in which we numerically determined that the dispersion relation Eq. 4.3.9 holds for $\bar{B} = 0.4$. The green lines indicate the boundaries for $B = 0$.

Unlike in the previous cases, it is not so clear in which region the dispersion relation is valid, and hence in which region surface states are supported. The region in which it is valid for $\bar{B} = 0.4$ is given in Fig. 4.4. Plotted here is the region in which the determinant of the matching matrix vanishes, after substitution of the found dispersion relation, which is done numerically. Note that the "tips" should end exactly in a point at $\bar{k}_y = 0$, but do not due to numerical rounding errors.

Additionally, we see that the velocity is also no longer linear and constant throughout the dispersion region. We can compute the (dimensionless) velocity profile to be

$$\mathbf{v} = \nabla_{\mathbf{k}} E(\mathbf{k}) = \left(0, -\sqrt{1-\bar{B}^2\bar{k}_z^2}, -2\bar{B}\bar{k}_z + \frac{\bar{B}^2\bar{k}_z\bar{k}_y}{\sqrt{1-\bar{B}^2\bar{k}_z^2}}\right). \tag{4.3.10}$$

So the velocity is parallel to the surface, as is to be expected, but now does actually depend on $\bar{k}_z$ and $\bar{k}_y$. A plot of the direction of the flow overlayed on the dispersion region is given in Fig. 4.5. As can be seen, the flow eventually converges to the $\bar{k}_y$ axis from all sides.

We can investigate the determinant of the matchings matrix in order to attempt to discern what the boundaries of this region are analytically. Doing so will reveal that the term that has to vanish is given by

$$\begin{aligned} 0 =& (1-\bar{B}^2)(1-\bar{k}_z^2) + 2(1-\bar{B})\bar{E} + \bar{E}^2 - \left(\bar{k}_y - \sqrt{\bar{k}_y^2 + (1-\bar{B}^2)(1-\bar{k}_z)^2 + 2\bar{B}(1-\bar{k}_z)\bar{E} - \bar{E}^2}\right) \\ & \left(\bar{k}_y - \sqrt{\bar{k}_y^2 + (1-\bar{B}^2)(1+\bar{k}_z)^2 + 2\bar{B}(1+\bar{k}_z)\bar{E} - \bar{E}^2}\right), \end{aligned}$$

where $\bar{E}$ is the dispersion relation as in Eq. 4.3.9.

Looking at the full equation, it appears impossible to derive from this the boundaries of the region for the dispersion relation. However, they may be obtained by investigating the square roots that appear in the equation, and checking when the term underneath the root changes sign. So we look for the solutions of

$$\bar{k}_y^2 + (1-\bar{B}^2)(1\pm\bar{k}_z)^2 + 2\bar{B}(1\pm\bar{k}_z)\bar{E} - \bar{E}^2 = 0. \tag{4.3.11}$$

From this, we find that the region is bounded by two hyperbolic curves that are defined

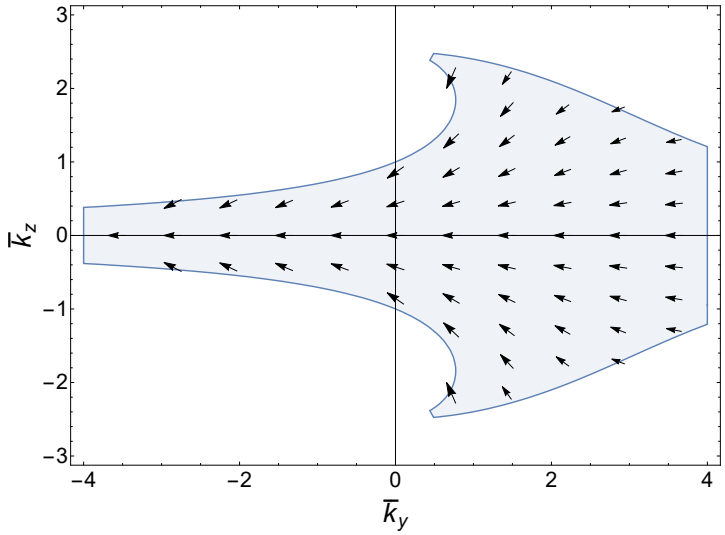

Figure 4.5 – Plot of the velocity field, which is indicated by the arrows, given in Eq. 4.3.10, overlayed on the region in which we numerically determined that the dispersion relation Eq. 4.3.9 is a solution, which is shaded in blue.

by

$$\bar{k}_y = \frac{\bar{k}_z \pm 1}{\bar{B}\bar{k}_z}\sqrt{1-\bar{B}^2\bar{k}_z^2}. \tag{4.3.12}$$

In Fig. 4.6 we have plotted these found expression for the boundaries on top of the region for which we numerically determined the dispersion relation to be a solution. We see that this indeed exactly gives the boundaries of the region. However, we see that the region does not exactly end in the point like the boundaries that were derived, which we attribute to numerical rounding errors.

The exact expression for the wave function can be obtained by substituting the found dispersion relation into the states computed through the WKB method, but are generally so complicated and extensive that it is not enlightening to show here.

Combined effect

Now that we have computed the effect of the individual terms on the dispersion relation, we can consider the effect of both combined. In this case we add the full one-loop correction term, given by

$$H_1 = -\gamma^5\left[\gamma^0\gamma^3\mu_2 + \mu_1(k_z + \gamma^5 b)\right]B,$$

to the Hamiltonian. With this, the effective matrix is then given by

$$Q(x) = -\imath\gamma^1\left\{\gamma^0\left[E + \gamma^5\mu_1(k_z - \gamma^5 b)B\right] - \gamma^2[k_y + eBx] - \gamma^3[k_z - \gamma^5(b + \mu_2 B)]\right\}.$$

Once again we can apply the same methods as used above to compute the surface state dispersion. In this instance it is given by

$$E = \mu_1 Bb\left(1 - \frac{k_z^2}{b(b+\mu_2 B)}\right) - k_y\sqrt{1-(\mu_1 B)^2\left(\frac{k_z}{b+\mu_2 B}\right)^2}. \tag{4.3.13}$$

This can again be cast into a dimensionless form. Introducing the ratio $\bar{r} \equiv \mu_2/\mu_1 b$, the

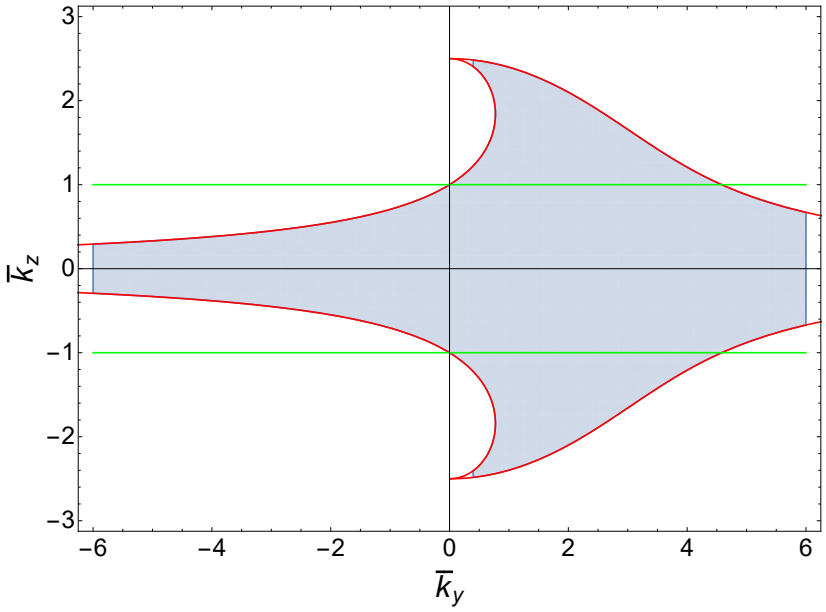

Figure 4.6 – Shaded in blue is the region in which we numerically determined that the dispersion relation Eq. 4.3.9 holds for $\bar{B} = 0.4$. The red curves denote the analytically found expressions for the boundaries given in Eq. 4.3.12. The green lines indicate the boundaries for $B = 0$.

dispersion relation can be written as

$$\bar{E} = \bar{B}\left(1 - \frac{\bar{k}_z^2}{1 + \bar{r}\bar{B}}\right) - \bar{k}_y\sqrt{1 - \bar{B}^2\frac{\bar{k}_z^2}{(1 + \bar{r}\bar{B})^2}}. \tag{4.3.14}$$

Curiously the dispersion relation now does depend on the Zeeman parameter μ_2, while it did not when we investigated that term alone. However, any term with μ_2 is multiplied with μ_1, so with $\mu_1 = 0$, we indeed see that the dispersion does not depend on μ_2, even when considering $\mu_2 \neq 0$. The flow field in this case is almost the same as with the previous case, but with some additional scaling factors.

Again we can check the limiting cases: taking $\mu_2 = 0$, which is equivalent to setting $\bar{r} = 0$, we recover the dispersion as in Eq. 4.3.9. Setting $\mu_1 = 0$ gives the correct result $\bar{E} = -\bar{k}_y$ for both the Zeeman and zero field cases.

The region in which it is valid for $\bar{B} = 0.4$ and $\bar{r} = 1$ is shown in Fig. 4.7. It is very similar to the case for only $\mu_1 \neq 0$, except slightly broadened in the $\bar{k}_z$ direction. So it is indeed a combination of the two, as the $\mu_2 \neq 0$ case also caused a broadening of the band. Again the boundaries of the dispersion region can be found by looking at the square root terms in the determinant of the matching matrix, and are found to be given by the two hyperbolas defined by:

$$\bar{k}_y = \frac{\bar{k}_z \pm (1 + \bar{r}\bar{B})}{\bar{B}\bar{k}_z}\sqrt{(1 + \bar{r}\bar{B})^2 - \bar{B}^2\bar{k}_z^2}. \tag{4.3.15}$$

As with the previous case, the tips of the zone should end exactly at $\bar{k}_y = 0$, but do not in the figure because of numerical rounding. Setting $\mu_2 = 0$, or equivalently $\bar{r} = 0$, will give us the boundaries we found earlier for just $\mu_1 \neq 0$.

Finally we can investigate the $B \to 0$ limit. If these formulas are to be correct, then they should allow us to recover the zero field boundaries through this limit. Taking this limit, we see that the limit diverges everywhere, except at two special values for $\bar{k}_z$, namely $\bar{k}_z = \pm 1$, at which point the limit simply goes to $\bar{k}_z = \pm 1$, which are exactly the boundaries for the zero-field case.

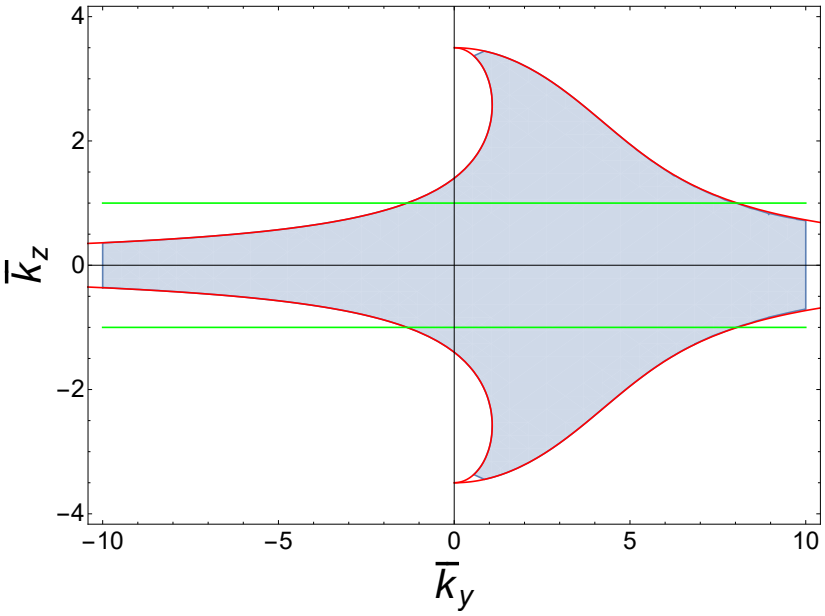

Figure 4.7 – The region in which we numerically found that the dispersion relation Eq. 4.3.14 with both $\mu_1 \neq 0$ and $\mu_2 \neq 0$ holds for $\bar{B} = 0.4$ and $\bar{r} = 1$ is shaded in blue. The green lines indicate the boundaries in the absence of a magnetic field. The red curves denote the analytical expressions for the boundaries, given in Eq. 4.3.15.

Effect	Dispersion relations	Boundaries
B=0	$E = -k_y$	$k_z = \pm b$
B=B$\hat{\mathbf{z}}$	$E = -k_y$	$k_z = \pm b$
$\mu_2 \neq 0$	$E = -k_y$	$k_z = \pm(b + \mu_2 B)$
$\mu_1 \neq 0$	$\bar{E} = \bar{B}\left(1 - \bar{k}_z^2\right) - \bar{k}_y\sqrt{1 - \bar{B}^2\bar{k}_z^2}$	$\bar{k}_y = \frac{\bar{k}_z \pm 1}{\bar{B}\bar{k}_z}\sqrt{1 - \bar{B}^2\bar{k}_z^2}$
$\mu_1 \neq 0$ and $\mu_2 \neq 0$	$\bar{E} = \bar{B}\left(1 - \frac{\bar{k}_z^2}{1+\bar{r}\bar{B}}\right) - \bar{k}_y\sqrt{1 - \frac{\bar{B}^2\bar{k}_z^2}{(1+\bar{r}\bar{B})^2}}$	$\bar{k}_y = \frac{\bar{k}_z \pm (1+\bar{r}\bar{B})}{\bar{B}\bar{k}_z}\sqrt{(1+\bar{r}\bar{B})^2 - \bar{B}^2\bar{k}_z^2}$

Table 4.1 – Summary of the obtained results on the surface state dispersion relations and the regions in which they are a solution.

Finally, a summary of the found results for the surface state dispersion relations and the regions in which they are valid is given in Table 4.1.

4.4 Conclusion

In this chapter we have computed the effect of electromagnetic fields and the anomalous magnetic moment on the conducting surface states on the interface between a Weyl semimetal and a massive Dirac vacuum. We started by computing the surface state dispersion in the absence of any gauge fields, in order to establish a general procedure for computing these states, and to be able to compare the result with the states in the presence of these fields. After that we show the result of an electric field and its corresponding term in a vertex correction, which is a Rashba-like term, on the energy states.

Next we used the WKB approximation in order to find the surface states in the presence of a magnetic field with a direction parallel to the interface. We have shown that at

tree level, the magnetic field does not influence the surface state dispersion. This was expected based on the gauge coupling vanishing at the surface and a physical argument. After that we show that the anomalous magnetic moment terms actually do influence the dispersion relation as long as the tilt parameter μ_1 is non-zero, which is a novel result, and change the direction of flow as well as the region in which the dispersion relation holds. We show that instead of two straight lines, the region is now bound by two hyperbolas, which reduce to the two straight lines in the zero field limit.

Chapter 5

Conclusion & Outlook

In this chapter we summarize the results and conclusions that were obtained during this thesis. Afterwards we look ahead to what unanswered questions remain and could be interesting for further research.

5.1 Results

In this thesis we have investigated the effects of magnetic fields on the energy states of a Weyl semimetal, both in the bulk and on the interface with a Dirac vacuum. Starting from the known effects of a magnetic field on the energy levels in bulk, giving us the Landau levels, we have added more terms to the Hamiltonian. The first extra terms under consideration were those corresponding to the anomalous magnetic moment, consisting of two terms. The first term is proportional to $\boldsymbol{\sigma} \cdot \mathbf{B}$, which gives us an anomalous Zeeman shift. This effect shifted the two Weyl cones in momentum space, breaking the spin degeneracy that is present in the normal Landau levels. The second term is proportional to $\mathbf{k} \cdot \mathbf{B}$, which tilts the Weyl cones, also breaking the degeneracy. Both effects could be incorporated analytically into the expression for the energy levels.

The next effect under consideration is the explicit shifting of the Weyl cones in momentum space, away from each other, which is necessary to form a stable Weyl semimetal, rather than a Dirac semimetal. We have shown that shifting the cones in either energy space or along the direction of the magnetic field yields analytically computable energy states. In contrast, shifting the cones perpendicular to the direction of the magnetic field gives non-trivial results, such as a non-linear dispersion relation for the lowest Landau level and a topological phase transition. These energy states need to be computed numerically, due to Fock space no longer being a suitable basis for these states. Perturbation theory is then used to compute the lowest Landau level for small shift parameters, which shows excellent agreement with the numerical results.

After the bulk problem, the effect on surface states was considered. For this we looked at a Weyl semimetal bordering a massive Dirac vacuum, and a magnetic field parallel to this interface. The mass was taken sufficiently large as to act as a work function to prevent the fermions from leaving the Weyl semimetal easily. To find surface states we solve the Dirac equation in both half-planes separately and demand continuity of the solutions at the boundary. To solve this problem in the presence of magnetic field, the WKB approximation for matrix Hamiltonians is used. This method of computing is developed in the appendix and gives us a tool to calculate the wave functions of the bound states for a general matrix Hamiltonian and allows for the addition of more terms in the Hamiltonian, which could be useful for future work. From this we conclude that a magnetic field along the boundary does not influence the surface state dispersion, as expected.

We then added the anomalous magnetic moment terms like before and asked the same

question again. Here we found that the anomalous Zeeman term on its own does not influence the dispersion relation, but does broaden the region in which it is a solution. The tilt term does influence the dispersion relation, and significantly alters the region in which the solution is valid. The region changes from being bound by two straight lines to being confined to the interior of two hyperbolic curves. Combining the two effects, we find that the Zeeman shift then also contributes to the dispersion relation, but only in combination with the tilt term. The region here is then similar to the one found in the case of just the tilt, but broadened, as in the case with just Zeeman. Taking the zero field limit on the found hyperbolic curves again reduces them to the straight lines like before.

5.2 Outlook

As with any research project, unanswered questions still remain at the end of this thesis. The bulk problem is now reasonably well understood, but there are still some aspects of the bound surface states that we wanted to investigate. We have only looked at a magnetic field parallel to the boundary, but having it perpendicular to the boundary instead would be the logical next step. Physical intuition tells us that in this case, even without interaction effects, the magnetic field would change the surface state dispersion relation: in the same vein as our argument against having a parallel field not alter it, the cyclotron orbits due to this field would now be exactly in the surface plane. Hence, we expect it to affect the dispersion this way. However, computations in this case will yield another difficulty: where we only had to break one translational invariance in the case of a magnetic field along the boundary, we will need to break a second one if we put it perpendicular to the surface. In this case, the method we developed for the surface states will need to be improved further, but could lead to some very interesting results. The theory on which my method is based is valid for general matrix Hamiltonians. Thus, we expect that it should be possible to derive from that a method that allows for the breaking of multiple translational invariances.

Appendix A

Dirac equation with magnetic field

In this appendix we shall explicitly show how to construct solutions for the Dirac equation in the presence of a magnetic field. It will consist of two parts. In the first part we shall construct the regular solutions, which are again the Landau solutions as seen before. The second part will concern itself with the classically forbidden regime, the tunneling solutions, which are found using the WKB approximation, as these solutions cannot be found through analytical solutions of the Dirac equation.

A.1 Landau levels

The Dirac Hamiltonian, minimally coupled to a magnetic field reads

$$H = \gamma^0 \left[\boldsymbol{\gamma} \cdot (-\imath\nabla + e\mathbf{A}) + m\right] = \begin{pmatrix} -\boldsymbol{\sigma} \cdot (-\imath\nabla + e\mathbf{A}) & m \\ m & \boldsymbol{\sigma} \cdot (-\imath\nabla + e\mathbf{A}) \end{pmatrix}. \tag{A.1.1}$$

We take our choice of gauge to be $\mathbf{A} = B(0, x, 0)$, such that translational invariance in the $\hat{y}$ direction is conserved and the magnetic field is uniform in the $\hat{z}$ direction. Due to the structure, we look for solutions of the form $\Psi = (\psi, \phi)^T$, leaving us with two equations:

$$\begin{aligned} -\boldsymbol{\sigma} \cdot (-\imath\nabla + e\mathbf{A})\psi + m\phi &= E\psi \\ m\psi + \boldsymbol{\sigma} \cdot (-\imath\nabla + e\mathbf{A})\phi &= E\phi \end{aligned}$$

Solving for ϕ using the first equation yields $m\phi = [E + \boldsymbol{\sigma} \cdot (-\imath\nabla + e\mathbf{A})]\psi$. Inserting this into the second equation and mulitplying both sides by the mass, we obtain

$$[\boldsymbol{\sigma} \cdot (-\imath\nabla + e\mathbf{A})]^2\psi = [E^2 - m^2]\psi. \tag{A.1.2}$$

Next we expand the square of the operator, keeping in mind that Pauli matrices do not commute.

$$\begin{aligned} [\boldsymbol{\sigma} \cdot (-\imath\nabla + e\mathbf{A})]^2 &= (-\imath\boldsymbol{\sigma} \cdot \nabla + eBx\sigma_y)^2 \\ &= -\nabla^2 + (eBx)^2 - \imath\boldsymbol{\sigma} \cdot \nabla(eBx\sigma_y) - \imath eBx\sigma_y(\boldsymbol{\sigma} \cdot \nabla) \\ &= -\nabla^2 + (eBx)^2 - \imath eBx\sigma_x \cdot \sigma_y - \imath eBx\{\boldsymbol{\sigma} \cdot \nabla, \sigma_y\} \\ &= -\nabla^2 + (eBx)^2 + eB\sigma_z - 2eBx\imath\partial_y. \end{aligned}$$

So we find that the equation above is given by

$$[-\nabla^2 + (eBx)^2 + eB\sigma_z - 2eBx\imath\partial_y - E^2 + m^2]\psi = 0. \tag{A.1.3}$$

Since translational invariance is only broken in the $\hat{x}$ direction we can make a planewave ansatz in the other two directions, and write the spinor as $\psi = f(x)e^{\imath(k_y y + k_z z)}$, with $f(x)$ a two-component spinor. Inserting this ansatz then reduces the above equation to a one-dimensional equation for x:

$$[\partial_x^2 - (k_y + eBx)^2 + (E^2 - eB\sigma_z - m^2 - k_z^2)]f(x) = 0. \tag{A.1.4}$$

Since this is a matrix equation, we expect to find a two dimensional eigenspace. Without loss of generality, we take the basis of this space to be eigenstates of the σ_z operator:

$$f_+(x) = F_+(x)\begin{pmatrix}1\\0\end{pmatrix}, \qquad f_-(x) = F_-(x)\begin{pmatrix}0\\1\end{pmatrix}. \tag{A.1.5}$$

In this way we find that $\sigma_z f_s(x) = s f_s(x)$, with $s = \pm 1$. Using this, the solutions are given by the two (scalar) functions that satisfy the equations

$$[\partial_x^2 - (k_y + eBx)^2 + (E^2 - eBs - m^2 - k_z^2)]F_s(x) = 0. \tag{A.1.6}$$

We can reduce these equations to a known one by introducing $\kappa = \sqrt{eB}\,(x + k_y/eB)$ and writing the equations as

$$(\partial_\kappa^2 - \kappa^2 + \alpha_s)F_s(\kappa) = 0, \tag{A.1.7}$$

where $\alpha_s = (E^2 - eBs - m^2 - k_z^2)/eB$.

This equation is a special case of the Hermite equation, which is also found in the harmonic oscillator. It has solutions exactly when $\alpha_s = 2n+1$, with n a non-negative integer, and its solutions are given by the Hermite functions. The solutions, after normalization are then given by

$$F_s(\kappa) = \left(\frac{\sqrt{eB}}{n!2^n\sqrt{\pi}}\right)e^{-\kappa^2/2}H_n(\kappa) \equiv G_n(\kappa). \tag{A.1.8}$$

Since we require that $\alpha_s = 2n + 1$, we find that the eigenvalues are given by

$$E^2 = m^2 + k_z^2 + eBs + eB(2n+1) = m^2 + k_z^2 + 2eB\left(n + \frac{1+s}{2}\right) \equiv m^2 + k_z^2 + 2eBl, \tag{A.1.9}$$

where l is again the Landau index, which we require to also be a non-negative integer. Hence, we find that there are not just two solutions, but infinitely many, labelled by the Landau index l. This should not come as a surprise to anyone familiar with the harmonic oscillator. We conclude that the eigenstates are given by

$$f_+^{(l)}(\kappa) = \begin{pmatrix}G_{l-1}(\kappa)\\0\end{pmatrix}, \qquad f_-^{(l)}(\kappa) = \begin{pmatrix}0\\G_l(\kappa)\end{pmatrix}. \tag{A.1.10}$$

From here we also see that the lowest Landau level is non-degenerate, since we must set $G_{-1}(\kappa) = 0$ to make sure that $l \geq 0$. So again we find that the lowest level is chiral, or spin-polarized, because only the $s = -1$ state is an eigenstate of this level.

Now that we have found one half of the solution to the Dirac equation, we can apply the relation $m\phi = [E + \boldsymbol{\sigma}\cdot(-\imath\nabla + e\mathbf{A})]\psi$ to construct the full solutions. To this end, we shall use E_l to denote the positive root of $E^2 = m^2 + k_z^2 + 2eBl$.

We will also need a recursion relation for the Hermite functions, which is given by

$$\partial_x G_n(x) = xG_n(x) - \sqrt{2(n+1)}G_{n+1}(x).$$

We start with computing $\boldsymbol{\sigma}\cdot(-\imath\nabla + e\mathbf{A})\psi$ for the $s=1$ state:

$$\begin{aligned}\boldsymbol{\sigma}\cdot(-\imath\nabla + e\mathbf{A})\psi_+^{(l)}(\kappa) &= \begin{pmatrix} -\imath\partial_z & -\imath\partial_x - \partial_y - \imath eBx \\ -\imath\partial_x + \partial_y + \imath eBx & \imath\partial_z \end{pmatrix}\begin{pmatrix} G_{l-1}(\kappa) \\ 0 \end{pmatrix} e^{\imath(k_y y + k_z z)} \\ &= \begin{pmatrix} k_z & -\imath(\partial_x + k_y + eBx) \\ -\imath(\partial_x - k_y - eBx) & -k_z \end{pmatrix}\begin{pmatrix} G_{l-1}(\kappa) \\ 0 \end{pmatrix} e^{\imath(k_y y + k_z z)} \\ &= \begin{pmatrix} k_z G_{l-1}(\kappa) \\ -\imath(\partial_x - k_y - eBx)G_{l-1}(\kappa) \end{pmatrix} e^{\imath(k_y y + k_z z)}\end{aligned}$$

Now we apply the recursion relation given above. First note that $\partial_x - k_y - eBx = \sqrt{eB}(\partial_\kappa - \kappa)$. From this follows that

$$\sqrt{eB}(\partial_\kappa - \kappa)G_{l-1}(\kappa) = (\kappa - \kappa)G_{l-1}(\kappa) - \sqrt{2eBl}G_l(\kappa) = -\sqrt{2eBl}G_l(\kappa).$$

So we find that

$$\boldsymbol{\sigma}\cdot(-\imath\nabla + e\mathbf{A})\psi_+^{(l)}(\kappa) = \begin{pmatrix} k_z G_{l-1}(\kappa) \\ \imath\sqrt{2eBl}G_l(\kappa) \end{pmatrix} e^{\imath(k_y y + k_z z)}.$$

The $s=-1$ state can be computed in a similar way:

$$\boldsymbol{\sigma}\cdot(-\imath\nabla + e\mathbf{A})\psi_-^{(l)}(\kappa) = \begin{pmatrix} -\imath\sqrt{2eBl}G_{l-1}(\kappa) \\ -k_z G_l(\kappa) \end{pmatrix} e^{\imath(k_y y + k_z z)}.$$

Having obtained these results, we can now write down the full solutions to the Dirac equation:

$$\Psi_+^{(l)} = \begin{pmatrix} G_{l-1}(\kappa) \\ 0 \\ \frac{1}{m}(E_l + k_z)G_{l-1}(\kappa) \\ \frac{\imath}{m}\sqrt{2eBl}G_l(\kappa) \end{pmatrix} e^{\imath(k_y y + k_z z)}, \qquad \Psi_-^{(l)} = \begin{pmatrix} 0 \\ G_l(\kappa) \\ -\frac{\imath}{m}\sqrt{2eBl}G_{l-1}(\kappa) \\ \frac{1}{m}(E_l - k_z)G_l(\kappa) \end{pmatrix} e^{\imath(k_y y + k_z z)}. \tag{A.1.11}$$

These are the solutions to the positive energy states. However, we know that the negative states also exist. Those states are simply found by flipping the sign on E_l:

$$\Phi_+^{(l)} = \begin{pmatrix} G_{l-1}(\kappa) \\ 0 \\ \frac{1}{m}(k_z - E_l)G_{l-1}(\kappa) \\ \frac{\imath}{m}\sqrt{2eBl}G_l(\kappa) \end{pmatrix} e^{\imath(k_y y + k_z z)}, \qquad \Phi_-^{(l)} = \begin{pmatrix} 0 \\ G_l(\kappa) \\ -\frac{\imath}{m}\sqrt{2eBl}G_{l-1}(\kappa) \\ \frac{-1}{m}(E_l + k_z)G_l(\kappa) \end{pmatrix} e^{\imath(k_y y + k_z z)}. \tag{A.1.12}$$

A.2 WKB states

The Landau solution to the Dirac equation allows us to find exact solutions to the equation. However, it only gives us the classically allowed harmonic oscillator states. We

are also interested in the classically forbidden states, the tunneling states, which give us exponentially decaying states. These are the states of interest when considering edge modes.

Solutions in this regime cannot be found analytically, instead we apply the WKB approximation, named after Wentzel, Kramers and Brillouin, who all developed this method independently in 1926 [31, 32, 33]. This approximation is used to solve differential equations with spatially varying coefficienst, and where the highest order derivative is multiplied by a small number, denoted by ϵ. In quantum mechanics, $\hbar$ generaly plays the role of this parameter ϵ.

A.2.1 Scalar WKB

The approximation proposes the ansatz $\psi(x) \propto e^{\frac{1}{\hbar}\sum_{n=0}^{\infty}\hbar^n f_n(x)}$, with usually only the first couple orders taken into account. We can now apply this method to the Dirac equation, specifically, the form we found from which we derived the Hermite equation:

$$\left[\partial_x^2 - (k_y + eBx)^2 + (E^2 - eBs - m^2 - k_z^2)\right] F_s(x) = 0.$$

If we now take care of the units and re-insert the factors of $\hbar$, we can write this equation as

$$\hbar^2 \partial_x^2 F_s(x) = Q(x) F_s(x), \tag{A.2.1}$$

where we define $Q(x) \equiv -E^2 + (p_y + eBx)^2 + eBs + m^2 + p_z^2$. This is exactly of the form we need for the WKB expansion. For this we shall consider the first two terms of the expansion and use the ansatz $F_s(x) = e^{\frac{1}{\hbar}f(x)+g(x)}$:

$$\begin{aligned}
\partial_x^2 F_s(x) &= \partial_x^2 e^{\frac{1}{\hbar}f(x)+g(x)} \\
&= \partial_x \left\{ \left[\frac{1}{\hbar} f'(x) + g'(x) \right] e^{\frac{1}{\hbar}f(x)+g(x)} \right\} \\
&= \left\{ \frac{1}{\hbar^2}\left[f'(x)\right]^2 + \frac{1}{\hbar}\left[f''(x) + 2f'(x)g'(x)\right] + g''(x) + \left[g'(x)\right]^2 \right\} e^{\frac{1}{\hbar}f(x)+g(x)}.
\end{aligned}$$

Ignoring $\hbar^2$ and higher terms, we find the equation

$$\left[f'(x)\right]^2 + \hbar\left[f''(x) + 2f'(x)g'(x)\right] = Q(x). \tag{A.2.2}$$

Comparing orders of $\hbar$, we find that the zeroeth order is given by

$$\left[f'(x)\right]^2 = Q(x). \tag{A.2.3}$$

This can be easily solved by taking the square root and integrating out the derivative to obtain

$$f(x) = \pm \int_{x_0}^{x} \sqrt{Q(y)}\, dy. \tag{A.2.4}$$

Now that we have solved the leading order term, we can use that to solve the next order in $\hbar$. This equation reads

$$f''(x) + 2f'(x)g'(x) = 0.$$

Rewriting this for the unknown function, we obtain

$$g'(x) = -\frac{1}{2}\frac{f''(x)}{f'(x)}.$$

Using that $f'(x) = \pm\sqrt{Q(x)}$ and $f''(x) = \pm Q'(x)/2\sqrt{Q(x)}$, we find that

$$g'(x) = -\frac{1}{4}\frac{Q'(x)}{Q(x)} = -\frac{1}{4}\partial_x \log[Q(x)].$$

Integrating this equation then gives us the solution, which is given by

$$g(x) = -\frac{1}{4}\log\left[Q(x)\right] + a, \tag{A.2.5}$$

where a is a constant of integration, which we will absorb into the normalization constant. Inserting the found functions into the ansatz, we find that the approximate solution to the equation for the first two orders are given by

$$F_s(x) = a_1 Q^{-1/4}(x) e^{\frac{1}{\hbar}\int_{x_0}^{x} dy\sqrt{Q(y)}} + a_2 Q^{-1/4}(x) e^{-\frac{1}{\hbar}\int_{x_0}^{x} dy\sqrt{Q(y)}}. \tag{A.2.6}$$

Since we require the solutions to not blow up on each side of the boundary, one of the two exponentials will be set to zero through their constants. Since we will be interested in a boundary at $x = 0$, it is an obvious choice to pick $x_0 = 0$. Note that in order for this to be exponentially decaying states, we require that $Q(x) \geq 0$, otherwise it becomes an oscillating state.

A.2.2 Matrix WKB

The above is valid in the case of a scalar equation. In the case of a matrix Hamiltonian, the method becomes a bit more complicated. The method used in this section is derived from the more general method used in Ref. [34]. In this case a slightly different ansatz is employed:

$$\psi(x) = \mathbf{v}(x) e^{\frac{1}{\hbar}f(x)}. \tag{A.2.7}$$

Instead of the second exponent being a scalar function, we make it a matrix function, which we then merge with a constant vector to form a vector function. We rewrite the Dirac equation to read $\hbar\partial_x\psi(x) = Q(x)\psi(x)$, with $Q(x)$ a matrix. Applying the ansatz above, we find

$$\hbar\partial_x\psi(x) = \hbar\partial_x\left[\mathbf{v}(x)e^{\frac{1}{\hbar}f(x)}\right] = \hbar\mathbf{v}'(x)e^{\frac{1}{\hbar}f(x)} + \mathbf{v}(x)f'(x)e^{\frac{1}{\hbar}f(x)},$$

with a prime denoting a derivative with respect to x. Multiplying both sides of the equation with $e^{-\frac{1}{\hbar}f(x)}$, we find

$$\hbar\mathbf{v}'(x) + \mathbf{v}(x)f'(x) = Q(x)\mathbf{v}(x).$$

Since $\mathbf{v}$ and f are still unknown, we need to apply some tricks. The first being the spectral decomposition of $Q(x)$, by setting $Q(x) = R(x)Q_D(x)R^{-1}(x)$, with $Q_D(x)$ being the diagonalized version of the matrix $Q(x)$, with its eigenvalues on the diagonal, and $R(x)$ being the matrix with the eigenvectors of $Q(x)$ as its columns. Next we define another vector $\mathbf{L}(x)$, by the relation $\mathbf{v}(x) = R(x)\mathbf{L}(x)$. Using this, we can rewrite the righthand side of the equation as

$$Q(x)\mathbf{v}(x) = R(x)Q_D(x)R^{-1}(x)R(x)\mathbf{L}(x) = R(x)Q_D(x)\mathbf{L}(x).$$

The lefthand side becomes

$$R(x)\mathbf{L}(x)f'(x)+\hbar\partial_x\left[R(x)\mathbf{L}(x)\right]f(x) = R(x)\mathbf{L}(x)f'(x)+\hbar\left[R'(x)\mathbf{L}(x)+R(x)\mathbf{L}'(x)\right]f(x).$$

If we now then equate the two sides and multiply from the left by $R^{-1}(x)$, we arrive at

$$Q_D(x)\mathbf{L}(x) = \mathbf{L}(x)f'(x)+\hbar\left[R^{-1}(x)R'(x)\mathbf{L}(x)+\mathbf{L}'(x)\right]f(x).$$

Regrouping this in terms of $\hbar$, we find

$$\left[Q_D(x)-f'(x)\right]\mathbf{L}(x)-\hbar\left[R^{-1}(x)R'(x)\mathbf{L}(x)+\mathbf{L}'(x)\right]f(x) = 0. \tag{A.2.8}$$

So now in zeroeth order of $\hbar$, we find the equation

$$\left[Q_D(x)-f'(x)\right]\mathbf{L}(x) = 0, \tag{A.2.9}$$

which we know only has non-trivial solutions in the case that $\mathrm{Det}[Q_D(x)-f'(x)] = 0$, meaning $f'(x)$ has to be equal to one of the eigenvalues of $Q(x)$.

One order higher we find that the equation that has to be satisfied is given by

$$R^{-1}(x)R'(x)\mathbf{L}(x)+\mathbf{L}'(x) = 0,$$

which then implies the following differential equation:

$$\mathbf{L}'(x) = -R^{-1}(x)R'(x)\mathbf{L}(x). \tag{A.2.10}$$

In the next sections we shall compute the solutions for the Dirac vacuum and and the WSM parts.

A.2.3 Dirac Vacuum

For the Dirac vacuum, the matrix $Q(x)$ is given by

$$Q(x) = -\imath\gamma^1\left[\gamma^0 E-\gamma^2(p_y+eBx)-\gamma^3 k_z-m\right]. \tag{A.2.11}$$

In order to have non-trivial solutions to the zeroeth order equation, we demand $\mathrm{Det}(Q_D(x)-f'(x)) = 0$. From this we conclude that $f'(x)$ has to be equal to one of the eigenvalues of the the matrix $Q(x)$, which are given by $\pm\lambda(x) = \pm\sqrt{-E^2+m^2+(p_y+eBx)^2+p_z^2}$, with both signs being doubly degenerate.

From this we conclude that

$$f(x) = \pm\int_0^x dy\sqrt{-E^2+m^2+(p_y+eBy)^2+p_z^2}, \tag{A.2.12}$$

the same as in the scalar case. Furthermore, we find from this equation that for $f'(x) = +\lambda$, which is the case that we are interested in, $L_1 = L_2 = 0$ in order to satisfy the relation.

Now the next order is a little bit more involved. Because we are interested in the evanescent solution, away from the classical turning points, we are going to assume that $f(x)\neq 0$. Defining $\alpha(x)\equiv p_y+eBx$, we find that the matrix multiplying the vector is given by

$$R^{-1}(x)R'(x) = \frac{eB}{2\lambda^2(x)}\begin{pmatrix} [\alpha(x)-\lambda(x)] & 0 & -[\alpha(x)+\lambda(x)] & 0 \\ 0 & [\alpha(x)+\lambda(x)] & 0 & -[\alpha(x)-\lambda(x)] \\ -[\alpha(x)-\lambda(x)] & 0 & [\alpha(x)+\lambda(x)] & 0 \\ 0 & -[\alpha(x)+\lambda(x)] & 0 & [\alpha(x)-\lambda(x)] \end{pmatrix}.$$

This immediately implies that $L_1'(x) = -L_3'(x)$ and $L_2'(x) = -L_4'(x)$. So the set of four differential equations are given by

$$
\begin{aligned}
L_1'(x) &= \frac{eB}{2\lambda^2(x)}\left\{[\lambda(x)-\alpha(x)]L_1(x) + [\lambda(x)+\alpha(x)]L_3(x)\right\},\\
L_2'(x) &= \frac{eB}{2\lambda^2(x)}\left\{-[\lambda(x)+\alpha(x)]L_2(x) + [-\lambda(x)+\alpha(x)]L_4(x)\right\},\\
L_3'(x) &= -\frac{eB}{2\lambda^2(x)}\left\{[\lambda(x)-\alpha(x)]L_1(x) + [\lambda(x)+\alpha(x)]L_3(x)\right\},\\
L_4'(x) &= -\frac{eB}{2\lambda^2(x)}\left\{-[\lambda(x)+\alpha(x)]L_2(x) + [-\lambda(x)+\alpha(x)]L_4(x)\right\}.
\end{aligned}
$$

It is at this point that we have seemingly reached a contradiction. Due to the earlier derived condition that $L_1 = L_2 = 0$ and the coupling between the derivatives of $L_1\&L_2$ and $L_3\&L_4$ it can be easily shown that it only has trivial solutions, which are useless. The solution to this problem lies in the degeneracy of the subspaces. We consider one degenerate subspace for $+\lambda$, containing the coefficients L_3 and L_4, while the coefficients L_1 and L_2 are outside of this space. It turns out that the coefficients outside of the considered space are of order $\hbar$, while those inside are of order 1, so the equations above are deceiving, due to this difference in order.

To correct orders, we find that the equations are given by

$$
\begin{aligned}
L_1'(x) &= 0,\\
L_2'(x) &= 0,\\
L_3'(x) &= -\frac{eB}{2\lambda^2(x)}[\lambda(x)+\alpha(x)]L_3(x),\\
L_4'(x) &= -\frac{eB}{2\lambda^2(x)}[-\lambda(x)+\alpha(x)]L_4(x).
\end{aligned}
$$

These equations can be solved fairly easily through integration, and yield results that are again consistent with the found results:

$$
\begin{aligned}
L_1 &= 0,\\
L_2 &= 0,\\
L_3 &= \frac{c_3}{\sqrt{\lambda(x)}}[\alpha(x)+\lambda(x)]^{-1/2},\\
L_4 &= \frac{c_4}{\sqrt{\lambda(x)}}[\alpha(x)+\lambda(x)]^{1/2}.
\end{aligned}
$$

The two coefficients can now be determined from the condition that in the limit $B \to 0$ it has to match the already known solution. It can be easily computed that the vectors in the $B \to 0$ limit are simply given by $L_3 = 1$ & $L_4 = 0$, or $L_3 = 0$ & $L_4 = 1$. So this gives us two cases. In the first we have $C_3 = \sqrt{\lambda_0}\sqrt{p_y+\lambda_0}$ and $c_4 = 0$, where $\lambda_0 \equiv \sqrt{m^2+p_y^2+p_z^2-\omega^2}$. The other option is given by $c_3 = 0$ and $c_4 = \sqrt{\lambda_0}/\sqrt{py+\lambda_0}$. If we now apply the matrix $R(x)$ to these vectors, we find that the WKB state vectors for the Dirac vacuum are given by

$$\mathbf{v}_1 = \sqrt{\frac{\lambda_0(p_y+\lambda_0)}{\lambda(x)[\alpha(x)+\lambda(x)]}}\begin{pmatrix} \frac{\imath[\alpha(x)+\lambda(x)]}{m} \\ \frac{pz-E}{m} \\ 0 \\ 1 \end{pmatrix}, \qquad \mathbf{v}_2 = \sqrt{\frac{\lambda_0[\alpha(x)+\lambda(x)]}{\lambda(x)(p_y+\lambda_0)}}\begin{pmatrix} \frac{-p_z+E}{m} \\ \frac{\imath[-\alpha(x)+\lambda(x)]}{m} \\ 1 \\ 0 \end{pmatrix}.$$

It is clear that these states are fairly similar in structure to the states without a magnetic field applied, but the main difference being the factor in front, which was not present earlier.

A.2.4 Weyl semimetal part

In order to find the solutions in the WSM half-space, we can use the same line of reasoning as in the previous section. In the semimetallic region, the matrix $Q(x)$ is given by

$$Q(x) = -\imath\gamma^1\left[\gamma^0 E - \gamma^2(p_y + eBx) - \gamma^3(p_z - \gamma^5 b)\right]. \tag{A.2.13}$$

The eigenvalues of this matrix are given by $\pm\lambda_\pm \equiv \pm\sqrt{-\omega^2 + (p_y+eBx)^2 + (p_z \pm b)^2}$. Note that we now have four non-degenerate eigenvalues. From the zeroeth order equation, and the requirement that the exponent does not blow up for $x \to \infty$, we conclude that $f'(x) = -\lambda_\pm$, and hence that

$$f_\pm(x) = -\int_0^x dy \lambda_\pm(y). \tag{A.2.14}$$

Furthermore, since $f'(x)$ now only equals one of the entries of $Q_D(x)$, we conclude that three of the four components have to vanish, instead of two as in the Dirac case. For the next order, we can again compute the matrix $M \equiv -R^{-1}(x)R'(x)$, which in this case is given by

$$M = \begin{pmatrix} M_+ & 0 \\ 0 & M_- \end{pmatrix},$$

where the matrices are defined as

$$M_\pm \equiv \frac{eB}{2\lambda_\pm^2}\begin{pmatrix} -\alpha(x)+\lambda_\pm(x) & \alpha(x)+\lambda_\pm(x) \\ \alpha(x)-\lambda_\pm(x) & -[\alpha(x)+\lambda_\pm(x)] \end{pmatrix}.$$

Due to this structure of M, it is evident that the upper two components of $\mathbf{L}$ are decoupled from the lower two, so we can write $\mathbf{L} = (\mathbf{L}_+, \mathbf{L}_-)^T$. Now the differential equations under consideration are

$$\begin{aligned} L'_{\pm,1}(x) &= \gamma_\pm\{[-\alpha(x)+\lambda_\pm(x)]L_{\pm,1} + [\alpha(x)+\lambda_\pm(x)]L_{\pm,2}\} \\ L'_{\pm,2}(x) &= \gamma_\pm\{-[-\alpha(x)+\lambda_\pm(x)]L_{\pm,1} - [\alpha(x)+\lambda_\pm(x)]L_{\pm,2}\} \end{aligned}$$

where we define $\gamma_\pm \equiv eB/2\lambda_\pm^2$.

However, from the zeroeth order equations, we have already determined that $L_{\pm,2} = 0$. So in order to again get a consistent set of equations, we require that the off-diagonal coupling terms in the differential equations are again of a different order. Doing so then allows us to write the following equations:

$$\begin{aligned} L'_{\pm,1}(x) &= \gamma_\pm[-\alpha(x) + \lambda_\pm(x)]L_{\pm,1}, \\ L'_{\pm,2}(x) &= 0. \end{aligned} \tag{A.2.15}$$

The second equation is consistent with $L_{\pm,2} = 0$. The first can be solved and yields

$$L_{\pm,1} = \frac{c_\pm}{\sqrt{\lambda_\pm(x)}}\sqrt{\alpha(x) + \lambda_\pm(x)}. \tag{A.2.16}$$

In the case $B = 0$, we require that $L_{\pm,1} = 1$, so we find that the constant has to be given by $c_\pm = \sqrt{\lambda_\pm(0)}/\sqrt{\alpha(0) + \lambda_\pm(0)}$. This leaves us with two solutions for the WKB state vectors:

$$\mathbf{v}_1 = \sqrt{\frac{\lambda_{-,0}}{\lambda_-(x)}}\sqrt{\frac{\alpha(x) + \lambda_-(x)}{p_y + \lambda_{-,0}}}\begin{pmatrix} 0 \\ 0 \\ -\imath\frac{\alpha(x)-\lambda_-(x)}{E-p_z+b} \\ 1 \end{pmatrix}, \qquad \mathbf{v}_2 = \sqrt{\frac{\lambda_{+,0}}{\lambda_+(x)}}\sqrt{\frac{\alpha(x) + \lambda_+(x)}{p_y + \lambda_{+,0}}}\begin{pmatrix} \imath\frac{\alpha(x)-\lambda_+(x)}{E+p_z+b} \\ 1 \\ 0 \\ 0 \end{pmatrix}.$$

Note that we did not need the exact form of the eigenvalues for the computation on the states. So we expect that this result is a general one and valid even under addition of more terms to the Hamiltonian. Adding more terms would change the eigenvalues, but not the method itself.

Bibliography

[1] Nobelprize.org, *The nobel prize in physics 2016* (2016), URL http://www.nobelprize.org/nobel_prizes/physics/laureates/2016/.

[2] C. L. Kane and E. J. Mele, Phys. Rev. Lett. **95**, 146802 (2005).

[3] X. Chen, Z.-X. Liu, and X.-G. Wen, Phys. Rev. B **84**, 235141 (2011).

[4] J. von Neumann and E. Wigner, Phys. Z. **467** (1929).

[5] H. Weyl, Proceedings of the National Academy of Sciences U.S.A **15**, 323 (1929).

[6] H. Kramer, Proceedings Koninklijke Akademie van Wetenschappen **33**, 959 (1930).

[7] K. S. Novoselov, A. K. Geim, S. V. Morozov, D. Jiang, Y. Zhang, S. V. Dubonos, I. V. Grigorieva, and A. A. Firsov, Science **306**, 666 (2004).

[8] Nobelprize.org, *The nobel prize in physics 2010* (2016), URL http://www.nobelprize.org/nobel_prizes/physics/laureates/2010/.

[9] A. H. Castro Neto, F. Guinea, N. M. R. Peres, K. S. Novoselov, and A. K. Geim, Rev. Mod. Phys. **81**, 109 (2009).

[10] S. Borisenko, Q. Gibson, D. Evtushinsky, V. Zabolotnyy, B. Büchner, and R. J. Cava, Phys. Rev. Lett. **113**, 027603 (2014).

[11] S.-Y. Xu, I. Belopolski, N. Alidoust, M. Neupane, G. Bian, C. Zhang, R. Sankar, G. Chang, Z. Yuan, C.-C. Lee, et al., Science **349**, 613 (2015).

[12] M. V. Berry, Proceedings of the Royal Society of London A: Mathematical, Physical and Engineering Sciences **392**, 45 (1984).

[13] S. Chern, Annals of Mathematics **46**, 674 (1945), ISSN 0003486X.

[14] H. Nielsen and M. Ninomiya, Physics Letters **130B** (1983).

[15] K. Fukushima, D. E. Kharzeev, and H. J. Warringa, Phys. Rev. D **78**, 074033 (2008).

[16] Q. Li, D. E. Kharzeev, C. Zhang, Y. Huang, I. Pletikosic, A. V. Fedorov, R. D. Zhong, J. A. Schneeloch, G. D. Gu, and T. Valla, Nat. Phys. (2016).

[17] E. Hall, American Journal of Mathematics **2**, 287 (1879).

[18] E. Hall, Philos. Mag. **12** (1881).

[19] N. Nagaosa, J. Sinova, S. Onoda, A. H. MacDonald, and N. P. Ong, Rev. Mod. Phys. **82**, 1539 (2010).

[20] A. Burkov, arXiv:1406.3033v2 [cond-mat.mes-hall] (2014).

[21] X. Wan, A. M. Turner, A. Vishwanath, and S. Y. Savrasov, Phys. Rev. B **83**, 205101 (2011).

[22] B. Q. Lv, S. Muff, T. Qian, Z. D. Song, S. M. Nie, N. Xu, P. Richard, C. E. Matt, N. C. Plumb, L. X. Zhao, et al., Phys. Rev. Lett. **115**, 217601 (2015).

[23] S.-Y. Xu, I. Belopolski, N. Alidoust, M. Neupane, G. Bian, C. Zhang, R. Sankar, G. Chang, Z. Yuan, C.-C. Lee, et al., Science (2015), ISSN 0036-8075.

[24] P. A. M. Dirac, Proceedings of the Royal Society of London A: Mathematical, Physical and Engineering Sciences **117**, 610 (1928).

[25] M. O. Goerbig, arXiv:0909.1998v2 [cond-mat.mes-hall] (2009).

[26] E. J. Ferrer and V. de la Incera, Nuclear Physics B **824**, 217 (2010).

[27] V. P. J. Jacobs, P. Betzios, U. Gürsoy, and H. T. C. Stoof, Phys. Rev. B **93**, 195104 (2016).

[28] E. C. I. van der Wurff and H. T. C. Stoof, Phys. Rev. B **94**, 155118 (2016).

[29] P. Goswami and S. Tewari, Phys. Rev. B **88**, 245107 (2013).

[30] A. Igarashi and M. Koshino, Phys. Rev. B **95**, 195306 (2017).

[31] G. Wentzel, Zeitschrift für Physik **38**, 518 (1926).

[32] H. Kramers, Zeitschrift für Physik **39**, 828 (1926).

[33] L. Brillouin, Comptes Rendus de l'Academie des Sciences **183** (1926).

[34] J. D. Bjorken and H. S. Orbach, Phys. Rev. D **23**, 2243 (1981).

Acknowledgements

Throughout this past year I have had help from a lot of different people. All of them contributed to the final result in one way or another, and all of them deserve to be mentioned here.

First and foremost, I would like to thank my supervisors Henk Stoof and Erik van der Wurff for their guidance and input. Henk, even though you are a very busy man, you still found the time to supervise me (and others) and have weekly meetings to discuss progress. I greatly enjoyed our discussions and I feel that I have learned a lot this past year, both about (condensed matter) physics and doing research in general. Doing this project has only further strengthened my passion for physics and motivation to continue on this path. Erik, thank you so much for all the help that you have provided, especially in the last couple of months. You were always willing to make time to answer my questions, which is very much appreciated. I am also very grateful for the fact that you took the time to scrutinize my draft version. I feel that your remarks have greatly improved the quality of this final version.

I would also like to thank my family for their continued interest in my progress and support. I am especially grateful to my father for reading through this thesis multiple times and commenting on my use of English, picking out the typo's and strange structures. Furthermore, I would like to say that I am extremely fortunate to have some of my good friends around here. Without their unwavering support during the times where things did not go as smoothly, this journey would have been a more difficult one. You know who you are. Finally, I would like to give a shout-out to Laurens for providing the latex template that was used here.